Electron Transfer in Structurally Engineered Metalloproteins

Thesis by

Stephen L. Mayo

In partial fulfillment of the requirements
for the degree of Doctor of Philosophy

California Institute of Technology

Pasadena, California

1988

(Submitted December 21, 1987)

to my family

and

our first Ph.D.

Acknowledgements

I would like to start off by saying that my stay at Caltech has been among the best of my educational experiences. Not only have I learned more about the "science" of science, but I have also become educated in the more pragmatic aspects of doing science in the 80's.

I would like to thank the Campbell, Goddard, Gray, and Richards groups for allowing me to move freely throughout their research empires.

I would also like to acknowledge AT&T Bell Labs for providing financial support during my tenure as a graduate student.

And finally, *very* special thanks goes to Jae....

Abstract

This thesis is concerned with experimental approaches for studying electron transfer in metalloproteins. The material presented traces the development of experimental techniques aimed at elucidating the mechanism of intramolecular metalloprotein electron transfer. The first chapter includes a reprint of an *Inorganic Chemistry* paper that describes the bimolecular reaction of small inorganic redox complexes with blue-copper proteins. The second chapter illustrates the use of covalently attached redox probes for studying rate-distance relationships. And the third chapter documents our progress in using genetic methods to structurally engineer yeast iso-1 cytochrome *c* into an idealized system for studying the distance dependence of intramolecular electron-transfer events.

Contents

Thesis Overview

The chapters of this thesis follow the historical development of experiments aimed at elucidating the mechanism of biological electron transfer in our laboratories.[1] To this end, Chapter 1 includes a paper exemplifying the use of small inorganic redox complexes and bimolecular kinetics in "early" attempts to understand the mechanistic details of metalloprotein electron transfer.[2] Its inclusion serves to point out the nearly insurmountable difficulties that arise when one is forced to examine the problem of electron transfer at a level of complexity that is divergent to the goal of understanding the fundamental transfer process. That is, a bimolecular system adds unwanted complexity to studying electron transfer because the actual transfer event (an intramolecular process) must be deconvoluted from the dominant bimolecular process. In addition, since donor-acceptor distance is a prime concern in mechanistic considerations of electron transfer,[3] bimolecular events are very difficult to study because the detailed geometry of the reacting species is seldom known.

The frustration generated by experiments of the type described in Chapter 1 catalyzed the development of unimolecular systems that allow the examination of the electron-transfer events without the complexity of bimolecular reactions. One such system was developed by Gray and coworkers[4] and involved attaching a probe redox center directly to the protein of interest. Since the 3-D structures of the target proteins are generally available, it is possible to know the geometry of the complex with some degree of certainty. These experiments have proven to be very successful in providing rate-distance data that can be evaluated in terms of Marcus theory, which is the subject of Chapter 2. However, even these experiments do not provide the ultimate answer. As indicated in the papers of Chapter 2,[5] the number of rate-distance points is not yet sufficient to make definitive statements concerning the correlation of electron-transfer rates and donor-acceptor distances. And, the data

indicate that factors other than distance (the electron-transfer path in particular) might play an important role in determining the rate at which the electron-transfer takes place.

Given these additional considerations, the experiment described in Chapter 3 follows naturally. It occurred to us that one method of ensuring the generation of "consistent" rate-distance data is to engineer the protein in addition to using a covalently attached redox probe. That is, the use of genetic engineering in combination with the techniques developed for studying intramolecular electron transfer provide tremendous control over the entire system. The full meaning of "structurally engineered" is now clear. Chapter 3 documents our progress in using genetic engineering methodology to build an optimal metalloprotein system for studying biological electron transfer.

References

[1] For a review on biological electron transfer see (and references therein): Mayo, S. L.; Ellis, W. R., Jr.; Crutchley, R. L.; Gray, H. B. *Science* **1986**, *233*, 948-952.

[2] Brunschwig, B. S.; DeLaive, P. J.; English, A. M.; Goldberg, M.; Gray, H. B.; Mayo, S. L.; Sutin, N. *Inorg. Chem.* **1985**, *24*, 3743-3749.

[3] Marcus, R. A.; Sutin, N. *Biochim. Biophys. Acta* **1985**, *811*, 265-322.

[4] (a) Yocum, K. M.; Shelton, J. B.; Shelton, J. R.; Schroeder, W. A.; Worosila, G.; Isied, S. S.; Bordignon, E.; Gray, H. B.; *Proc. Nat. Acad. Sci. USA* **1982**, *79*, 7052-7055. (b) Winkler, J. R.; Nocera, D. G.; Yocom, K. M.; Bordignon, E.; Gray, H. B. *J. Am. Chem. Soc.* **1982**, *104*, 5798-5800. (c) Yocom, K. M.; Winkler, J. R.; Nocera, D. G.; Bordignon, E.; Gray, H. B. *Chem. Scr.* **1983**, *21*, 29-33.

[5] (a) Axup, A. W.; Albin, M.; Mayo, S. L.; Crutchley, R. J.; Gray, H. B. *J. Am. Chem. Soc*, in press. (b) Lieber, C. M.; Karas, J. L.; Mayo, S. L.; Albin, M.; Gray, H. B. *Welch Conference Proceedings*, in press.

Chapter 1

A Structural Model of a Biomolecular Electron-Transfer Complex

The text of this chapter contains a paper co-authored with Bruce S. Brunschwig, Patricia J. DeLaive, Ann M. English, Michel Goldberg, Harry B. Gray and Norman Sutin, which appeared in *Inorganic Chemistry*. It is concerned with the kinetics and mechanism of electron transfer between blue copper proteins and electronically excited small, inorganic redox complexes. My contribution to this effort was the creation of a structural model of the interaction between plastocyanin and chromium tris-1,10-phenanthroline. Because of the poor reproduction of the paper's color figure, an appendix containing this figure is also included.

Reprinted from Inorganic Chemistry, 1985, 24, 3743

Contribution from the Chemistry Department, Brookhaven National Laboratory, Upton, New York 11973, and Contribution No. 7144 from the Arthur Amos Noyes Laboratory, California Institute of Technology, Pasadena, California 91125

Kinetics and Mechanisms of Electron Transfer between Blue Copper Proteins and Electronically Excited Chromium and Ruthenium Polypyridine Complexes

BRUCE S. BRUNSCHWIG,[1] PATRICIA J. DeLAIVE,[2] ANN M. ENGLISH,[2,3] MICHEL GOLDBERG,[2] HARRY B. GRAY,*[2] STEPHEN L. MAYO,[2] and NORMAN SUTIN*[1]

Received January 28, 1985

The kinetics of the quenching of the long-lived excited states of CrL_3^{3+} and RuL_3^{2+} complexes (L is 1,10-phenanthroline and 2,2'-bipyridine or substituted derivatives) by the copper proteins plastocyanin, azurin, and stellacyanin have been studied in aqueous solution. The rate constants for quenching by the Cu(I) proteins approach a limiting value of $\sim 10^6$ s^{-1} at high protein concentration. The kinetic behavior for plastocyanin is discussed in terms of a model in which the metal complex binds at a remote site 10–12 Å from the copper center. The model allows for electron transfer both from this remote site and by attack of the metal complex adjacent to the copper center. The results show that at low protein concentration the adjacent pathway is about 10 times faster than the remote pathway. The rate constant for the intramolecular electron transfer from the remote site is consistent with the value expected on the basis of theoretical calculations.

Introduction

The use of inorganic complexes to study the electron-transfer reactions of metalloproteins has been exploited in a number of laboratories.[4-7] In recent years increasing use has been made of electronically excited complexes.[8,9] The use of an oxidant (or reductant) that can be "instantaneously" generated by a laser pulse

(1) Brookhaven National Laboratory.
(2) California Institute of Technology.
(3) Present address: Department of Chemistry, Concordia University, Montreal, Quebec, Canada H3G 1M8.
(4) Sutin, N. *Nature (London)* **1961**, *190*, 438.

(5) (a) Wherland, S.; Gray, H. B. In "Biological Aspects of Inorganic Chemistry"; Addison, A. W., Cullen, W. R., Dolphin, D., James, B. R., Eds.; Wiley: New York, 1977; p 289, and references therein. (b) Cummins, D.; Gray, H. B. *J. Am. Chem. Soc.* **1977**, *99*, 5158. (c) McArdle, J. V.; Coyle, C. L.; Gray, H. B.; Yoneda, G. S.; Holwerda, R. A. *J. Am. Chem. Soc.* **1977**, *99*, 2483. (d) Holwerda, R. A.; Knaff, D. B.; Gray, H. B.; Clemmer, J. D.; Crowley, R.; Smith, J. M.; Mauk, A. G. *J. Am. Chem. Soc.* **1980**, *102*, 1142. (e) Mauk, A. G.; Scott, R. A.; Gray, H. B. *J. Am. Chem. Soc.* **1980**, *102*, 4360.

0020-1669/85/1324-3743$01.50/0

affords an opportunity for the study of reactions that are too fast to be observed with conventional mixing techniques. In addition, since the excited state can be a powerful oxidant or reductant, the electron-transfer kinetics can be studied under highly exergonic conditions. An early application[8,9] of this technique exploited the properties of tris(2,2'-bipyridine)ruthenium(II) ($Ru(bpy)_3^{2+}$), which is both a very good reductant ($E^\circ = -0.84$ V) and a moderately strong oxidant ($E^\circ = +0.84$ V) in its excited state. Additional studies with the ruthenium(II) complex, as well as with tris(1,10-phenanthroline)chromium(III) ($Cr(phen)_3^{3+}$), which is a very strong oxidant in its excited state ($E^\circ = +1.42$ V),[10] and with other CrL_3^{3+} complexes are described here.

Discussions of the kinetics of reactions between oxidation–reduction metalloproteins and inorganic redox agents often have centered on the role played by encounter or precursor complexes formed from the separated reactants.[5,6] Some studies suggest that the associative interaction between the protein (e.g., blue copper proteins, iron sulfur proteins, *c*-type cytochromes) and its redox partner is quite strong, with association constants up to 10^4 M^{-1}.[6] On the other hand, the results of the other studies[5] can be analyzed in terms of a bimolecular model requiring nothing more than a weak binding and reasonably close approach of the inorganic redox agent to the protein redox site.

The blue copper proteins plastocyanin, azurin, and stellacyanin studied in this work contain one copper atom per molecule. Plastocyanin and azurin function in the electron-transport chain of biological organisms.[11] The function of stellacyanin is unknown. In their oxidized (Cu(II)) state the copper proteins have an intense absorption in the visible region (~600 nm) and are colorless when the copper center is reduced (Cu(I)). The crystal structures of plastocyanin[12] (*Populus nigra, var. italacia*) and *Pseudomonas* azurin[13] have been determined and their molecular structures compared.[14] In general the copper atom is located at one end of the protein in a hydrophobic pocket formed by three loops in the polypeptide backbone. The residues near the pocket are highly evolutionarily conserved.[14] The copper is coordinated by two nitrogens (histidines) and two sulfurs (methionine and cysteine). The copper(II)–ligand bond lengths are ~2.1 Å except for Cu–S(Met), which is 2.9 Å.[15] The Cu(I) bond lengths for plastocyanin determined by X-ray crystallography depend on the pH of the solution from which the crystals were prepared. The variations in distance are interpreted as indicating two forms of the Cu(I) protein. The form that is assumed to be redox active has copper–nitrogen bond distances that are ~0.1 Å longer for the Cu(I) than for the Cu(II) protein. The low-pH (redox-inactive) form of the Cu(I) protein has one long copper–nitrogen bond (3.2 Å) and a short copper–sulfur bond (~2.5 Å).[15] Plastocyanin has a negative, acidic patch and a hydrophobic region on one side of the protein that is conserved and located 10–15 Å from the Cu atom. Azurin has no similar negative patch, but the same region has a conserved hydrophobic region.[15]

The tyrosine-83 region of plastocyanin has been shown to be a binding site for $Cr(phen)_3^{3+}$,[16,17] and a purpose of the present study was to determine whether this binding site opens up a pathway for (long-range) electron transfer from the excited phenanthroline or bipyridine complexes to the copper center, as has been proposed for the analogous $Co(phen)_3^{3+}$ reaction.[16] This pathway will be called the remote pathway in order to distinguish it from the adjacent pathway, which involves "direct" electron transfer at the copper site.

Experimental Section

Preparation and Purification of Materials. Plastocyanin (*Phaseolus vulgaris*) was isolated from the leaves of 6-week-old French bean plants and purified (absorbance ratio $A_{278}/A_{597} = 1.0$) by methods described by Milne and Wells;[18] azurin (*Pseudomonas aeruginosa*) was purified ($A_{280}/A_{625} = 1.9$) from the acetone extract by the method of Ambler,[19] and Japanese lacquer tree (*Rhus vernicifera*) stellacyanin was isolated ($A_{280}/A_{604} = 5.8$) from the acetone extract by the method of Reinhammar.[20] *Commercial tris(2,2'-bipyridine)ruthenium(II) chloride* was used as received from G. Frederick Smith Chemical Co. Tris(1,10-phenanthroline)chromium(III) perchlorate, tris(5-chloro-1,10-phenanthroline)chromium(III) perchlorate, and tris(4,7-dimethyl-1,10-phenanthroline)chromium(III) perchlorate were prepared according to literature methods.[21]

Preparation of Samples. All protein experiments were performed with use of phosphate buffer at pH 7.0 (Na_2HPO_4, 27 mM; NaH_2PO_4, 20 mM) and an ionic strength of 0.1 M in deionized water (conductivity $<7 \times 10^{-6}$ cm Ω^{-1}). The blue copper proteins were reduced by either of two methods; chemical reduction by sodium ascorbate followed by a 4-h dialysis against phosphate buffer to ensure that little or no excess ascorbate or dehydroascorbate was present in the final solutions or hydrogen reduction over platinum metal. These two procedures were performed under nitrogen or argon flushing to prevent air oxidation of the proteins. Stock solutions of the inorganic reagent were deaerated by nitrogen (or argon) flushing for at least 30 min prior to sample preparation in an anaerobic environment.

Spectral Measurements. All absorption spectra were recorded on a *Cary 219 UV–visible recording spectrophotometer. Concentrations of* the proteins in the final solutions were determined spectrophotochemically with use of the following data: plastocyanin $\lambda_{max} = 597$ nm ($\epsilon = 4500$ M^{-1} cm^{-1}),[18] azurin $\lambda_{max} = 625$ nm ($\epsilon = 5700$ M^{-1} cm^{-1}),[6c] and stellacyanin $\lambda_{max} = 604$ nm ($\epsilon = 4080$ M^{-1} cm^{-1}).[20] Emission spectra were recorded on a Perkin-Elmer Hitachi MPF-4 spectrofluorimeter.

Photochemical Experiments. The transient emission and absorption measurements were made with either a Phase-R D-1100 dye laser system (fwhm 0.5 μs) or Quanta Ray DC-R Nd:YAG (fwhm 8 ns) laser. In the former case the active dye was coumarin 440 with an output at ~440 nm. For absorption measurements the probe beam source (positioned at 90° to the laser beam) was a 150-W tungsten–halogen lamp filtered to remove light at wavelengths shorter than the monitoring wavelength. The probe beam (or the emission) passed through a Jarrell-Ash monochromator and was detected by a photomultiplier tube and preamplifier. The signal from the preamplifier was digitized and stored in a Biomation 8100 transient recorder. The data were then transferred to a PDP-11/23 computer, where the 2000 data points were averaged in sets of 10 (converted to change in absorbance when necessary) and fit by a nonlinear least-squares fitting routine to a first-order decay. For the Nd laser the emission was detected by a photomultiplier tube and digitized by a Biomation 6500. Thirty to sixty curves were summed to get the decay curve that was then analyzed on a MINC-11/03 computer. The measurements were performed at room temperature unless otherwise noted. The $Cr(phen)_3^{3+}$ emission was monitored at 730 nm and excited either at 440 nm or with the third harmonic of the Nd laser (353 nm). The $Ru(bpy)_3^{2+}$ was excited with the second harmonic of the Nd laser (532 nm) and the emission observed at 610 nm. The metal complex concentration was 2.5×10^{-5} M for $Ru(bpy)_3^{2+}$ and 3×10^{-5} M for $Cr(phen)_3^{3+}$; the protein concentration was varied from zero to 5×10^{-3} M.

The intensity of the emission from the polypyridine chromium(III) complexes was also measured as a function of protein concentration ($<10^{-4}$ M) on a spectrofluorimeter. Solutions of the protein and the chromium complex were excited at 350 nm, and the emission was monitored at the emission maximum of the complex (720–730 nm). Plots

(6) (a) Segal, M. G.; Sykes, A. G. *J. Chem. Soc., Chem. Commun.* **1977**, 764. (b) Segal, M. G.; Sykes, A. G. *J. Am. Chem. Soc.* **1978**, *100*, 4585. (c) Chapman, S. K.; Davies, D. M.; Watson, A. D.; Sykes, A. G. *ACS Symp. Ser.* **1983**, *No. 211*, 177. (d) Armstrong, F. A.; Henderson, R. A.; Sykes, A. G. *J. Am. Chem. Soc.* **1980**, *102*, 6545. (e) Goldberg, M.; Pecht, I. *Biochemistry* **1976**, *15*, 4197.
(7) Morton, R. A.; Overnell, J.; Harbury, H. A. *J. Biol. Chem.* **1970**, *245*, 4653.
(8) Sutin, N. *Adv. Chem. Ser.* **1977**, *No. 162*, 156.
(9) English, A. M.; Lum, V. R.; DeLaive, P. J.; Gray, H. B. *J. Am. Chem. Soc.* **1982**, *104*, 870.
(10) Sutin, N. *J. Photochem.* **1979**, *10*, 19.
(11) Fee, J. A. *Struct. Bonding (Berlin)* **1975**, *23*, 1.
(12) Coleman, P. M.; Freeman, H. C.; Guss, J. M.; Murata, M.; Norris, V. A.; Ramshaw, J. A. M.; Venkatappa, M. P. *Nature (London)* **1978**, *272*, 319.
(13) Adman, E. T.; Jensen, L. H. *Isr. J. Chem.* **1981**, *21*, 8.
(14) Norris, G. E.; Anderson, B. F.; Baker, E. N.; Rumball, S. V. *J. Mol. Biol.* **1979**, *125*, 309.
(15) Freeman, H. C. *Proc. Int. Conf. Coord. Chem.* **1980**, *21*, 29.
(16) Handford, P. M.; Hill, H. A. O.; Lee, R. W.-K.; Henderson, R. A.; Sykes, A. G. *J. Inorg. Biochem.* **1980**, *13*, 83.
(17) Cookson, D. J.; Hayes, M. T.; Wright, P. E. *Biochim. Biophys. Acta* **1980**, *591*, 162. Cookson, D. J.; Hayes, M. T.; Wright, P. E. *Nature (London)* **1980**, 283, 682.
(18) Milne, P. R.; Wells, J. R. E. *J. Biol. Chem.* **1970**, *245*, 1566.
(19) Ambler, R. P.; Brown, L. M. *Biochem. J.* **1967**, *104*, 784.
(20) Reinhammar, B. *Biochim. Biophys. Acta* **1970**, *205*, 35. Malmström, B. G.; Reinhammar, B.; Vänngard, T. *Biochim. Biophys. Acta* **1970**, *205*, 48.
(21) Brunschwig, B. S.; Sutin, N. *J. Am. Chem. Soc.* **1978**, *100*, 7568.

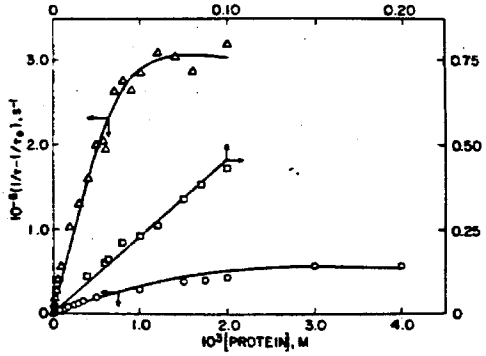

Figure 1. Plot of $1/\tau - 1/\tau_0$ vs. protein concentration for the reaction of reduced plastocyanin (Δ), azurin (□), and stellacyanin (○) with the excited state of $Cr(phen)_3^{3+}$ at pH 7.0, 0.1 M ionic strength, and 25 °C.

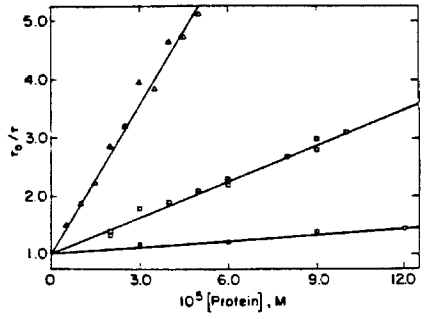

Figure 2. Plot of τ_0/τ vs. protein concentration for the reaction of oxidized plastocyanin (Δ), azurin (□), and stellacyanin (○) with the excited state of $Cr(phen)_3^{3+}$ at pH 7.0, 0.1 M ionic strength, and 25 °C.

Table I. Rate Constants for Reaction of the Oxidized Blue Copper Proteins with $*Cr(phen)_3^{3+}$, $Cr(phen)_3^{2+}$, and $*Ru(bpy)_3^{2+}$ at pH 7.0, 0.1 M Ionic Strength, and 25 °C

protein	sensitizer	$\Delta E°$, V	$10^{-8}k_q$, M^{-1} s^{-1}
plastocyanin(II)	$*Cr(phen)_3^{3+}$		6.0
	$Cr(phen)_3^{2+}$	0.64	23
	$*Ru(bpy)_3^{2+}$	1.20	42
azurin(II)	$*Cr(phen)_3^{3+}$		1.0
	$*Ru(bpy)_3^{2+}$	1.14	12
stellacyanin(II)	$*Cr(phen)_3^{3+}$		0.49
	$*Ru(bpy)_3^{2+}$	1.03	13

of I_0/I vs. protein concentration gave values of $k_q\tau_0$, where k_q is the quenching rate constant and τ_0 is the lifetime of the excited state in the absence of the metalloprotein.

Results

Quenching of the CrL_3^{3+} Excited State. Rate parameters ($1/\tau$) for quenching of the $Cr(phen)_3^{3+}$ emission by plastocyanin, azurin, and stellacyanin are presented in Supplementary Tables 1–3 and are plotted vs. protein concentration in Figure 1 ($1/\tau - 1/\tau_0$) for the reduced metalloproteins and in Figure 2 (τ_0/τ) for the oxidized metalloproteins. The quenching at low protein concentration was also studied by steady-state emission methods with similar results. The plots for the quenching by the reduced protein (Figure 1) were all similar with a "normal" region at low protein concentration, where $1/\tau - 1/\tau_0$ is proportional to the protein concentration, and a "plateau" region at higher concentration, where $1/\tau - 1/\tau_0$ is independent of protein concentration.[22] The Stern–Volmer plots for the quenching by the oxidized protein were all normal, with no departure from linearity up to 0.1 mM protein. The quenching rate constants are given in Table I. The effect of driving force on the rate constant for the quenching of the chromium(III) excited state by reduced azurin was studied by use of $Cr(5\text{-}Clphen)_3^{3+}$ ($E° = +1.53$ V)[21] or $Cr(4,7\text{-}(CH_3)_2phen)_3^{3+}$ ($E° = +1.23$ V)[21] instead of $Cr(phen)_3^{3+}$. The rate constants for these reactions agreed to within 10% with those found with $Cr(phen)_3^{3+}$.

The spectrum of a solution containing $Cr(phen)_3^{3+}$ and reduced plastocyanin, measured ~1 μs after the laser flash at high protein concentration, revealed approximately uniform bleaching from 500 to 700 nm. This is expected for production of Cu(II) protein and $Cr(phen)_3^{2+}$.[23] The rate constant for the back-reaction between the oxidized metalloprotein and $Cr(phen)_3^{2+}$ is 2.3×10^9 M^{-1} s^{-1} and is independent of monitoring wavelengths between 500 and 650 nm. The second-order fit of the bleaching at 597 nm is shown in Figure 3.

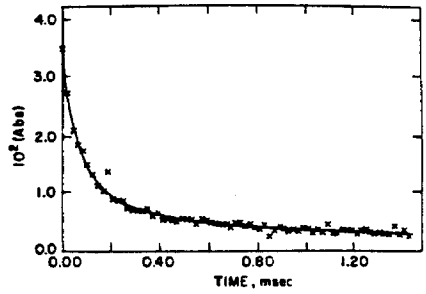

Figure 3. Decay of the transient absorption at 597 nm in a solution of reduced plastocyanin (2×10^{-3} M) and $Cr(phen)_3^{3+}$ (5×10^{-4} M). The solid line is the fit of the data points (×) to a second-order plot (pH 7.0, 0.1 M ionic strength, and 25 °C).

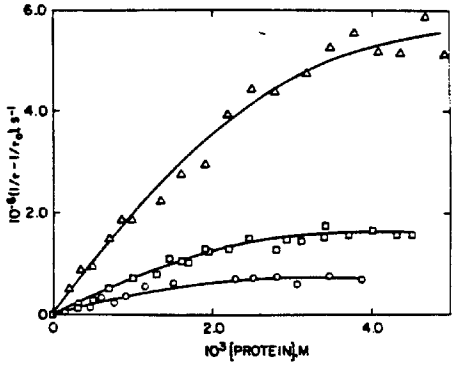

Figure 4. Plot of $1/\tau - 1/\tau_0$ vs. protein concentration for the reaction of reduced plastocyanin (Δ), azurin (□), and stellacyanin (○) with the excited state of $Ru(bpy)_3^{2+}$ at pH 7.0, 0.1 M ionic strength, and 25 °C.

Quenching of the $Ru(bpy)_3^{2+}$ Excited State. The $1/\tau - 1/\tau_0$ vs. protein concentration plots for the quenching of the $Ru(bpy)_3^{2+}$ emission by the three reduced copper proteins are shown in Figure 4. The plots are qualitatively similar to those for quenching of $Cr(phen)_3^{3+}$ emission and show a linear region at low metalloprotein concentrations and a plateau at higher concentrations. The results at low protein concentrations were reported previously.[9] The absorption spectra taken 5.0–160 μs after the laser flash for a solution of $Ru(bpy)_3^{2+}$ and reduced plastocyanin show the ab-

(22) (a) The data for azurin(I) quenching of the $Cr(phen)_3^{3+}$ excited state do not show limiting behavior for [Az(I)] ≤ 0.1 mM; however, data under slightly different conditions show the plateau region beginning at [Az(I)] ≈ 2 mM.[22b] Therefore, all the data for quenching by the reduced protein were treated in the same manner. (b) English, A.; DeLaive, P.; Gray, H. B., unpublished results.

(23) (a) The production of equal concentrations of $Cr(phen)_3^{2+}$ and Cu(II) plastocyanin would produce a fairly uniform change in absorbance in the region monitored since $Cr(phen)_3^{2+}$ has an absorption maximum at 700 nm ($\epsilon \approx 2500$ M^{-1} cm^{-1}).[23b] (b) Serpone, N.; Jamieson, M. A.; Emmi, S. S.; Fouchi, P. G.; Mulazzani, Q. G.; Hoffman, M. Z. *J. Am. Chem. Soc.* **1981**, *103*, 1091.

Table II. Quenching of $^*Cr(phen)_3^{3+}$ and $^*Ru(bpy)_3^{2+}$ Emission by Blue Copper(I) Proteins at 22 °C

protein	complex	$-\Delta G°$,[a] V	$10^{-9}(k_1$ or $k_4)$,[b] M^{-1} s^{-1}	K_1, M^{-1}	$10^{-6}k_2$, s^{-1}	$10^{-3}K_3$, M^{-1}	k_{adj}/k_{rem}[c]
plastocyanin(I)	CrL_3^{3+}	1.06	3.5	250	2.5	4.2	7
plastocyanin(I)	RuL_3^{2+}	0.48	1.9	100	3.0	0.2	7
azurin(I)	CrL_3^{3+}	1.11	0.40	60	1.2[d]		7
azurin(I)	RuL_3^{2+}	0.53	0.65	40	1.2	2.3	14
stellacyanin(I)	CrL_3^{3+}	1.23	0.35	60	0.20	1.3	30
stellacyanin(I)	RuL_3^{2+}	0.65	0.40	40	0.20	1.4	51

[a] References 10, 21, and 37a. [b] The rate constants were calculated by fitting the data to eq 1 with $k_1 = k_4$ and K_1 ($=k_1/k_{-1}$) equal to the values given in the table. [c] The ratio of the adjacent to remote paths at low protein concentration calculated from $k_4(k_{-1} + k_2)/k_1k_2$. [d] Calculated from the initial slope of $1/\tau$ vs. protein concentration with the values of the other parameters given in the table.

Scheme I

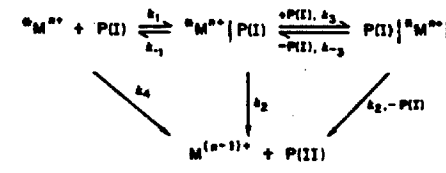

sorbance changes expected for electron-transfer products. The spectrum shows a bleach at 430–450 nm due to the loss of $Ru(bpy)_3^{2+}$ and absorbance increases at 470–530 and 550–700 nm due to the formation of $Ru(bpy)_3^{+}$ and oxidized plastocyanin.[18,24]

The quenching of the $Ru(bpy)_3^{2+}$ emission by the oxidized copper proteins gave normal τ_0/τ plots up to 5 mM protein. No indication of rate saturation was observed. The quenching rate constants are included in Table I. Control experiments showed that the $Ru(bpy)_3^{2+}$ emission was not quenched by the apoproteins.

Discussion

It is necessary to consider energy-transfer as well as electron-transfer pathways for the quenching of the excited states of the metal complexes. Oxidation of the copper(II) proteins by the excited state of $Cr(phen)_3^{3+}$ is thermodynamically unfavorable; however, there is significant overlap between the proteins' absorption spectra and the chromium(III) emission and the observed quenching very probably proceeds by an energy-transfer pathway. By contrast, the quenching of the emission of the excited chromium(III) and ruthenium(II) complexes by the reduced metalloprotein can be ascribed to an electron-transfer mechanism since the transient spectra identify the reduced complex and the oxidized protein as the quenching products. An energy-transfer mechanism is not likely for these systems because there is no overlap between the absorption spectrum of the reduced protein (the reduced protein has no absorption between 400 and 800 nm) and the emission of the excited metal complex ($Cr(phen)_3^{3+}$, $\lambda_{em} = 727$ nm; $Ru(bpy)_3^{2+}$, $\lambda_{em} = 607$ nm).

We next consider adjacent and remote pathways for the electron-transfer quenching. These are shown in Scheme I, which also includes a 2:1 complex that may be formed at high protein concentrations. In this scheme $^*M^{n+}|P(I)$ is a complex in which the excited inorganic complex $^*M^{n+}$ is bound at a remote site from the copper. The formation constant of the 1:1 complex is K_1 ($=k_1/k_{-1}$), the formation constant of the 2:1 complex (formed between two reduced protein molecules and the inorganic complex) is K_3 ($=k_3/k_{-3}$), k_2 is the intramolecular (remote) electron-transfer rate constant, and k_4 is the bimolecular electron-transfer rate constant for adjacent attack, that is, for the pathway that involves close approach of $^*M^{n+}$ to the copper(I) site. We assume that the ground and excited states of the inorganic complex bind with the same equilibrium constant to the metalloprotein and that the bound inorganic complexes have the same intrinsic lifetimes (τ_0) as the free complexes. The various equilibria between the proteins and the ground-state metal complexes are established prior to the laser flash. These equilibria are, of course, still maintained immediately after the excitation of the metal complex.

The above kinetic scheme is intrinsically multiphasic. In order to simplify the resulting kinetic expressions, we assume that the 2:1 complex is in equilibrium with the 1:1 complex. Under these conditions the differential equations for the above scheme can be solved to yield two (first-order) rate constants given by[25]

$$\theta_{1(2)} = \frac{S_1 + S_2}{2} + (-)\left[\frac{(S_1 - S_2)^2}{4} + \frac{k_1k_{-1}}{1 + K_3[P(I)]}\right]^{1/2} \quad (1)$$

where $\theta = 1/\tau - 1/\tau_0$, $S_1 = (k_1 + k_4)[P(I)]$, and $S_2 = k_2 + k_{-1}/(1 + K_3[P(I)])$. Trial values of the various parameters indicate that the negative root (θ_2) is the appropriate one under the conditions used. The low- and high-[protein] limits of this root are of interest: in the low-[protein] limit the value of θ_2 is given by

$$\theta_2 = k_4[P(I)] + \frac{k_1k_2[P(I)]}{k_{-1} + k_2} \quad (2)$$

and the quenching rate constant is directly proportional to the protein concentration. At high protein concentrations θ_2 is given by

$$\theta_2 = k_2 \quad (3)$$

and the rate constant is independent of protein concentration. In the intermediate region the rates have a complex dependence on protein concentration.

The first term on the right-hand side of eq 2 is the rate constant for adjacent attack while the second term is the effective rate constant for the remote electron-transfer pathway. If $k_4 \gg k_1k_2/(k_{-1} + k_2)$, then the adjacent-attack pathway predominates with the remote pathway being relatively slow.[26] On the other hand, if $k_1k_2/(k_{-1} + k_2) \gg k_4$, then the remote electron-transfer path predominates. At high protein concentration only the remote pathway is available for reaction (eq 3).

Not all five constants (k_1, K_1, k_2, K_3, and k_4) can be calculated from the four parameters in eq 1 without introducing additional assumptions. Unconstrained fits of the data indicated that k_4 is very large, and we shall assume that $k_4 = k_1$: this assumption seems reasonable since k_1 is a rate constant for diffusion and, because of the large driving force for the electron transfer and the high probability of electron transfer at the adjacent site, it is likely that k_4 is also diffusion controlled. In addition, we assume that K_1 is equal to 250 and 100 M^{-1} for the association of reduced plastocyanin with $Cr(phen)_3^{3+}$ and $Ru(bpy)_3^{2+}$, respectively, and

(24) Creutz, C.; Sutin, N. *J. Am. Chem. Soc.* **1976**, *98*, 6384.

(25) Bamford, C. H.; Tipper, C. F. H. "Comprehensive Chemical Kinetics"; Elsevier: New York, 1969; Vol. 2, p 31. Rybak, W.; Haim, A.; Netzel, T. L.; Sutin, N. *J. Phys. Chem.* **1981**, *85*, 2856.

(26) The limiting form of this case is the so-called "dead-end" mechanism. In fact, it may be advantageous to refer to it as an unproductive binding mechanism. Because the protein is present in excess, "dead-end" refers to the activity of the oxidant, not of the protein. It would be erroneous to assume that this mechanism necessarily means that $Cr(phen)_3^{3+}$ or $Ru(bpy)_3^{2+}$ inactivates the protein redox site. Nor does it imply photophysical or chemical inactivation of the redox agent by the protein. We only postulate that in this mechanism the oxidant enters a cul-de-sac; i.e., it is bound at a site sufficiently remote from the Cu center so that intramolecular electron transfer is slower than that along an alternative (bimolecular) pathway, which presumably involves encounter of $^*M^{n+}$ very near the copper center (adjacent attack). At high protein concentrations, under saturation conditions, all the $^*Cr(phen)_3^{3+}$ or $^*Ru(bpy)_3^{2+}$ is bound at the remote site. Provided that the intramolecular electron-transfer rate is significantly slower than the effective dissociation rate, reaction takes place only when the oxidant dissociates from the remote site and then follows the fast bimolecular pathway.

to 40–60 M^{-1} for the other systems. The value assumed for the association constant for reduced plastocyanin with $Cr(phen)_3^{3+}$, while slightly larger than the value reported by Sykes et al.,[27] is more consistent with the present data.[28a] The larger values of K_1 for the plastocyanin reaction are consistent with the more negative charge on reduced plastocyanin (−10)[5d,29] compared with those on azurin (−2)[5d] and stellacyanin (0).[5d] These values are also consistent with the results of kinetic and binding studies that are described below.[6a,b,16,27,29]

The values of k_1, K_1, k_2, K_3, and k_4 for the $Cr(phen)_3^{3+}$ and $Ru(bpy)_3^{2+}$ data determined for Scheme I subject to the above constraints are given in Table II. The curves calculated with these constants are shown in Figures 1 and 2. The values of the quenching rate constants in the low-[protein] limit (eq 2) calculated by using the constants in Table II are within 25% of their measured values. The value of K_3 is very sensitive to the curvature in the $1/\tau - 1/\tau_0$ vs. protein concentration plots, and because of the scatter in the high-[protein] data, K_3 is the least well-determined parameter. The k_1 values seem consistent with diffusion-controlled rates when the steric factors for the reaction are considered. The larger values of k_1 for the plastocyanin reactions are expected on the basis of the larger charge products for these reactions (−30 and −20 for the $Cr(phen)_3^{3+}$ and $Ru(bpy)_3^{2+}$ reactions, respectively, compared with −6 and −4 for the azurin and zero for the stellacyanin reactions).[5d,29] Moreover, the k_1 value of 2×10^9 M^{-1} s^{-1} for the reaction of $^*Ru(bpy)_3^{2+}$ with reduced plastocyanin is in excellent agreement with the value directly measured for the reaction of $Cr(phen)_3^{2+}$ with the oxidized protein (the reactants have similar charge products). Although the k_2 values are large, at low protein concentration the remote electron-transfer path is about 1 order of magnitude slower than the adjacent path, i.e., $k_1k_2/(k_{-1} + k_2) < k_4$ for the systems studied (Table II); this is a consequence of the fact that k_4 is comparable to k_1 while $k_2 \ll k_{-1}$.

The association of a second protein molecule renders more abrupt the transition from a roughly linear concentration dependence of the quenching lifetime to an almost concentration-independent region. Saturation is accelerated because the effective dissociation rate constant of the 1:1 complex is lowered by the binding of the additional protein molecule, $k'_{-1} = k_{-1}/(1 + K_3[P(I)])$. Note that a rate effect is only observed because the formation of a dimeric species is affected by the presence of the bound oxidant. If a protein dimer were formed in the absence of a redox partner, but with the same equilibrium constant (K_3), there would be no modulation effect. We conclude that the oxidant is somehow "sandwiched" between two protein molecules. It is also worth noting that the association of the second P(I) exhibits positive cooperativity for all proteins ($K_3 > K_1$).

Sykes et al.[6a,b,16,27] have reported kinetics for the oxidation of reduced plastocyanin and azurin by $Co(phen)_3^{3+}$. Their plots of the observed first-order rate constant vs. cobalt(III) concentration at pH 7.5 exhibit slight downward curvature for plastocyanin but none for azurin. They interpret this curvature in terms of complex formation at the remote site and derive $K_1 = 170$ and ≤ 40 M^{-1} for plastocyanin and azurin, respectively (ionic strength 0.1 M, pH 7.5).[28a] They also studied[27] the $Cr(phen)_3^{3+}$ inhibition of the $Co(phen)_3^{3+}$ oxidation of reduced plastocyanin and found $K_1 \approx 180$ M^{-1} for binding of the chromium(III) complex at pH 7.5. NMR studies clearly show that $Cr(phen)_3^{3+}$ binds to plastocyanin at or near Tyr-83, which is in the vicinity of the negative patch formed by the carboxylate groups of residues 42–45 (and residues 51 and 59).[16,17] This region is 10–15 Å from the copper site. Because $Co(phen)_3^{3+}$ is structurally very similar to $Cr(phen)_3^{3+}$ and because its reaction with reduced plastocyanin is blocked by the latter, $Co(phen)_3^{3+}$ almost certainly binds at the same site. This is consistent with the exothermic character of the precursor-complex formation ($\Delta H^\circ \simeq 10$ kcal mol^{-1}),[6b] which indicates that electrostatic factors dominate the interaction of $Co(phen)_3^{3+}$ with the reduced plastocyanin. It is also proposed that $Ru(bpy)_3^{2+}$ binds in the region of Tyr-83. Its association constant, though not known exactly, is certainly smaller than that for the phenanthroline complexes. Moreover, the oxidation of reduced plastocyanin by $Co(phen)_3^{3+}$ is inhibited by $Co(NH_3)_6^{3+}$, $Pt(NH_3)_6^{4+}$, and $(Co(NH_3)_5)_2NH_2^{5+}$, suggesting that all these complexes associate in the same region.[6c] Further support for the above interpretation is provided by the k_2 values. Since the magnitude of k_2 is governed primarily by the distance from the copper center to the binding site (see below), the similarity in the k_2 values for $Cr(phen)_3^{3+}$ and $Ru(bpy)_3^{2+}$ would indicate that both metal complexes bind at similar positions for a given protein.

The association constants of reduced plastocyanin with $Co(NH_3)_6^{3+}$, $Pt(NH_3)_6^{4+}$, and $(Co(NH_3)_5)_2NH_2^{5+}$ are large.[6c] However, the rate decreases observed even at high inhibitor concentration are only about twofold. The fact that the blocking is only partial suggests that more than one pathway is effective in the $Co(phen)_3^{3+}$ oxidation. The blocking agent can totally inhibit only the remote pathway by binding to the protein: the adjacent pathway can operate even when the blocking agent is present provided that the binding is at the remote site. The ratios of rate constants for the adjacent and remote pathways are significantly different for the $Co(phen)_3^{3+}$ and $^*Cr(phen)_3^{3+}$ oxidations, ≤ 1 and ~ 7, respectively. For the $Co(phen)_3^{3+}$ reaction neither pathway has a rate constant close to the diffusion limit and the rate ratio reflects the relative association constants at the adjacent and remote sites, as well as the rate difference arising from the difference in distance between the metal complex and the copper center for the two paths. On the other hand, for the $Cr(phen)_3^{3+}$ reaction the adjacent pathway is diffusion-controlled and the rate ratio reflects only the relative magnitudes of k_{-1} and k_2.[28b]

Table III. Distances in the Computer-Generated Complex Formed between Plastocyanin and $Cr(phen)_3^{3+}$

	dist, Å
cysteine-84 S to nearest phen C	10.3
Cu center to nearest phen C	12.7
Cu to Cr	18.4
tyrosine-83 *o*-C to Cr	8.0, 8.7
tyrosine-83 *m*-C to Cr	9.4, 10.0
valine-40 Me C to Cr	8.5, 11.5

Binding Site for $Cr(phen)_3^{3+}$. As discussed in the Introduction, NMR studies of reduced plastocyanin have shown that the proton resonances of tyrosine-83 (as well as the methyl group resonances of an aliphatic side chain, possibly valine-40) are broadened by added $Cr(phen)_3^{3+}$. The former residue affords a particularly attractive binding site because of the possibility of hydrophobic interactions between the phenyl ring of the tyrosine-83 and a phenanthroline ring of the chromium complex.[30] In order to further examine this possibility, computer simulations of the docking of $Cr(phen)_3^{3+}$ with the tyrosine region of plastocyanin were performed.[31] The best-fit docked complex, obtained by

(27) Lappin, A. G.; Segal, M. G.; Weatherburn, D. C.; Henderson, R. A.; Sykes, A. G. *J. Am. Chem. Soc.* **1979**, *101*, 2302. Lappin, A. G.; Segal, M. G.; Weatherburn, D. C.; Sykes, A. G. *J. Am. Chem. Soc.* **1979**, *101*, 2297.

(28) (a) It should be recognized that parallel adjacent and remote pathways may also operate in the $Co(phen)_3^{3+}$ reaction. A least-squares analysis of the published data[6] in terms of the corresponding rate law gave an excellent fit with the $K_1 = 220 \pm 40$ M^{-1}. (b) For the $Co(phen)_3^{3+}$ oxidation $k_{adj}/k_{rem} \approx (K_{adj}/K_{rem}) \exp(-\beta(d_{adj} - d_{rem}))$, where we assume that ΔG° is the same for the two pathways, $K_{rem} = K_1$, and K_{adj} is the association constant for the adjacent pathway. For the $^*Cr(phen)_3^{3+}$ oxidation $k_{adj}/k_{rem} \approx 1 + k_{-1}/k_2$; see eq 4.

(29) Augustin, M. A.; Chapman, S. K.; Davies, D. M.; Watson, A. D.; Sykes, A. G. *J. Inorg. Biochem.* **1984**, *20*, 281.

(30) (a) Farver and Pecht have presented evidence that Cr^{2+} binds to oxidized plastocyanin at a residue near Tyr-83 prior to electron transfer.[30b] (b) Farver, O.; Pecht, I. *Proc. Natl. Acad. Sci. U.S.A.* **1981**, *78*, 4190.

(31) (a) Computer graphics were done with the program BIOGRAF/1 (written by S. L. Mayo, B. D. Olafson, and W. A. Goddard, III) and a VAX 11/780-supported Evans and Sutherland PS300 interactive graphics terminal. The metal complex used as a structural model was $Co(phen)_3^{3+}$ (Niederhoffer, E. C.; Martell, A. E.; Rudolf, P.; Clearfield, A. *Cryst. Struct. Commun.* **1982**, *11*, 1951). (b) The surfaces of the protein and of the metal complex were calculated by using the program MS: Connolly, M. *Quant. Chem. Program Exchange Bull.* **1981**, *1*, 75.

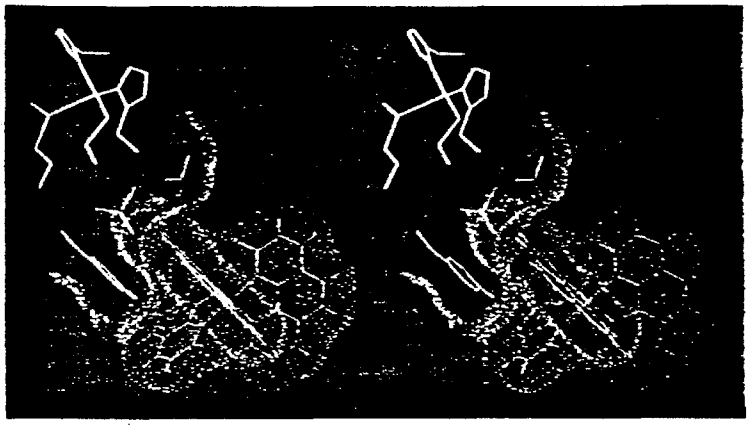

FIG 5

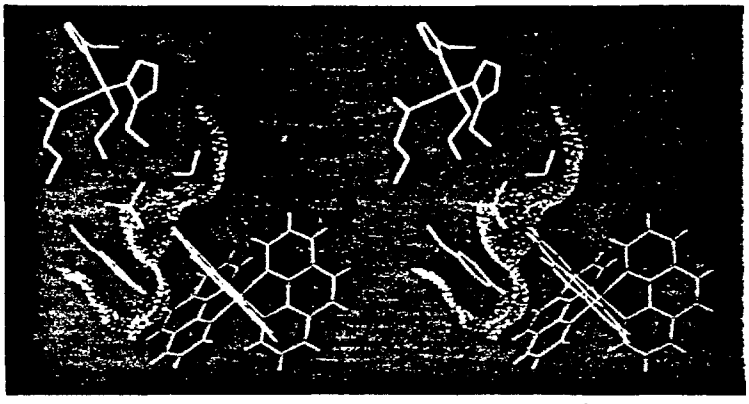

Figure 5. Computer-generated stereoviews of the complex formed between plastocyanin and $Cr(phen)_3^{3+}$. The lower view shows the copper atom with its four ligands (light blue), three nearby residues, valine-40, serine-85, tyrosine-83 (green), the docked $Cr(phen)_3^{3+}$ (orange), and the solvent-accessible surface (blue) of the atoms near tyrosine-83. The upper view also shows the van der Waals surface of $Cr(phen)_3^{3+}$ (orange).

rotation of the phenyl ring of the tyrosine, is shown in Figure 5. It is evident that very good overlap between the phenyl ring and a phenanthroline ligand of the complex can be achieved. Various distances determined from the computer-generated complex are presented in Table III. The closest lead-in atom to the copper site is the coordinated sulfur of cysteine-84. The distance from this sulfur atom to the nearest phenanthroline carbon of the bound $Cr(phen)_3^{3+}$ complex is 10.3 Å. This is the edge-to-edge electron-transfer distance for the remote pathway, and its implications for the electron-transfer rate are discussed next.

Rate Constant for the Remote Pathway. When nuclear tunneling can be neglected, the first-order rate constant for electron transfer can be expressed as

$$k_{el} = \kappa_{el}\nu_n \exp[-(\lambda + \Delta G^\circ)^2/4\lambda RT] \qquad (4)$$

where κ_{el} is the electronic transmission coefficient, ν_n is the effective nuclear vibration frequency that destroys the activated complex configuration, λ is the vertical reorganization energy, and ΔG° is the free energy change for the reaction.[32-36] When the electronic coupling of the two redox sites is relatively strong, the electron transfer will be adiabatic: for such systems $\kappa_{el} \approx 1$ and $\nu_n \approx 10^{13}$ s^{-1}.[32,35,36] On the other hand, if the two redox sites are relatively far apart, as is the case for the remote pathway, then the coupling between the redox sites will be weak and the electron transfer will be nonadiabatic. The product $\kappa_{el}\nu_n$ is then independent of the frequency for nuclear motion and is given by[32-36]

$$\kappa_{el}\nu_n = 10^{13} \exp(-\beta d)\ s^{-1} \qquad (5)$$

where d is the electron-transfer distance defined so that $\kappa_{el}\nu_n$ is equal to some nuclear vibration frequency, typically 10^{13} s^{-1}, when $d = 0$; i.e., the reaction is adiabatic when $d = 0$. The measured rate constants for the reactions of a reduced protein with $*Cr(phen)_3^{3+}$ or $*Ru(bpy)_3^{2+}$ have similar values despite the different driving forces for the reactions. This suggests that these reactions are essentially barrierless. In the barrierless regime $\lambda + \Delta G^\circ \approx 0$ so that $\lambda \approx 0.9$ eV[37] for the cross-reactions of the proteins. The vertical reorganization energies for the cross-reactions are given by $\lambda = (\lambda_{11} + \lambda_{22})/2$, where λ_{11} and λ_{22} are the vertical reorganization energies for the self-exchange reactions of the $*Cr(phen)_3^{3+/2+}$ (or $*Ru(bpy)_3^{2+/+}$) and protein(II/I) couples, respectively. The value of λ_{11} for $*Cr(phen)_3^{3+/2+}$ is 22 kcal mol^{-1}.[38] This yields a vertical reorganization energy for the proteins of ~20 kcal mol^{-1}. This value can be compared with the measured self-exchange rate constants of $\leq 2 \times 10^4$ (50 °C), 2×10^6 (50

(32) Sutin, N.; Brunschwig, B. S. *ACS Symp. Ser.* **1982**, *198*, 105.
(33) Hopfield, J. J. *Proc. Natl. Acad. Sci. U.S.A.* **1967**, *215*, 642; **1974**, *71*, 3640.
(34) Buhks, E.; Jortner, J. *FEBS Lett.* **1980**, *109*, 117.
(35) Sutin, N., *Prog. Inorg. Chem.* **1983**, *30*, 441.
(36) Marcus, R. A.; Sutin, N. *Biochim. Biophys. Acta* **1985**, *811*, 265.

(37) (a) The reduction potentials for the plastocyanin(II/I), azurin(II/I), and stellacyanin(II/I) couples are 0.36, 0.31, and 0.19 V, respectively.[39b] (b) Taniguchi, V. T.; Sailasuta-Scott, N.; Anson, F. C.; Gray, H. B. *Pure Appl. Chem.* **1980**, *52*, 2275.

to 40–60 M^{-1} for the other systems. The value assumed for the association constant for reduced plastocyanin with $Cr(phen)_3^{3+}$, while slightly larger than the value reported by Sykes et al.,[27] is more consistent with the present data.[28a] The larger values of K_1 for the plastocyanin reaction are consistent with the more negative charge on reduced plastocyanin (−10)[5d,29] compared with those on azurin (−2)[5d] and stellacyanin (0).[5d] These values are also consistent with the results of kinetic and binding studies that are described below.[6a,b,16,27,29]

The values of k_1, K_1, k_2, K_3, and k_4 for the $Cr(phen)_3^{3+}$ and $Ru(bpy)_3^{2+}$ data determined for Scheme I subject to the above constraints are given in Table II. The curves calculated with these constants are shown in Figures 1 and 2. The values of the quenching rate constants in the low-[protein] limit (eq 2) calculated by using the constants in Table II are within 25% of their measured values. The value of K_3 is very sensitive to the curvature in the $1/\tau - 1/\tau_0$ vs. protein concentration plots, and because of the scatter in the high-[protein] data, K_3 is the least well-determined parameter. The k_1 values seem consistent with diffusion-controlled rates when the steric factors for the reaction are considered. The larger values of k_1 for the plastocyanin reactions are expected on the basis of the larger charge products for these reactions (−30 and −20 for the $Cr(phen)_3^{3+}$ and $Ru(bpy)_3^{2+}$ reactions, respectively, compared with −6 and −4 for the azurin and zero for the stellacyanin reactions).[5d,29] Moreover, the k_1 value of 2×10^9 M^{-1} s^{-1} for the reaction of $^*Ru(bpy)_3^{2+}$ with reduced plastocyanin is in excellent agreement with the value directly measured for the reaction of $Cr(phen)_3^{2+}$ with the oxidized protein (the reactants have similar charge products). Although the k_2 values are large, at low protein concentration the remote electron-transfer path is about 1 order of magnitude slower than the adjacent path, i.e., $k_1k_2/(k_{-1} + k_2) < k_4$ for the systems studied (Table II); this is a consequence of the fact that k_4 is comparable to k_1 while $k_2 \ll k_{-1}$.

The association of a second protein molecule renders more abrupt the transition from a roughly linear concentration dependence of the quenching lifetime to an almost concentration-independent region. Saturation is accelerated because the effective dissociation rate constant of the 1:1 complex is lowered by the binding of the additional protein molecule, $k'_{-1} = k_{-1}/(1 + K_3[P(I)])$. Note that a rate effect is only observed because the formation of a dimeric species is affected by the presence of the bound oxidant. If a protein dimer were formed in the absence of a redox partner, but with the same equilibrium constant (K_3), there would be no modulation effect. We conclude that the oxidant is somehow "sandwiched" between two protein molecules. It is also worth noting that the association of the second P(I) exhibits positive cooperativity for all proteins ($K_3 > K_1$).

Sykes et al.[6a,b,16,27] have reported kinetics for the oxidation of reduced plastocyanin and azurin by $Co(phen)_3^{3+}$. Their plots of the observed first-order rate constant vs. cobalt(III) concentration at pH 7.5 exhibit slight downward curvature for plastocyanin but none for azurin. They interpret this curvature in terms of complex formation at the remote site and derive $K_1 = 170$ and ≤ 40 M^{-1} for plastocyanin and azurin, respectively (ionic strength 0.1 M, pH 7.5).[28a] They also studied[27] the $Cr(phen)_3^{3+}$ inhibition of the $Co(phen)_3^{3+}$ oxidation of reduced plastocyanin and found $K_1 \approx 180$ M^{-1} for binding of the chromium(III) complex at pH 7.5. NMR studies clearly show that $Cr(phen)_3^{3+}$ binds to plastocyanin at or near Tyr-83, which is in the vicinity of the negative patch formed by the carboxylate groups of residues 42–45 (and residues 51 and 59).[16,17] This region is 10–15 Å from the copper site. Because $Co(phen)_3^{3+}$ is structurally very similar to $Cr(phen)_3^{3+}$ and because its reaction with reduced plastocyanin is blocked by the latter, $Co(phen)_3^{3+}$ almost certainly binds at the same site. This is consistent with the exothermic character of the precursor-complex formation ($\Delta H^\circ \simeq 10$ kcal mol^{-1}),[6b] which indicates that electrostatic factors dominate the interaction of $Co(phen)_3^{3+}$ with the reduced plastocyanin. It is also proposed that $Ru(bpy)_3^{2+}$ binds in the region of Tyr-83. Its association constant, though not known exactly, is certainly smaller than that for the phenanthroline complexes. Moreover, the oxidation of reduced plastocyanin by $Co(phen)_3^{3+}$ is inhibited by $Co(NH_3)_6^{3+}$, $Pt(NH_3)_6^{4+}$, and $(Co(NH_3)_5)_2NH_2^{5+}$, suggesting that all these complexes associate in the same region.[6c] Further support for the above interpretation is provided by the k_2 values. Since the magnitude of k_2 is governed primarily by the distance from the copper center to the binding site (see below), the similarity in the k_2 values for $Cr(phen)_3^{3+}$ and $Ru(bpy)_3^{2+}$ would indicate that both metal complexes bind at similar positions for a given protein.

The association constants of reduced plastocyanin with $Co(NH_3)_6^{3+}$, $Pt(NH_3)_6^{4+}$, and $(Co(NH_3)_5)_2NH_2^{5+}$ are large.[6c] However, the rate decreases observed even at high inhibitor concentration are only about twofold. The fact that the blocking is only partial suggests that more than one pathway is effective in the $Co(phen)_3^{3+}$ oxidation. The blocking agent can totally inhibit only the remote pathway by binding to the protein: the adjacent pathway can operate even when the blocking agent is present provided that the binding is at the remote site. The ratios of rate constants for the adjacent and remote pathways are significantly different for the $Co(phen)_3^{3+}$ and $^*Cr(phen)_3^{3+}$ oxidations, ≤ 1 and ~ 7, respectively. For the $Co(phen)_3^{3+}$ reaction neither pathway has a rate constant close to the diffusion limit and the rate ratio reflects the relative association constants at the adjacent and remote sites, as well as the rate difference arising from the difference in distance between the metal complex and the copper center for the two paths. On the other hand, for the $Cr(phen)_3^{3+}$ reaction the adjacent pathway is diffusion-controlled and the rate ratio reflects only the relative magnitudes of k_{-1} and k_2.[28b]

Binding Site for $Cr(phen)_3^{3+}$. As discussed in the Introduction, NMR studies of reduced plastocyanin have shown that the proton resonances of tyrosine-83 (as well as the methyl group resonances of an aliphatic side chain, possibly valine-40) are broadened by added $Cr(phen)_3^{3+}$. The former residue affords a particularly attractive binding site because of the possibility of hydrophobic interactions between the phenyl ring of the tyrosine-83 and a phenanthroline ring of the chromium complex.[30] In order to further examine this possibility, computer simulations of the docking of $Cr(phen)_3^{3+}$ with the tyrosine region of plastocyanin were performed.[31] The best-fit docked complex, obtained by

Table III. Distances in the Computer-Generated Complex Formed between Plastocyanin and $Cr(phen)_3^{3+}$

	dist, Å
cysteine-84 S to nearest phen C	10.3
Cu center to nearest phen C	12.7
Cu to Cr	18.4
tyrosine-83 *o*-C to Cr	8.0, 8.7
tyrosine-83 *m*-C to Cr	9.4, 10.0
valine-40 Me C to Cr	8.5, 11.5

(27) Lappin, A. G.; Segal, M. G.; Weatherburn, D. C.; Henderson, R. A.; Sykes, A. G. *J. Am. Chem. Soc.* **1979**, *101*, 2302. Lappin, A. G.; Segal, M. G.; Weatherburn, D. C.; Sykes, A. G. *J. Am. Chem. Soc.* **1979**, *101*, 2297.

(28) (a) It should be recognized that parallel adjacent and remote pathways may also operate in the $Co(phen)_3^{3+}$ reaction. A least-squares analysis of the published data[6] in terms of the corresponding rate law gave an excellent fit with the $K_1 = 220 \pm 40$ M^{-1}. (b) For the $Co(phen)_3^{3+}$ oxidation $k_{adj}/k_{rem} \approx (K_{adj}/K_{rem}) \exp(-\beta(d_{adj} - d_{rem}))$, where we assume that ΔG° is the same for the two pathways, $K_{rem} = K_1$, and K_{adj} is the association constant for the adjacent pathway. For the $^*Cr(phen)_3^{3+}$ oxidation $k_{adj}/k_{rem} \approx 1 + k_{-1}/k_2$; see eq 4.

(29) Augustin, M. A.; Chapman, S. K.; Davies, D. M.; Watson, A. D.; Sykes, A. G. *J. Inorg. Biochem.* **1984**, *20*, 281.

(30) (a) Farver and Pecht have presented evidence that Cr^{2+} binds to oxidized plastocyanin at a residue near Tyr-83 prior to electron transfer.[30b] (b) Farver, O.; Pecht, I. *Proc. Natl. Acad. Sci. U.S.A.* **1981**, *78*, 4190.

(31) (a) Computer graphics were done with the program BIOGRAF/I (written by S. L. Mayo, B. D. Olafson, and W. A. Goddard, III) and a VAX 11/780-supported Evans and Sutherland P5300 interactive graphics terminal. The metal complex used as a structural model was $Co(phen)_3^{3+}$ (Niederhoffer, E. C.; Martell, A. E.; Rudolf, P.; Clearfield, A. *Cryst. Struct. Commun.* **1982**, *11*, 1951). (b) The surfaces of the protein and of the metal complex were calculated by using the program MS: Connolly, M. *Quant. Chem. Program Exchange Bull.* **1981**, *1*, 75.

°C), and 1.2×10^5 (20 °C) M^{-1} s^{-1} for plastocyanin, azurin, and stellacyanin, respectively. From the λ_{22} values we estimate that $S\kappa_{el}$, the product of the steric and electronic factors,[38] is $\sim 10^{-4}$ for the protein self-exchange reactions.

The electron-transfer distance for the remote pathway can be estimated from eq 4. Since these reactions are essentially barrierless,[39] the last term in eq 4 is close to unity and the rate constant for the remote pathway reduces to

$$k_{el} = 10^{13} \exp(-\beta d) \text{ s}^{-1} \quad (6)$$

The value of β estimated from studies of electron transfer in frozen media and other systems[32,36,40] is ~ 1.2 Å^{-1}. Substitution of the experimental value of k_{el} (k_2) into eq 6 yields a value of 12 Å for d, the electron-transfer distance for the reaction of reduced plastocyanin with $^*Cr(phen)_3^{3+}$ by the remote pathway. The closest distance from the edge of the phenanthroline ring to the "lead-in" atom to the copper site (the sulfur atom of cysteine-84), is ~ 10 Å (Table III), in reasonable agreement with this value. The difference of 2 Å (approximately 1 order of magnitude in the rate) may suggest that the frequency factor of 10^{13} s^{-1} is too large and/or that the estimated β is too low.[41] However, considering the complexity of the protein system and the assumptions involved, the agreement can be regarded as satisfactory.

Electron Transfer at the Adjacent Site. We next consider the value of the diffusion-controlled rate constant for electron transfer at the adjacent site. This rate constant can be calculated from

$$k_{diff} = (4\pi ND/1000) / \int_{r=\sigma_{12}}^{\infty} \exp[-w(r)/RT] r^2 \, dr \quad (7)$$

$$w(r) = \frac{z_1 z_2 e^2}{D_s r} \left[\frac{\exp(B\sigma_1 \mu^{1/2})}{1 + B\sigma_1 \mu^{1/2}} + \frac{\exp(B\sigma_2 \mu^{1/2})}{1 + B\sigma_2 \mu^{1/2}} \right] \exp(-Br\mu^{1/2})$$

In these expressions D is the sum of the diffusion constants of the two reactants, $B = 0.329$ Å^{-1} for water at 25 °C, $\sigma_1 = a_1 + a_1'$, $\sigma_2 = a_2 + a_2'$, where a' is the radius of the dominant ion of opposite charge in the ionic atmosphere, and z_1 and z_2 are the charges of the reactants.[36] Substitution of $D = 2.70 \times 10^{-6}$ cm^2 s^{-1}, $a_1 = 15.8$ Å, $a_1' = 0.95$ Å, $z_1 = -10$, $a_2 = 7.0$ Å, $a_2' = 1.81$ Å, and $z_2 = +3$ gives $k_{diff} = 6 \times 10^9$ M^{-1} s^{-1}. This value is slightly larger than the observed value of k_1 for the reaction of reduced plastocyanin with $Cr(phen)_3^{3+}$ (3.5×10^9 M^{-1} s^{-1}) and may indicate that there is a rotational contribution to k_{diff} or, perhaps, that the reaction is activation controlled with the maximum value of the rate constant equal to $SK_A\kappa_{el}\nu_n$, where S is a steric factor.[35,36] The effect is small, and it is not possible to distinguish between these alternatives at this time.

Finally, for electron transfer at a remote site to successfully compete with adjacent electron transfer, it is necessary that the binding constant at the remote site be large enough to compensate for the larger electron-transfer distance. For $d - d' = 10$ Å, where d' is the (edge-to-edge) electron-transfer distance at the adjacent site, and $\beta = 1.2$ Å^{-1}, the binding constant at the remote site needs to be $\sim 10^5$ times larger than the binding constant at the adjacent site if the (bimolecular) remote path is to successfully compete with the (bimolecular) adjacent path. Although this may be the case for certain biological systems, it is unlikely to be the case for reactions of metalloproteins with most metal complexes. On the other hand, at high protein or metal complex concentrations the (intramolecular) remote path can be significant if the dissociation of the 1:1 complex is sufficiently slow. This is the case for the systems considered here.

Acknowledgment. Research at the California Institute of Technology was supported by National Institutes of Health Grant AM19038, and research at Brookhaven National Laboratory was carried out under contract DE-AC02-76CH00016 with the U.S. Department of Energy and supported by its Division of Chemical Sciences and Office of Basic Energy Sciences. A.M.E. acknowledges a postdoctoral fellowship from the NSERC (1980–1981). S.L.M. thanks AT&T Bell Laboratories for a predoctoral fellowship (1983–present). We wish to acknowledge helpful discussions with Dr. C. Creutz and the assistance of J. Horwitz of the University of California at Santa Cruz and Dr. R. Humphry-Baker of L'Ecole Polytechnique Fēderale de Lausanne during the early stages of this work.

Registry No. $Ru(bpy)_3^{2+}$, 15158-62-0; $Cr(phen)_3^{3+}$, 15276-16-1; $Cr(5\text{-}Clphen)_3^{3+}$, 51194-62-8; $Cr(4,7\text{-}Me_2phen)_3^{3+}$, 51194-72-0; L-Tyr, 60-18-4.

Supplementary Material Available: Tables of reciprocal lifetimes of $^*Cr(phen)_3^{3+}$ and $^*Ru(bpy)_3^{2+}$ as a function of plastocyanin (Table S1), azurin (Table S2), and stellacyanin (Table S3) concentration (3 pages). Ordering information is given on any current masthead page.

(38) (a) The values of λ_{ij} are estimated with use of[35,36] $k_{ij} = SK_A\kappa_{el}\nu_n \exp(-\lambda_{ij}/4RT)$, where k_{ij} is the self-exchange rate constant, S is a steric factor, and K_A is the association constant for the reactants. The association constant can be calculated from $(4 \times 10^{-3})\pi N\sigma^2(\delta r) \exp(-w_{ij}/RT)$, where N is Avogadro's number, σ is the close-contact distance for the exchange reaction, δr is 0.8 Å, and w is the electrostatic work required to bring the two reactants together.[35] The self-exchange rate for the $^*Cr(phen)_3^{3+/2+}$ couple has been estimated as $\sim 3 \times 10^5$ M^{-1} s^{-1} at 25 °C at 0.1 M ionic strength,[21] and the self-exchange rates for the plastocyanin(II/I), azurin(II/I), and stellacyanin(II/I) couples are $\leq 2 \times 10^4$, 2×10^6 (both at 50 °C), and 1.2×10^5 (at 20 °C) M^{-1} s^{-1}, respectively.[36b-d] The value of $S\kappa_{el}$ is unity for the $^*Cr(phen)_3^{3+/2+}$ exchange and $\sim 10^{-4}$ for the protein self-exchanges. (b) Beattie, J. K.; Fensom, D. J.; Freeman, H. C.; Woodcock, E.; Hill, H. A. O.; Stokes, A. M. *Biochim. Biophys. Acta* **1975**, *405*, 109. (c) Canters, G. W.; Hill, H. A. O.; Kitchen, N. A.; Adman, E. T. *J. Magn. Reson.* **1984**, *57*, 1. (d) Dahlin, S.; Reinhammar, B.; Wilson, M. T. *Biochem. J.* **1984**, *218*, 609.

(39) In the $Co(phen)_3^{3+}$ reaction,[6a,b,16,27] by contrast, the rate-determining step may be the reorganization of the precursor complex: note the large activation energy for the $Co(phen)_3^{2+}$ reaction.

(40) Miller, J. R.; Beitz, J. V.; Huddleston, R. K. *J. Am. Chem. Soc.* **1984**, *106*, 5057.

(41) In this connection it is interesting to compare intramolecular electron-transfer rates in $(NH_3)_5Ru(His\text{-}33)^{2+}$–ferricytochrome c (Ru^{II}–Fe^{III}) and $(NH_3)_5Ru(His\text{-}83)^{2+}$–azurin ($Ru^{II}$–$Cu^{II}$): the rate constants are 30 and 2 s^{-1}, respectively.[42,43] The distance between the two redox sites is very similar for the two reactions (11.8 Å), and both reactions are temperature independent over a wide range. The ΔS^* values for the two reactions are also very similar (−25.8 cal deg^{-1} mol^{-1} for Ru^{II}–Fe^{III} and −26.8 cal deg^{-1} mol^{-1} for Ru^{II}–Cu^{II}).[42-44]

(42) Nocera, D. G.; Winkler, J. R.; Yocom, K. M.; Bordignon, E.; Gray, H. B. *J. Am. Chem. Soc.* **1984**, *106*, 5145.

(43) Margalit, R.; Kostić, N. M.; Che, C.-M.; Blair, D. F.; Chiang, H.-J.; Pecht, I.; Shelton, J. B.; Shelton, J. R.; Schroeder, W. A.; Gray, H. B. *Proc. Natl. Acad. Sci. U.S.A.* **1984**, *81*, 6554.

(44) Kostić, N. M.; Margalit, R.; Che, C.-M.; Gray, H. B. *J. Am. Chem. Soc.* **1983**, *105*, 7765.

Appendix: Figure 5 from preceding paper

Because of the poor reproduction of Figure 5 in the preceding paper, it has been reproduced on the following pages.

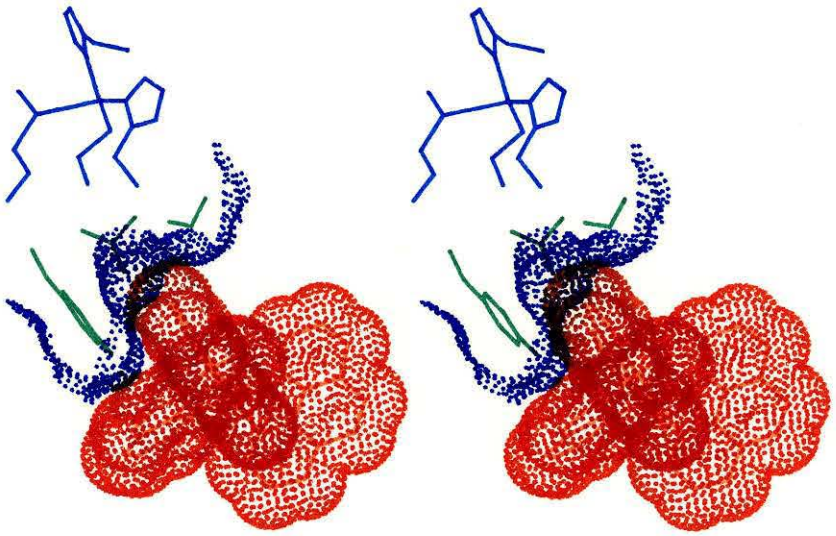

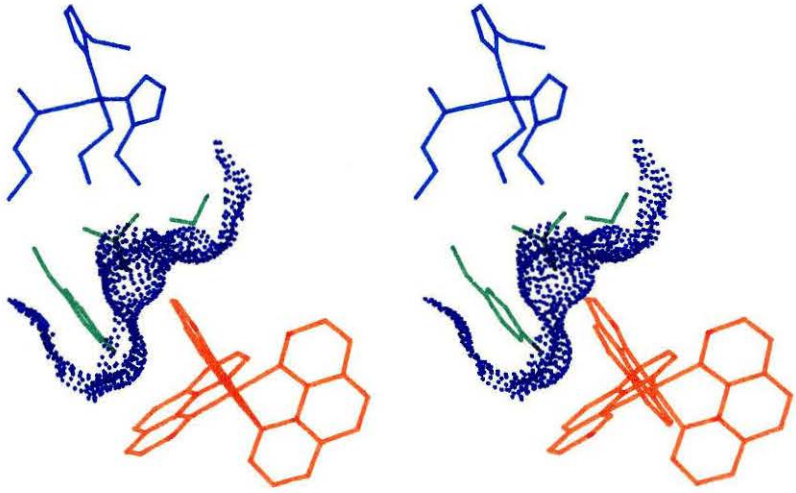

Chapter 2

The Determination of Electron-Transfer Geometries and Kinetic Parameters in Ruthenium-Modified Metalloproteins

The text of this chapter contains two preprints of papers concerned with the correlation of electron-transfer kinetic data with Marcus theory. The first paper was co-authored with Andrew W. Axup, Robert J. Crutchey and Harry B. Gray and has been accepted for publication in the *Journal of The American Chemical Society*. The second paper was co-authored with Charles M. Lieber, Jennifer L. Karas, Michael Albin and Harry B. Gray and has been accepted for publication in the *Welch Conference Proceedings*, November 1987. My contribution to this work was the determination of the electron-transfer geometries of the complexes of interest and the evaluation of the distance dependence of the electron-transfer rates in terms of Marcus theory. In addition to the papers an appendix of calculational details is also included.

Distance Dependence of Photoinduced Long-Range Electron Transfer in Zinc/Ruthenium-Modified Myoglobins

Andrew W. Axup, Michael Albin, Stephen L. Mayo,

Robert J. Crutchley,[1] and Harry B. Gray

Contribution No. 7588 from the Arthur Amos Noyes Laboratory of Chemical Physics, California Institute of Technology, Pasadena, California 91125

Abstract: An experimental investigation of the distance dependence of long-range electron transfer in zinc/ruthenium-modified myoglobins has been performed. The modified proteins were prepared by substitution of zinc-mesoporphyrin IX diacid (ZnP) for the heme in each of four previously characterized pentaammineruthenium(II)(a_5Ru) derivatives of sperm whale myoglobin (Mb): a_5Ru(His-48),a_5Ru(His-12),a_5Ru(His-116),a_5Ru(His-81). Electron transfer from the ZnP triplet excited state (^{3}ZnP*) to Ru^{3+}, ^{3}ZnP*-Ru^{3+} $\rightarrow$ZnP$^+$-Ru^{2+} (ΔE° $\sim$0.8V), was measured by time-resolved transient absorption spectroscopy: rate constants (k_f) are 7.0×10^4 (His-48), 1.0×10^2 (His-12), 8.9×10^1 (His-116), and 8.5×10^1 (His-81) at 25°C. Activation enthalpies calculated from the temperature dependences of the electron-transfer rates over the range 5-40°C are 1.7±1.6 (His-48), 4.7±0.9 (His-12), 5.4±0.4 (His-116), and 5.6±2.5 (His-81) kcal/mol^{-1}. Electron-transfer distances (d=closest ZnP edge to a_5Ru(His) edge) were calculated to fall in the following ranges: His-48, 11.8-16.6; His-12, 21.5-22.3; His-116, 19.8-20.4; His-81, 18.8-19.3Å. The rate-distance equation is $k_f=7.8\times10^8\exp[-0.91(d-3)]s^{-1}$. The data indicate that the ^{3}ZnP*-Ru(His-12)$^{3+}$ electronic coupling may be enhanced by an intervening tryptophan (Trp-14).

Introduction

Long-range electron transfers are important mechanistic steps in many biological oxidation-reduction reactions.[2,3,4,5,6,7,8,9,10,11,12,13,14,15,16] Although it is generally assumed that the rates of these transfers are determined to a large extent by the donor-acceptor separation and nature of the intervening medium,[17,18,19,20,21] very few experiments have addressed these points in a systematic manner.[7,8,11]

One approach to the study of long-range electron transfer is to attach a redox-active complex to a specific surface site of a structurally characterized heme or blue copper protein, thereby producing a two-site molecule with fixed, donor-acceptor distance. The redox-active complex that has been employed successfully in several previous experiments is $a_5Ru^{2+/3+}$ (a=NH_3), which covalently bonds to surface hisitidines.[8,9,10,11,12] This complex can be attached by the reaction of $a_5Ru(OH_2)^{2+}$ with native protein under mild conditions, and the ruthenated protein can be purified by ion-exchange chromatography.

In order to probe distance effects on long-range electron transfer, we have replaced the heme in four ruthenated myoglobins (a_5Ru(His-48)Mb; a_5Ru(His-12)Mb; a_5Ru(His-81)Mb; a_5Ru(His-116)Mb: Mb=sperm whale myoglobin)[10] by zinc-mesoporphyrin IX diacid (ZnP). The ZnP excited triplet state (^{3}ZnP*) is a much more powerful electron donor than a reduced heme ($\Delta E°(^3ZnP^*\text{-}Ru^{3+} \rightarrow ZnP^+\text{-}Ru^{2+}) \sim 0.8V$),[11] thereby allowing four different electron-transfer distances to be examined in a single protein molecule.

Experimental Section

Materials and Apparatus

Distilled water, filtered through a Barnstead Nanopure water purification system (No. 2794, specific resistance > 18MΩ-cm), was used in the preparation of all aqueous solutions. 2-Butanone (MCB) was stored over aluminum oxide (Woelm neutral, Waters Associates) at 4°C to prevent the accumulation of peroxides. All other reagents were used as received.

Carboxymethylcellulose cation exchange resis, CM-52 (Whatman, preswollen, microgranular), was equilibrated as indicated by the manufacturer (six aliquot buffer changes). Five column volumes of buffer were passed to pack the column prior to use. CM-52 resins were cleaned after use by washing with high salt solution (~1-3 M NaCl). Sephadex ion exchange gel, G-25-80 (Sigma, bead size 20-80μ) was equilibrated in the desired buffer, slurried and poured in a fashion similar to that described for CM-52. Sephadex gels were cleaned by multiple washings with buffer or water.

Samples were degassed and purged with purified argon (passed through a manganese oxide column) on a dual manifold vacuum-argon line. At least five vacuum/purge cycles were used to deoxygenate samples. Transfers were done anaerobically with a cannula (Aldrich, 20 ga. stainless, noncoring tips). Other air-sensitive manipulations were performed under argon in a Vacuum Atmospheres Co. HE-43-2 Dri Lab inert atmosphere box. Concentrations of protein solutions and removal of small molecules were achieved with an Amicon ultrafiltration system (YM-5 filter, 5000 molecular weight cutoff).

Preparations and Purifications

The perchlorate[22] and chloride[23] salts of tris-(1,10-phenanthroline)-cobalt(III), $Co(phen)_3^{3+}$ were used to oxidize the protein samples.

Aquopentaammineruthenium(II) ($a_5RuH_2O^{2+}$) was synthesized by reduction of chloro-pentaammineruthenium(III) (Strem) by zinc amalgam.[24] The product was precipitated as the hexafluorophosphate salt and stored under vacuum, or the $a_5RuH_2O^{2+}$ solution was used directly in the labelling reaction with protein.

Purification of sperm whale skeletal muscle ferrimyoglobin

Sigma ferrimyoglobin (6g), metMb, was dissolved in 20mL of Tris buffer (μ 0.05M, pH 7.2). The protein solution was centrifuged to separate the insoluble material. The supernatant was applied to a CM-52 column (4cm x 80cm) equilibrated with Tris buffer (μ 0.05M, pH 7.8) at 4°C. The sample was eluted at 50mL/h with Tris buffer (μ 0.05M, pH 7.2). Four separable bands were typically observed, and band IV (the richest in metMb) was used for these studies.

Preparation of pentaammineruthenium(III)ferrimyoglobin[10]

A solution containing 60mg (25mL of 1.3 mM metMb) of ferrimyoglobin in Tris buffer (μ 0.05 M, pH 7.2) was degassed and purged with argon in a septum-stoppered 120 mL bottle. Excessive foaming of the protein solution during degassing was avoided to minimize protein denaturation. 130mg of degassed aquopentaammineruthenium(II)-hexafluorophosphate were dissolved in 15mL of argon-purged Tris buffer (μ 0.05M, pH 7.2).

The aquopentaammineruthenium(II) was transferred under argon to the ferrimyoglobin solution. The ferrimyoglobin immediately reduced and the solution changed

color from brown to deep red. After the mixture had reacted without agitation at room temperature for thirty minutes, the reactin was quenched by elution at room temperature on a Sephadex G-25 column (Tris buffer, μ 0.05M, pH 7.2). The protein fraction was collected, oxidized with $Co(phen)_3^{3+}$, and stored at 4°C.

Purification of pentaammineruthenium(III)ferrimyoglobin[10]

The mixture of ruthenated myoglobins was desalted by five cycles of Amicon concentration and dilution with water, and then reduced to a final volume of 6mL (600mg, 5.6mM modified metMb). The modified myoglobins were separated by isoelectric focusing. An LKB system (2117 Multiphor, 2197 Electrofocusing Power Supply) was used. Two gels were prepared by standard procedures.[25] To each gel, 3mL of protein solution were applied, and the gels were run at 4°C (power supply settings: 1500V, 22mA, 10W). Progress of the focusing was monitored visually by observing the separation of the modified myoglobin bands. When sufficient resolution of native, singly modified, and doubly modified bands occurred, the gels were stopped. The band of singly modified derivatives was cut from the trays and eluted from the gel through a disposable frit with water. The ampholytes were removed from the collected protein solution by Amicon ultrafiltration.

The mixture of singly ruthenated myoglobin derivatives was concentrated and loaded onto a CM-52 column (equilibrated with μ 0.1M Tris buffer, pH 7.8, 4cm x 70cm) at 4°C. The protein was eluted with Tris buffer at 50mL/h. Four bands were collected and each was concentrated and rechromatographed, if necessary. Fractions were kept at 4°C for short-term storage or frozen at -60°C (0.1mM protein) in Tris buffer. $Co(phen)_3^{3+}$ was added to all modified protein solutions for storage. The order of elution from the CM-52 column is a_5Ru(His-12)Mb, a_5Ru(His-116)Mb, a_5Ru(His-

81)Mb, and a_5Ru(His-48)Mb.

Preparation of zinc-mesoporphyrin IX diacid

The porphyrin dimethyl ester was first saponified to the diacid. 250mg of mesoporphyrin IX dimethly ester (Sigma) were dissolved in 5mL of pyridine in a 50mL three-neck flask. The flask was wrapped in foil and placed under an argon flow. 20mL of 1% potassium hydroxide in methanol (0.29g KOH (89%) in 25mL MeOH) were added with 3mL of water. The reaction mixture was heated and refluxed for two hours. 6N hydrochloric acid was added to precipitate the porphyrin diacid. The reaction mixture was refrigerated overnight. The sample was centrifuged and decanted. Zinc(II) was inserted into the free base by standard methods.[26] Evaluation of the completeness of the reaction and purity of the product was done by thin layer chromatography (EM Reagents, silca gel 60 F_{254}). Samples were spotted from chloroform solution and an 85:13.5:1.5 (v/v/v) toluene/ethlyacetate/methanol solvent system was used as the developer.[27] Progress of the chromatography was followed by sample luminescence under UV light. The zinc-mesoporphyrin IX diacid was stored in a foil-wrapped vial at -60°C.

Preparation of apomyoglobin

The heme was removed from the myoglobin by the acidic 2-butanone extraction method.[28,29] On the final extraction, the aqueous apoprotein solution was removed and transferred to a Spectrapor dialysis bag (Spectrum Medical industries, 20.4mm diameter, 600-800 molecular weight cutoff, 3.2mL/cm) that had been previously cleaned by standard methods. The sample was twice dialyzed against 1L of 10mM sodium bicarbonate (3.36g $NaHCO_3$ in 4L H_2O) followed by three times against 1L of

μ 0.1M phosphate buffer, pH 7.0. Each dialysis was continued for six to twelve hours. The concentration of the apoprotein was determined from the absorption spectrum (ϵ_{280} 15.8mM^{-1}cm^{-1}).[30] A minor peak at 424nm indicated the incomplete removal of the iron porphyrin. Typically, heme removal in excess of 99% was achieved. Apoprotein prepared in this fashion was immediately used for reconstitution with the zinc mesoporphyrin.

Preparation of reconsituted myoglobins[31]

The apoprotein solution was maintained at 4°C or ice bath temperatures for the duration of the insertion process. Approximately 3mg of zinc mesoporphyrin IX diacid were dissolved in 10 drops of 0.1N NaOH(aq) in 5mL. 2mL of phosphate buffer (μ 0.1M, pH 7.0) were added to the porphyrin solution. The resulting solution was added dropwise to the apoprotein with gentle swirling. The mixture was stirred in the dark at 4°C for twelve hours. A second insertion was then made. After twelve more hours, the solution was left undisturbed overnight. The sample was centrifuged for one to two hours and the supernatant was decanted and saved for purification.

Purification of reconstitued myoglobins

The zinc-mesoporphyrin IX reconstituted myoglobin was applied to a Sephadex G-25-80 column, equilibrated with phosphate buffer (μ 0.01M, pH 7.0), and eluted with the same buffer at 4°C. The protein band was collected and concentrated by Amicon ultrafiltration for loading on the phosphate (μ 0.01M) equilibrated CM-52 column (3cm x 22cm). An ionic strength gradient, μ 0.01M to 0.1M, was used to elute the sample at 30mL/h. Unmodified zinc myoglobin typically required 30-36 h to elute, and 72-84 h were required for the ruthenated derivatives. Additional 0.1M buffer was

needed to complete some elutions. Zinc-substituted myoglobins were refrigerated in foil-wrapped vials and used as quickly as possible.

Analytical isoelectric focusing was used to determine the purity of the a_5Ru(His)-Mb(ZnP)'s following final purification.[32] The isolectric point (pI) of Mb(ZnP) is the same as the pI of ferromyoglobin (pI 7.4). Apomyoglobin is readily resolved from the reconstituted protein, because its pI is between ~8 and 9. The broad pI band indicates that apomyoglobin consists of multiple components, probably a result of degradation of the less stable apoprotein. The a_5Ru(His)Mb(ZnP) samples exhibit pI's that correspond to reduced a_5Ru(His)Mb derivates.[11]

Reconstitution of apomyoglobin with zinc mesoporphyrin IX diacid was greater than 90% based on protein recovery. The determination of Mb(ZnP) concentrations assumes that the A_{280} extinction coefficients for apomyoglobin and Mb(ZnP) are similar. This assumption is supported by experimental results that correlate the amount of protein present before and after reconstitution with UV-visible absorption data:[33] A_{414}/A_{280} ~16, so ϵ_{414} ~250mM^{-1}cm^{-1}.

Instrumentation

Transient absorption lifetime measurements were made with a pulsed laser system described previously.[9f] Modifications to the system for transient absorption measurements are indicated below. Samples (μ 0.1M, phosphate buffer pH 7.0, A_{414} ~1.25) were degassed in a vacuum cell with a 1cm fluorescence cuvette side-arm. A 500W continuous wave tungsten lamp with an Infrared Industries Model 518 Lamp Power Supply served as the probe beam source. The beam was collimated (f17.7cm, diam. 7.5cm) in the lamp housing and focused by a lens (f15.2cm, diam. 10.0cm) through a series of Corning filters, 0-52, 0-51, 5-57, and 5-58. The beam was cropped by an

0.8cm aperture and passed through the sample cell. The beam was refocused (f7.0cm, diam. 3.8cm) onto the slit of the monochromator (0.8mm) through a Corning 5057 filter. A Tektronix FET probe amplifier with a 5kΩ resistor was used for all transients except the a_5Ru(His-48)Mb(ZnP) system, in which case a LeCroy amplifier was used. 40 pulses were taken at 1Hz and the data were averaged on a PDP computer. Data were serially transferred to an IBM PCAT for later analysis and graphics. Data were analyzed with nonlinear least-squares routines. Both monophasic and biphasic first-order fits with zero and nonzero endpoints were made.

Results and Discussion

Rate Constants

Electron-transfer rates were determined from the quenching of the ^{3}ZnP* decay. The long-lived triplet excited state reduces histidine-bound ruthenium(III)(ΔE° ~0.8V), and back electron transfer to ZnP^+ rapidly returns the system to its initial state ($k_b > k_f$):[11,34,35]

$$\begin{array}{ccc} \text{ZnP-Ru}^{3+} & \underset{k_d}{\overset{h\nu}{\rightleftharpoons}} & {}^3\text{ZnP*-Ru}^{3+} \\ & k_b \searrow \quad \swarrow k_f & \\ & \text{ZnP}^+\text{-Ru}^{2+}. & \end{array} \qquad (3.1)$$

The native Mb(ZnP) data fit a monophasic first-order nonzero endpoint expression for at least four half-lives. The rate constant (k_d) obtained from this fit is $40\pm2s^{-1}$ at 25°C. The Mb(^{3}ZnP*) decay rate does not vary significantly from 7.6°C ($38\pm5s^{-1}$) to 38.6°C ($42\pm1s^{-1}$) (Table I). Values of k_d determined a 3 and 90 μM are $41\pm2s^{-1}$ and $46\pm s^{-1}$, respectively, confirming that no bimolecular quenching of

Mb(^{3}ZnP*) occurs.

The a_5Ru(His-48)Mb(ZnP) data also fit a monophasic first-order nonzero endpoint expression for at least four half-lives (Figure 1). A rate constant of $7.0\pm0.8\text{x}10^4\text{s}^{-1}$ was obtained. Subtraction of the intrinsic decay rate ($40\pm2\text{s}^{-1}$) does not affect this result ($k_{obs}\sim k_f$). The decay of photoexcited a_5Ru(His-48)Mb(ZnP) was also measured following dithionite reduction[36] of a_5Ru(His-48)$^{3+}$; the observed decay rate ($50\pm5\text{s}^{-1}$) is nearly the same as k_d. The a_5Ru(His-48)Mb(^{3}ZnP*) quenching rate constant exhibits a slight temperature dependence (Table I), ranging from $5.4\pm0.9\text{x}10^4\text{s}^{-1}$ (7.6°C) to $8.1\pm1.4\text{x}10^4\text{s}^{-1}$ (38.6°C).

Residuals corresponding to a monophasic first-order nonzero endpoint fit of the a_5Ru(His-81)Mb(ZnP) data indicate a deviation from monophasic dehavior. These data can be satisfactorily fit to a biphasic first-order zero endpoint expression. Nine half-lives of the fast component were used in the analysis. The observed rate ($126\pm12\text{s}^{-1}$) corresponds to a k_f of $86\pm12\text{s}^{-1}$. The second component contributes less than 10% to the transient absorption measurement and was observed for less than two half-lives. Over the range 3-15μM a_5Ru(His-81)Mb(ZnP) showed no variation in k_{obs}; following reduction[36] of a_5Ru(His-48)$^{3+}$, the observed rate ($45\pm4\text{s}^{-1}$) was found to be within experimental error of k_d.

Similar analyses of the a_5Ru(His-116)Mb(ZnP) and a_5Ru(His-12)Mb(ZnP) data yielded electron-transfer rate constants of $89\pm3\text{s}^{-1}$ and $101\pm11\text{s}^{-1}$, respectively. The His-81, 116, and 12 derivatives exhibit moderate temperature dependences (Table I). Enthalpies of activation ($\Delta H^{\ddagger}$) are as follows: Mb(ZnP), 0.0 ± 0.9; a_5Ru(His-48)Mb(ZnP), 1.7 ± 1.6; a_5Ru(His-81)Mb(ZnP), 5.6 ± 2.5; a_5Ru(His-116)Mb(ZnP), 5.4 ± 0.4; and a_5Ru(His-12)Mb(ZnP), 4.7 ± 0.9 kcal mol^{-1}.[37]

Distance Dependence

Theory indicates that the rate of long-range electron transfer will fall off exponentially with donor-acceptor distance.[17] Both edge-edge (d) and metal-metal (d_m) distances were examined in our analysis.[38] Assuming an electronic transmission coefficient of unity when ^{3}ZnP* and a_5Ru(His)$^{3+}$ are in van der Waals edge-edge contact (d=3Å),[39] the standard theoretical expression for the electron-transfer rate constant is Eq. (3.2):

$$k_f = 10^{13} exp[-(\lambda + \Delta G^\circ)^2/4\lambda RT] exp[-\beta(d-3)] s^{-1}, \qquad (3.2)$$

where λ is the vertical reorganization energy and ΔG° is the reaction free energy.[17]

Electron-transfer distances for the various Mb derivatives (Figure 2) and for a_5Ru(His-33)cytochrome *c* were obtained from a rigid-body conformational search[40] of the appropriately modified sperm whale and tuna cytochrome *c* structures.[41] The searches were performed by evaluating the van der Waals energy of the 10^4 unique conformations that are generated by successively incrementing each of the two histidine (modified with a_5Ru) sidechain dihedral angles by 3.6°. The calculation included only the van der Waals contribution of those atoms within 8.5Å of the ruthenated histidine in each conformation. Pseudopotential-energy surfaces were obtained by plotting conformational energy *vs.* electron-transfer distance (d or d_m) and by fitting a smooth curve under the generated points. A comparison of the experimental structure[42] of a_5Ru(His-48)Mb reveals an uncertainty of at least 6.5kcal in our calculations. That is, the experimental d_m of 24Å falls on our potential-energy surface approximately 6.5kcal above the calculated minimum. The d and d_m ranges in our analysis of the rates reflect this 6.5kcal uncertainty (Table II).

The $\ln k_f$ *vs.* d plot for the a_5RuMb and a_5Rucyt*c*[34] experiments is shown in Figure 3. The experimental distance dependence of the rate constant is given by Eq.

(3.3):

$$k_f = 7.8 \times 10^8 exp[-0.91(d-3)]s^{-1}. \quad (3.3)$$

Best fits to the lower and upper limits of the d ranges give k_f=2.8x10^{8}exp[-0.87(d-3)]s^{-1} and k_f=5.8x10^{9}exp[-0.99(d-3)]s^{-1}, respectively, thereby providing a measure of the uncertainty in Eq. (3.3).[43]

Our finding that β for long-range protein electron transfers (0.9-1.0Å^{-1}) is somewhat smaller than the commonly assumed values (1.2-1.4Å^{-1}) is supported by the observation that the three longest transfers all occur at roughly the same rate, even though d is 2 to 3Å larger for the His-12 derivative than for the other two species. Examination of a_5Ru(His-12)Mb with computer graphics shows that an aromatic group (Trp-14) is parallel-planar to ZnP in the medium between the porphyrin and His-12 (Figure 4), thereby raising the possibility that weak ^{3}ZnP*(Trp-14)a_5Ru(His-12)$^{3+}$ charge-transfer interactions might facilitate electron transfer.[44] However, an extensive theorectical analysis of the ZnP to a_5Ru(His-12) pathway by Kuki and Wolynes[45] does not support a special role for the intervening tryptophan, and the relatively small departure of the His-12 derivative from the rate-distance correlation (Eq. 3.3) may have an entirely different origin. Hoffman, Mauk, and coworkers have found only minor effects on cytochrome *c* peroxidase (^{3}ZnP*):cytochrome *c*(Fe^{3+}) long-range electron-transfer rates upon changing Phe-82 of cyt*c* to other residues, although dramatic differences in the reverse-direction transfers (Fe^{2+}-ZnP$^+$) were observed.[14] Further work on the influence of the medium in well-defined electron-transfer systems is called for, because it is apparent from these early experimental and theoretical results that many issues need to be explored in greater depth.

Acknowledgments

We thank Charlie Lieber, Jenny Karas, Walter Ellis, Lorne Reid, Jose Onuchic, David Beratan, A. Kuki, Harvey Schugar, R. A. Marcus, and Jay Winkler for helpful discussions. A.W.A. acknowledges a fellowship from the Fannie and John Hertz Foundation. S.L.M. acknowledges a fellowship from AT&T Bell Laboratories. This research was supported by National Science Foundation Grants CHE85-18793 and CHE85-09637.

References

[1] Present address: Department of Chemistry, Carleton University, Ottawa, Canada K1S 5B6.

[2] Hatefi, Y. *Annu. Rev. Biochem.* **1985**, *54*, 1015-1069.

[3] Dixit, B. P. S. N.; Vanderkooi, J. M. *Curr. Top. Bioenerg.* **1984**, *13*, 159-202.

[4] Michel-Beyerle, M. E., Ed., *Antennas and Reaction Centers of Photosynthetic Bacteria*, Springer-Verlag, Berlin, **1985**.

[5] DeVault, D. *Quantum Mechanical Tunnelling in Biological Systems*, Cambridge Univ. Press, Cambridge, ed. 2, **1984**.

[6] Sykes, A. G. *Chem. Soc. Rev.* **1985**, *14*, 283-315.

[7] Brunschwig, B. S.; DeLaive, P. J.; English, A. M.; Goldberg, M.; Gray, H. B.; Mayo, S. L.; Sutin, N. *Inorg. Chem.* **1985**, *24*, 3743-3749.

[8] (a) Gray, H. B. *Chem. Soc. Rev.* **1986**, *15*, 17-30. (b) Mayo, S. L.; Ellis, W. R., Jr.; Crutchley, R. J.; Gray, H. B. *Science* **1986**, *233*, 948-952.

[9] (a) Yocum, K. M.; Shelton, J. B.; Shelton, J. R.; Schroeder, W. A.; Worosila, G.; Isied, S. S.; Bordignon, E.; Gray, H. B.; *Proc. Nat. Acad. Sci. USA* **1982**, *79*, 7052-7055. (b) Winkler, J. R.; Nocera, D. G.; Yocom, K. M.; Bordignon, E.; Gray, H. B. *J. Am. Chem. Soc.* **1982**, *104*, 5798-5800. (c) Yocom, K. M.; Winkler, J. R.; Nocera, D. G.; Bordignon, E.; Gray, H. B. *Chem. Scr.* **1983**, *21*, 29-33. (d) Kostic, N. M.; Margalit, R.; Che, C.-M.; Gray, H. B. *J. Am. Chem. Soc.* **1983**, *105*, 7765-7767. (e) Margalit, R.; Kostic, N. M.; Che, C.-M.; Blair,

D. F.; Chiang, H.-J.; Pecht, I.; Shelton, J. B.; Shelton, J. R.; Schroeder, W. A.; Gray, H. B. *Proc. Nat. Acad. Sci. USA* **1984**, *81*, 6554-6558. (f) Nocera, D. G.; Winkler, J. R.; Yocom, K. M.; Bordignon, E.; Gray, H. B. *J. Am. Chem. Soc.* **1984**, *106*, 5145-5150. (g) Crutchley, R. J.; Ellis, W. R., Jr.; Gray, H. B. *J. Am. Chem. Soc.* **1985**, *107*, 5002-5004. (h) Lieber, C. M.; Karas, J. L.; Gray, H. B. *J. Am. Chem. Soc.* **1987**, *109*, 3778-3779.

[10] (a) Crutchley, R. J.; Ellis, W. R.,Jr.; Gray, H. B. *Frontiers in Bioinorganic Chemistry*, Xavier, A. V., ed. VCH Verlagsgesellschaft: Weinheim, FRG, **1986**, pp. 679-693; (b) Crutchley, R. J.; Ellis, W. R., Jr.; Shelton, J. B.; Shelton, J. R.; Schroeder, W. A.; Gray, H. B., in preparation.

[11] Axup, A. W. Ph.D. Thesis, California Institute of Technology, Pasadena, CA, **1987**.

[12] (a) Isied, S. S.; Worosila, G.; Atherton, S. J. *J. Am. Chem. Soc.* **1982**, *104*, 7659-7661. (b) Isied, S. S.; Kuehn, C.; Worosila, G. *J. Am. Chem. Soc.* **1984**, *106*, 1722-1726. (c) Bechtold, R.; Gardineer, M. B.; Kazmi, A.; van Hemelryck, B.; Isied, S. S. *J. Phys. Chem.* **1986**, *90*, 3800-3804. (d) Bechtold, R.; Kuehn, C.; Lepre, C.; Isied, S. S. *Nature* **1986**, *322*, 286-288.

[13] (a) McGourty, J. L.; Blough, N. V.; Hoffman, B. M. *J. Am. Chem. Soc.* **1983**, *105*, 4470-4472. (b) Ho, P. S.; Sutoris, C.; Liang, N.; Margoliash, E.; Hoffman, B. M. *J. Am. Chem. Soc.* **1985**, *107*, 1070-1071. (c) Peterson-Kennedy, S. E.; McGourty, J. L.; Kalweit, J. A.; Hoffman, B. M. *J. Am. Chem. Soc.* **1986**, *108*, 1739-1746.

[14] Liang, N.; Pielak, G. J.; Mauk, A. G.; Smith, M.; Hoffman, B. M. *Proc. Nat.*

Acad. Sci. USA **1986**, *83*, 1249-1252.

[15] (a) Simolo, K. P.; McLendon, G. L.; Mauk, M. R.; Mauk, A. G. *J. Am. Chem. Soc.* **1984**, *106*, 5012-5013. (b) McLendon, G. L; Winkler, J. R.; Nocera, D. N.; Mauk, M. R.; Mauk, A. G.; Gray, H. B. *J. Am. Chem. Soc.* **1985**, *107*, 739-740. (c) McLendon, G.; Miller, S. R. *J. Am. Chem. Soc.* **1985**, *107*, 7811-7816. (d) Cheung, E.; Taylor, K.; Kornblatt, J. A.; English, A. M.; McLendon, G. L.; Miller, J. R. *Proc. Natl. Acad. Sci. USA* **1986**, *83*, 1330-1333. (e) Conklin, K. T.; McLendon, G. L. *Inorg. Chem.* **1986**, *25*, 4804-4806.

[16] (a) Williams, G.; Moore, G. R.; Williams, R. J. P. *Comments Inorg. Chem.* **1985**, *4*, 55-98. (b) Williams, R. J. P.; Concar, D. *Nature* **1986**, *322*, 213-214. (c) Pielak, G. J.; Concar, D. W.; Moore, G. R.; Williams, R. J. P. *Protein Engineering* **1987**, *1*, 83-88.

[17] Marcus, R. A.; Sutin, N. *Biochim. Biophys. Acta* **1985**, *811*, 265-322.

[18] Hopfield, J. J. *Proc. Natl. Acad. Sci. USA* **1974**, *71*, 3640-3644.

[19] Hush, N. S. *Coord. Chem. Rev.* **1985**, *64*, 135-157.

[20] Larsson, S. *J. Chem. Soc., Faraday Trans.* **1983**, *79*, 1375-1388.

[21] Scott, R. A.; Mauk, A. G.; Gray, H. B. *J. Chem. Educ.* **1985**, *62*, 932-938.

[22] Schilt, A. A.; Taylor, R. C. *J. Inorg. Chem.* **1959**, *9*, 211-221.

[23] Pfeiffer, P.; Werdelmann, B. *Z. Anorg. Allg. Chem.* **1950**, *263*, 31-38.

[24] Ford, P.; Rudd, De F. P.; Gaunder, R.; Taube, H. *J. Am. Chem. Soc.* **1968**, *90*, 1187-1194.

[25] Winter, A.; Perlmutter, H.; Davies, H. *Preparative Flat-Bed Electrofocusing in a Granulated Gel with the LKB 2117 Multiphor*, Application Note 198, revised **1980.**

[26] Adler, A. D.; Longo, F. R.; Kampas, F.; Kim, J. *J. Inorg. Nucl. Chem.* **1970**, *32*, 2443-2445.

[27] Doss, M. *Z. Klin. Chem. u. Klin. Biochem.* **1970**, *8*, 208-211.

[28] Teale, F. W. *Biochem. Biophys. Acta* **1959**, *35*, 543.

[29] Yonetani, T. *J. Biol. Chem.* **1967**, *242*, 5008-5013.

[30] Stryer, L. J. *J. Mol. Biol.* **1965**, *13*, 482-495.

[31] Leonard, J. J.; Yonetani, T.; Callis, J. B. *Biochemistry* **1974**, *13*, 1460-1464.

[32] LKB Ampholine polyacrylamide gel plates (PAG plates were used: pH range 3.5-9.5 (LKB 1804-101).

[33] After heme extraction, 17.2mg (A_{280} 0.355, ϵ 15.8mM^{-1}cm^{-1}, 17200 daltons (Edmundson, A. B.; Hirs, C. H. W. *J. Mol. Biol.* **1962**, *5*, 663-682), 45mL) of protein were available for reconstruction. The zinc mesoporphyrin was inserted, and following centrifugation and a Sephadex G-25 column, 17.5mg (A 0.403, 40mL) were recovered. The amount of reconstituted protein is in apomyoglobin equivalents (the zinc porphyrin is not included in the calculation).

[34] Elias, H.; Chou, M. H.; Winkler, J. R. *J. Am. Chem. Soc*, in press.

[35] Under pulsed laser experimental conditions, the a_5Ru(His)Mb(ZnP) samples are quite stable. The absorption spectra remain unchanged after 500 laser pulses. A

slow reversible decay amounting to about 10% of the transient optical density change is attributable to protein impurites.[30] The initial optical density is restored within one second of the excitation pulse (8 ns FWHM, 1 Hz repetition). In contrast, when using a broad-band, microsecond excitation source, the sample undergoes significant decomposition (~50%) within five flashes.

[36] Samples were treated with sodium dithionite in an inert atmosphere box. Excess dithionite was removed by four cycles of concentration and dilution with an Amicon ultrafiltration unit.

[37] The results of more extensive studies of the effects of temperature on electron-transfer rates in a_5RuMb(ZnP) and a_5RuMb(MgP) derivatives are discussed elsewhere: Cowan, J. A.; Upmacis, R. K.; Gray, H. B. *Recl. Trav. Chim. Pays-Bas* **1987**, *106*, 289. Cowan, J. A.; Gray, H. B. *Chem. Scr.*, in press. Upmacis, R. K.; Gray, H. B., in preparation.

[38] The distance between Ru and Zn is d_m; the closest distance between the Ru ligand atoms (the five ring atoms of histidine and the five nitrogen atoms of the ammines) and the Zn ligand atoms (the five ring atoms of the histidine and the porphyrin-ring atoms) is d.

[39] Electron transfer should be facile at the van der Waals edge-edge contact because there are relatively low-lying imidazole to Ru^{3+} charge-transfer states that should interact strongly with the delocalized π-donor level of $^3ZnP^*$: Krogh-Jespersen, K.; Schugar, H. J., *Inorg. Chem.* **1984**, *23*, 4390-4393. Krogh-Jespersen, K.; Westbrook, J. D.; Potenza, J. A.; Schugar, H. J., *J. Am. Chem. Soc.*, in press.

[40] (a) Gelin, B. R.; Karplus, M. *Biochemistry* **1979**, *18*, 1256-1268. (b) Calculations were performed using BIOGRAF/III version 1.23: BIOGRAF was designed and written by S. L. Mayo, B. D. Olafson, and W. A. Goddard III.

[41] (a) Protein coordinates were obtained from Brookhaven Protein Data Bank: Bernstein, F. C.; Koetzle, T. F.; Williams, G. J. B.; Meyer, Jr., E. F.; Brice, M. D.; Rodgers, J. R.; Kennard, O.; Shimanouchi, T.; Tasumi, M. *J. Mol. Biol.* **1977**, *112*, 535-542. (b) Tuna cytochrome *c* (Trp-33 replaced by a_5Ru(His)) served as the structural model for the horse heart protein.

[42] Mottonen, J; Ringe, D.; Petsko, G. A., unpublished results.

[43] For comparison, the β's are 0.75 and 0.90Å^{-1} for the lower and upper d_m limits. The driving-force dependences of the electron-transfer rates indicate that λ is 2.15-2.40eV for Ru(His-48)Mb if β is 0.91Å^{-1}: Karas, J. L.; Lieber, C. M.; Gray, H. B. Abstracts , 193rd ACS National Meeting; Denver, CO; April 1987; INOR 149. *J. Am. Chem. Soc.*, submitted for publication.

[44] Calculations assuming a nearly optimal orientation indicate that Trp-14 could enhance the donor-acceptor electronic coupling: Onuchic, J. N.; Beratan, D. N. *J. Am. Chem. Soc.*, submitted for publication.

[45] Kuki, A.; Wolynes, P. G. *Science* **1987**, *236*, 1647-1652.

Table I. Electron-transfer rate constants for a_5Ru(His)Mb(ZnP) derivatives

Temp. 0°C (±0.1)	Mb(ZnP) $k_{obs}(=k_d)\times10^{-1}$ (s^{-1})	His-48 $k_{obs}(=k_f)\times10^{-4}$ (s^{-1})	His-81		His-116		His-12	
			k_{obs}[a] (s^{-1})	k_f[b] (s^{-1})	k_{obs}[a] (s^{-1})	k_f[b] (s^{-1})	k_{obs}[a] (s^{-1})	k_f[b] (s^{-1})
7.6	3.8 ± 0.5	5.4 ± 0.9	7.4 ± 0.2	3.6 ± 0.5	8.6 ± 0.6	4.8 ± 0.8	9.9 ± 0.7	6.1 ± 0.9
11.8	3.9 ± 0.4	6.2 ± 0.8	9.0 ± 1.3	5.1 ± 1.4	9.2 ± 0.4	5.4 ± 0.6	10.3 ± 0.3	6.4 ± 0.5
16.2	3.9 ± 0.3	6.2 ± 0.6	9.7 ± 0.8	5.8 ± 0.9	10.5 ± 0.2	6.6 ± 0.4	11.7 ± 0.3	7.8 ± 0.4
20.6	4.0 ± 0.3	6.3 ± 1.3	11.2 ± 1.0	7.3 ± 1.0	11.4 ± 1.2	7.5 ± 1.2	11.9 ± 1.6	8.0 ± 1.6
25.0	4.0 ± 0.2	7.0 ± 0.8	12.6 ± 1.2	8.6 ± 1.2	13.0 ± 0.2	8.9 ± 0.3	14.1 ± 1.1	10.1 ± 1.1
29.4	4.1 ± 0.2	7.7 ± 1.4	13.8 ± 0.5	9.7 ± 0.5	14.4 ± 0.7	10.3 ± 0.7	15.7 ± 1.9	11.6 ± 1.9
34.0	4.2 ± 0.2	8.0 ± 1.0	15.2 ± 2.2	11.0 ± 2.2	15.9 ± 0.1	11.7 ± 0.2	17.4 ± 0.5	13.3 ± 0.5
38.6	4.2 ± 0.1	8.1 ± 1.4	17.2 ± 2.1	13.0 ± 2.1	18.3 ± 2.2	14.1 ± 2.2	19.2 ± 1.7	15.0 ± 1.7

a. $k_{obs}\times10^{-1}$.
b. $k_f\times10^{-1}$.

Table II. Electron-transfer distances for ruthenated heme proteins.[a]		
Derivative	d range (Å)	d_m range (Å)
a_5Ru(His-33)cyt c	10.8-11.7 [11.6]	16.1-18.8 [18.3]
a_5Ru(His-48)Mb	11.8-16.6 [12.7]	16.6-23.9 [17.1]
a_5Ru(His-81)Mb	18.8-19.3 [19.3]	24.1-26.6 [25.1]
a_5Ru(His-116)Mb	19.8-20.4 [20.1]	26.8-27.8 [27.7]
a_5Ru(His-12)Mb	21.5-22.3 [22.0]	27.8-30.5 [29.3]

a. The distances are lower and upper values at 6.5 kcal above the potential energy minimum. The value at the minimum is in brackets.

Figure 1.

(a) Time-resolved 414 nm transient absorption of a_5Ru(His-48)Mb(ZnP) at 25°C following 532 nm laser excitation; (b) analysis of a_5Ru(His-48)Mb(ZnP) data (monophasic, first-order, nonzero endpoint).

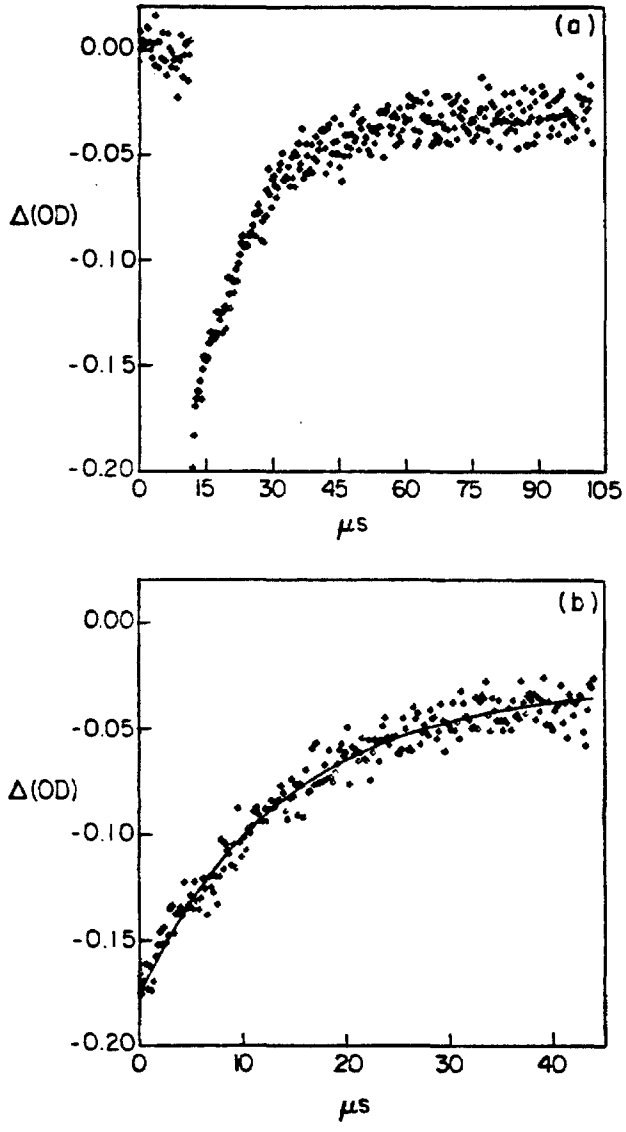
(a)
0.00
-0.05
-0.10
-0.15
-0.20
Δ(OD)
0
15
30
45
60
75
90
105
μs
(b)
0.00
-0.05
-0.10
-0.15
-0.20
Δ(OD)
0
10
20
30
40
μs

Figure 2.

View of the heme and the surface histidines that are modified in the four ruthenated myoglobins.

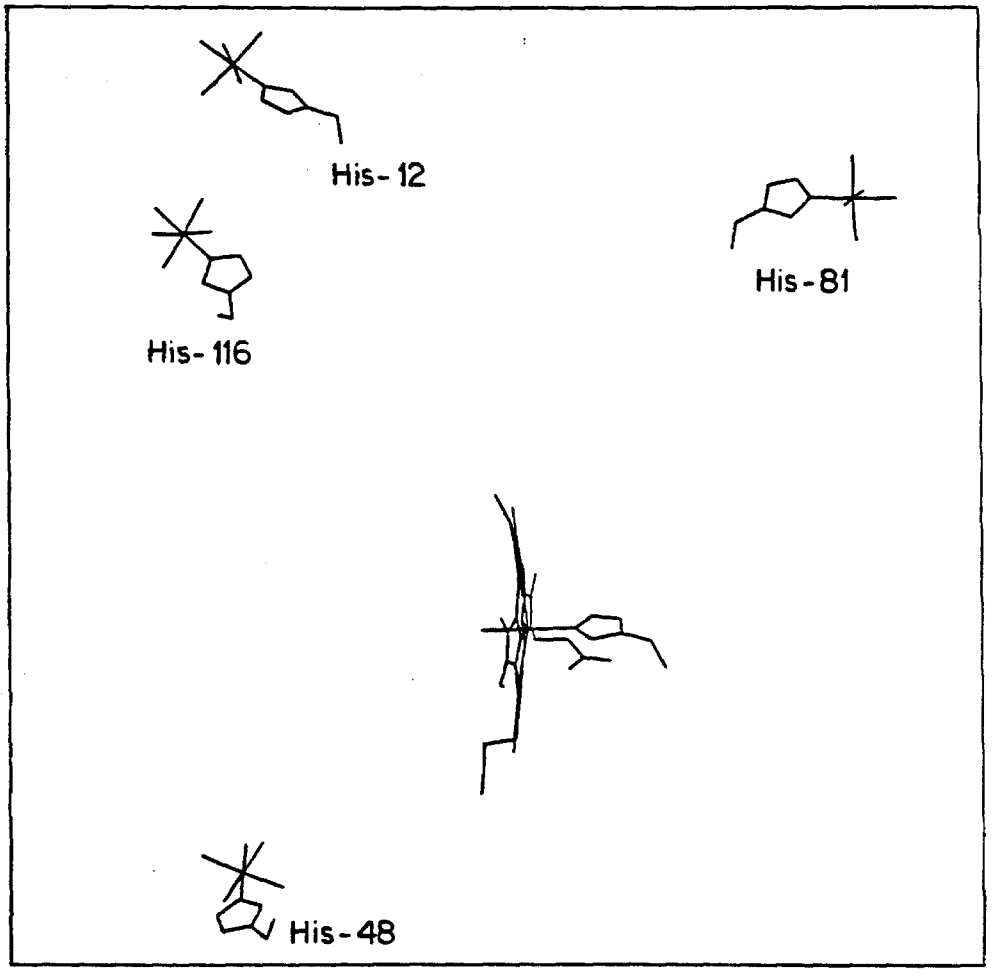
His-12
His-116
His-81
His-48

Figure 3.

Distance dependence of $\ln k_f$: 33, a_5Ru(His-33)cyt*c*(ZnP); other numbers are the a_5Ru(His)Mb(ZnP) derivatives. The lines are least-squares fits to 6.5 kcal lower-limit/upper-limit (- - - -) and minimum-energy (——) d values.

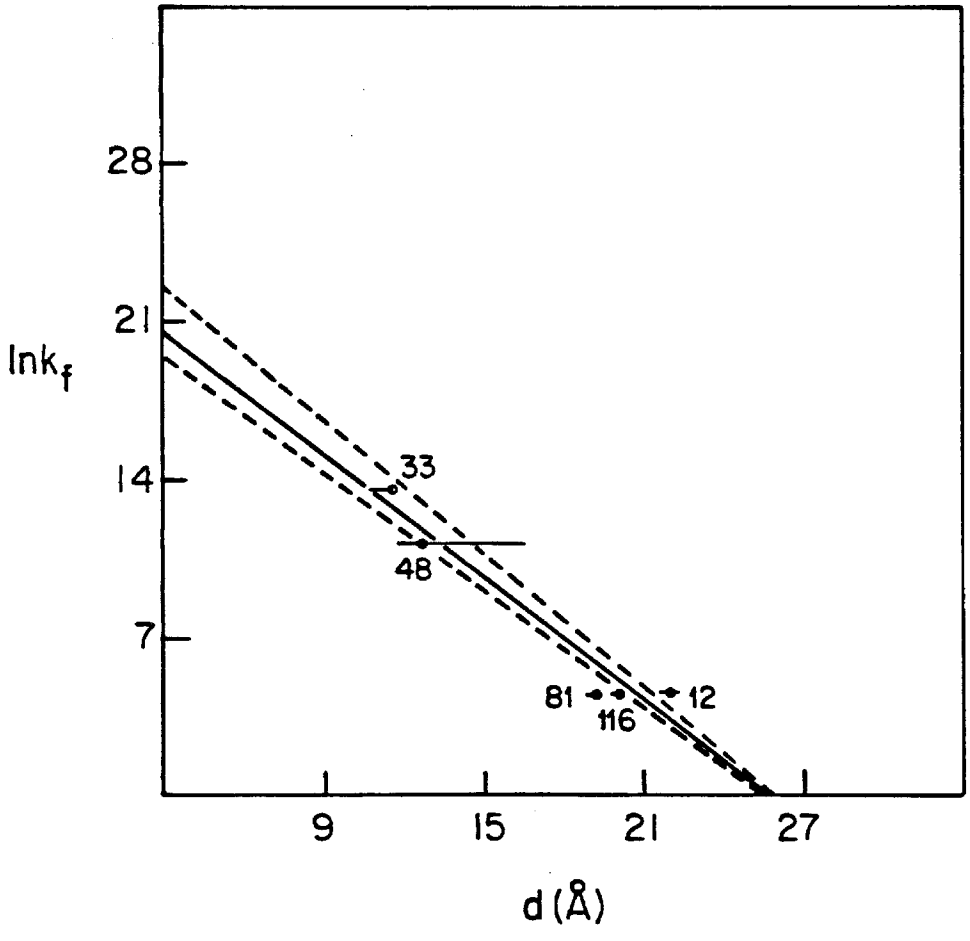
28
21
14
7
lnk$_f$
33
48
81
116
12
9
15
21
27
d (Å)

Figure 4.

View of the Trp-14 between the porphyrin and Ru(His-12)$^{3+}$ in a_5Ru(His-12)Mb.

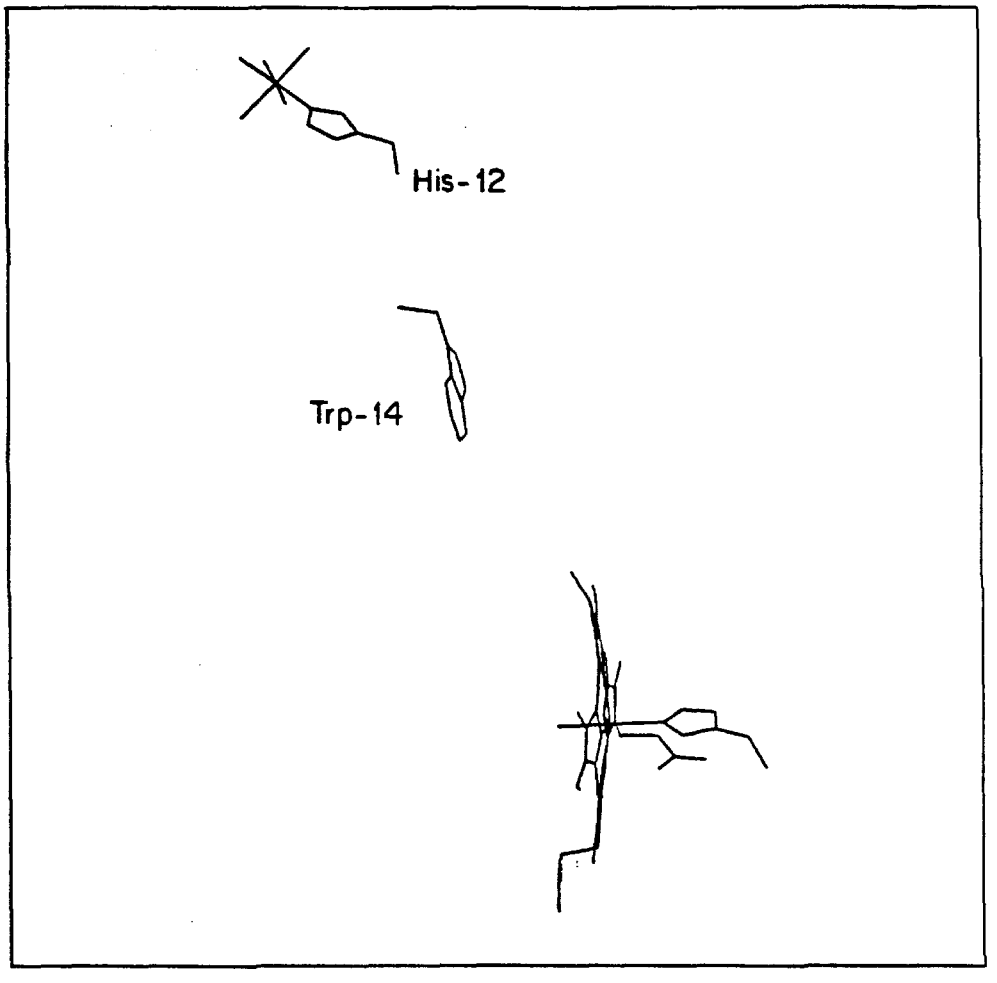
His-12
Trp-14

Long-Range Electron Transfer in Ruthenium-Modified Proteins

Charles M. Lieber, Jennifer L. Karas, Stephen L. Mayo,

Michael Albin, and Harry B. Gray

Contribution No. 7677 from the Arthur Amos Noyes Laboratory of Chemical Physics, California Institute of Technology, Pasadena, California 91125

Introduction

Long-range electron-transfer (ET) reactions are important mechanistic steps in many biological processes.[1,2,3,4,5] Research in our laboratory in this area is focused on elucidating the factors that control ET processes in fixed-distance donor-acceptor (D-A) molecules.[5,6,7,8,9] The ET process in a D-A molecule, D-A$\rightarrow$D$^+$-A$^-$, can be described in terms of classical Marcus theory.[2] The ET rate (k_{ET}), $k_{ET}=\Gamma\exp(-\Delta G^*/RT)$, contains an electronic term, Γ, and a free-energy term, ΔG^* (Eqns. 1a and 1b, respectively).

1a. $\Gamma=10^{13}\exp(-\beta(d-3))s^{-1}$

1b. $\Delta G^*=(\Delta G^\circ+\lambda)^2/4\lambda$

The electron part, Eqn. 1a., is the product of a frequency factor (barrier crossing rate) and an exponential decay. The exponential decay reflects the decrease in D-A electronic coupling with distance (d), and the rate of this decay is given by the parameter β. The activation energy factor ΔG^* (Eqn. 1b) is dependent on the overall reaction free energy (or driving force), ΔG°, and the reorganization energy, λ. With this theorectical framework as a guide, we have investigated the dependence of the ET rate on ΔG° and d, using the experiments described below.

Experimental System

The approach that we employ to prepare our D-A molecules involves covalently linking a redox-active ruthenium complex to a surface histidine of a crystallographically characterized metalloprotein.[5,6,7,8,9] Using this strategy, it possible to prepare D-A

systems in which the ET distance and intervening medium are known. In addition, we can tune the reaction free energy through systematic changes in the ruthenium complex.

A particularly attractive metalloprotein system for ET studies is sperm whale myoglobin (Mb). This structurally characterized heme protein has four surface histidine residues that lie between 13 and 22Å from the heme center (Figure 1).[10]

These four histidine residues have been modified with several different ruthenium reagents using procedures developed in our laboratory.[6,7,8] For example, pentaammineruthenium (a_5Ru) has been attached to each of the histidine residues in Mb (Figure 2).[11] Native Mb is reacted with excess $a_5Ru^{2+}(OH_2)$ to form singly and multiply labeled species. The singly modified derivatives are separated from unreacted and multiply labeled Mb using preparative IEF, and the four isomerically pure Ru(His-X)Mb species are isolated using cation-exchange chromaography. The specific labeling sites have been identified by peptide mapping and proton NMR studies.

An assumption important in the analysis of our data is that the ruthenium group does not perturb the native crystal structure. Spectroscopic evidence (UV-Vis, CD, EPR) has been used to support this contention; in addition, the recent structural determination of a_5Ru(His-48)Mb[12] demonstrates that the native and ruthenium-modified structures are virtually the same (Figure 3). Therefore, we can prepare ruthenium-modified Mb with one Ru per molecule attached to a specific histidine residue (any one of the four) at a known distance. In the following sections we will discuss the results we have obtained in studying ET in these systems.

Distance Dependence

Our intial studies[6a,c] with a_5Ru(His-48)MbFe (Fe denotes the native heme center) indicated that a large driving force would be required to study ET to the three long-distance sites (histidines 12, 81, and 116). The driving force in the heme system is only 20mV.

To prepare a high driving force system, we have removed the heme in Mb and replaced it with a photactive porphyrin, Zn(mesoporphyrin IX) (ZnP). The triplet excited state of ZnP (ZnP*) is long-lived and highly reducing, properties that are ideal for distance studes. The ET rates in these systems can be determined by monitoring the change in the ground-state Soret absorbance, as outlined in Scheme 1.

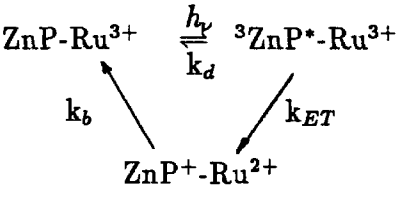

Scheme 1

Pulsed laser excitation generates ZnP*, which subsequently returns to the ground state via nonradiative decay and ET pathways. Since $k_b > k_{ET}$, the observed decay rate is equal to $k_D + k_{ET}$. The driving force for this reaction is 0.88(10)V.[9,13]

The exponential damping factor β (Eqn. 1a) can be determined from a plot of $\ln(k_{ET})$ *vs.* d: $\ln(k_{ET})=-\beta(d-3)+\text{constant}$; however, the actual value of d requires some discussion. The through-space ET distance can be evaluated by several methods including measurement of the edge-edge (E-E) and metal-metal (M-M) distances. The E-E distance corresponds to that measured from the edge of the porphyrin ring

to the edge of the histidine imidazole to which ruthenium is bound. The actual E-E and M-M distances used in the following analysis have been determined from a rigid body conformational search of the ruthenium-modified proteins; the uncertainty in distance was taken to be the variation found at 0.3eV above the calculated potential minimum.[11b]

The E-E and M-M $\ln(k_{ET})$ *vs.* distance plots using our experimental data and the results for a_5Ru-modified Zn-substituted cytochrome c[13] are shown in Figure 4. The β limits determined from least-squares analyses of 4a and 4b are 0.87-0.99 and 0.73-0.90Å^{-1}, respectively.[9] These two β ranges overlap somewhat, indicating that the method of defining the site-to-site distance is not that crucial in our system. One question of interest[14,15,16] is whether ET is facilitated by an aromatic group in the medium separating the donor and acceptor. Since there is some evidence that the ET rate determined for a_5Ru(His-12)Mb is enhanced via electronic interactions with the Trp-14 residue that lies in the ET pathway (Figure 5),[14] we have replotted Figures 4a and 4b without the His-12 data (Figure 6). The limits on β obtained from least-squares analysis of E-E (6a) and M-M (6b) plots are 0.99-1.12 and 0.84-1.09Å^{-1}.[17] The larger β extracted from these plots indicates a less efficient D-A electronic coupling at long range. With the limited data we have, however, we cannot say firmly that the ET rate in a_5Ru(His-12)Mb is enhanced by the medium.

In summary, the unbiased range of β determined using all of our experimental points and E-E distances is 0.87-0.99Å^{-1}. Although both E-E and M-M plots have been used to evaluate β, we favor the E-E measurement because the ZnP excited state is delocalized and because the ruthenium and imidazole wavefunctions interact strongly.[18] Additional work on the distance dependence (i.e., more points) and the influence of the medium (e.g., Trp-14 question) is needed to explore these

issues more fully. Studies employing site-directed mutagenesis to prepare systems that can address these points are currently in progress in our laboratory (i.e., we plan to introduce histidines at varying distance and with specific residues in the ET pathway).

Reorganization Energy

In this section we report investigations of the dependence of k_{ET} on driving force, which have allowed us to estimate the reorganization energy in the myoglobin system. Our experimental approach involves changing the redox potential of either D or A to vary $\Delta G°$, using substituted ruthenium complexes of the general form a_4LRu- (L=ammine (a), pyridine (py), etc.) and/or different metal-porphyrin centers.

Using flash photolysis, we have measured the Fe^{2+} to Ru^{3+} ET rates in myoglobin that had been modified at histidine-48 with a_5Ru and a_4pyRu: Ru^{3+}(His-48)$MbFe^{2+} \rightarrow Ru^{2+}$(His-48)$MbFe^{3+}$.[6a,c] Although the increase in rate, 0.04 to 2.5s^{-1}, observed when changing from the a_5Ru^{3+} acceptor ($\Delta E°$=0.02V) to a_4pyRu^{3+} ($\Delta E°$ =0.275V), agrees with that predicted by Marcus theory (Figure 7), with only two experimental points we cannot distinguish between small (1ev) and large (2eV) values of λ. ET experiments at higher driving forces would be especially helpful, because the change in rate for a well-defined step in driving force (i.e., a_5Ru to a_4pyRu) at an overall $\Delta G°$ near 1V is predicted to be small for the λ=1eV curve and significantly larger for λ=2eV.

To address this problem, we have replaced the heme in the above two ruthenium-modified derivatives with Pd(mesoporphyrin IX) (PdP).[6b] PdP possesses a highly reducing excited state (PdP*) and therefore can be used to study ET in ruthenium-

modified (His-48)Mb at much larger $\Delta E°$'s. The ET rates, Ru^{3+}(His-48)MbPdP* $\rightarrow$ Ru^{2+}(His-48)MbPdP$^+$, in the a_5Ru ($\Delta E°$=0.72(10)V) and $a_4$pyRu ($\Delta E°$=0.98(10)V) systems were determined by monitoring the quenching of the PdP* emission following pulsed laser excitation.

These kinetic results are displayed in a Marcus free-energy plot (Figure 8) together with theoretical curves for three values of λ. It is apparent that the reorganization energy is large; the experimental limits on λ for the myoglobin system are 1.90-2.45eV. Recent reports indicate that λ is also large in ruthenium-modified/zinc-cytochrome c[13] and in [Zn,Fe] hybrid hemoglobin.[19] We believe that the large λ values for ruthenium-modified myoglobin and cytochrome c are due mainly to the large changes in the structure of the aqueous medium around the redox sites that accompany electron transfer. Our analysis of these fixed-distance systems indicates that the outer-sphere (solvation) contribution to the λ for ET in RuMb is greater than commonly assumed.

There are several important conclusions to be drawn from this work. Since the electron-transfer rate is strongly dependent on the magnitude of λ, we suggest that long-range ET reactions may be controlled through variations in the reorganization energy. The large degree of control potentially available is illustrated by the calculated values of k_{ET} set out in Figure 9. The calculations were made using our experimentally determined value of β (0.91Å^{-1}). It may be possible by judicious use of this table to extract ET rates from estimated distances or ET distances from rates in systems that are not completely characterized. The strikingly large variations in k_{ET} at constant d and $\Delta G°$ indicate that specificity in biological ET reactions could be achieved through changes in the reorganization energy. We are currenlty investigating this matter through the synthesis of systems in which the redox-active

metal complex has a substantially lower λ than the ruthenium complexes used in this study.

Acknowledgments

Our research on metalloprotein electron-transfer reactions is supported by grants from the National Science Foundation and the National Institutes of Health. S.L.M. acknowledges a predoctoral fellowship from AT&T Bell Laboratories; C.M.L. held an NIH postdoctoral fellowship during 1985-87. This is contribution no. 7677 from the Arthur Amos Noyes Laboratory.

References

[1] (a) Hatefi, Y. *Annu. Rev. Biochm.* **1985**, *54*, 1015. (b) Dixit, B. P. S. N.; Vanderkooi, J. M. *Curr. Top. Bioenerg.* **1984**, *13*, 159.

[2] (a) Marcus, R. A.; Sutin, N. Biochim. Biophys. Acta **1985**, *811*, 265. (b) D. DeVault *Quantum-Mechanical Tunneling in Biological Systems*, Cambridge Univ. Press, Cambridge, ed. 2, **1984**.

[3] McLendon, G.; Gauarr, T.; McGuire, M.; Simolo, K.; Strauch, S.; Taylor, K. *Coord. Chem. Rev.* **1985**, *64*, 113.

[4] Peterson-Kennedy, S. E.; McGourty, J. L.; Ho, P. S.; Sutoris, C. J.; Liang, N.; Zemel, H.; Blough, N. V.; Margoliash, E.; Hoffman, B. M. *Coord. Chem. Rev.* **1985**, *64*, 125.

[5] (a) Mayo, S. L.; Ellis, W. R., Jr.; Crutchley, R. J.; Gray, H. B. *Science* **1986**, *233*, 948. (b) Gray, H. B. *Chem. Soc. Rev.* **1986**, *15*, 17.

[6] (a) Lieber, C. M.; Karas, J. L.; Gray, H. B. *J. Am. Chem. Soc.* **1987**, *109*, 3778. (b) Karas, J. L.; Lieber, C. M.; Gray, H. B. *J. Am. Chem. Soc.*, in press. (c) Crutchley, R. J.; Ellis, W. R., Jr.; Gray, H. B. *J. Am. Chem. Soc.* **1986**, *107*, 5002. (d) Crutchley, R. J.; Ellis, W. R., Jr.; Gray, H. B. *Frontiers in Bioinorganic Chemistry*, Xavier, A. V., ed., VCH Verlagsgesellschaft, Weinheim, FRG, **1986**.

[7] (a) Yocom., K. M.; Shelton, J. B.; Shelton, J. R.; Schroeder, W. A.; Worosila, G.; Isied, S. S.; Bordignon, E.; Gray, H. B. *Proc. Natl. Acad. Sci. USA* **1982**, *79*, 7052. (b) Nocera, D. G.; Winkler, J. R.; Yocom, K. M.; Bordignon, E.; Gray,

H. B. *J. Am. Chem. Soc.* **1984**, *106*, 5145. (c) Isied, S. S.; Kuehn, C.; Worosila, G. *J. Am. Chem. Soc.* **1984**, *106*, 1722.

[8] (a) Kostic, N. M.; Margalit, R.; Che, C.-M.; Gray, H. B. *J. Am. Chem. Soc.* **1983**, *105*, 7765. (b) Margalit, R.; Kostic, N. M.; Che, C.-M.; D.; Chiang, H.-J.; Pecht, I.; Shelton, J. B.; Shelton, J. R.; Schroeder, W. A.; Gray, H. B. *Proc. Natl. Acad. Sci. USA* **1984**, *81*, 6554.

[9] Axup, A. W.; Albin, M.; Mayo, S. L.; Crutchley, R. J.; Gray, H. B. *J. Am. Chem. Soc.*, in press.

[10] Protein coordinates were obtained from Brookhaven Protein Data Bank: Bernstein, F. C.; Koetzle, T. F.; Williams, G. J. B.; Meyer, E. F., Jr.; Brice, M. D.; Rodgers, J. R.; Kennard, O.; Shimanouchi, T.; Tasumi, M. *J. Mol. Biol.* **1977**, *112*, 535.

[11] (a) Gelin B. R.; Karplus, M. *Biochemistry* **1979**, *18*, 1256. (b) Calculations were performed using BIOGRAF/III version 1.21: BIOGRAF was designed and written by S. L. Mayo, B. D. Olafson, and W. A. Goddard III.

[12] Mottonen, J.; Ringe, D.; Petsko, G. unpublished results.

[13] Elias, H.; Chou, M. H.; Winkler, J. R. *J. Am. Chem. Soc.*, in press.

[14] Calculations assuming a nearly optimal orientation indicate that Trp-14 could enhance the donor-acceptor electronic coupling: Onuchic J. N.; Beratan, D. N. *J. Am. Chem. Soc.*, submitted for publication.

[15] Kuki A.; Wolynes, P. G. *Science* **1987**, *236*, 1647.

[16] Liang, N.; Pielak, G. J.; Mauk, A. G.; Smith, M.; Hoffman, B. M. *Proc. Natl. Acad. Sci. USA* **1986**, *83*, 1249.

[17] Mayo, S. L. unpublished results.

[18] Krogh-Jespersen, K.; Westbrook, J. D.; Potenza, J. A.; Schugar, H. J. *J. Am. Chem. Soc.*, in press.

[19] Peterson-Kennedy, S. E.; McGourty, J. L.; Kalweit, J. A.; Hoffman, B. M. *J. Am. Chem. Soc.* **1986**, *108*, 1739.

Figure 1.

Computer graphics projection of the four histidines of sperm whale myoglobin[10] that bind ruthenium in the form a_4LRu-(L=ammine (a), pyridine (py), etc.). The edge-edge donor-acceptor distances for these residues range from approximately 13Å for His-48 to 22Å for His-12. The histidines are shown along with the C_α protein trace and the heme center with its proximal histidine ligand.

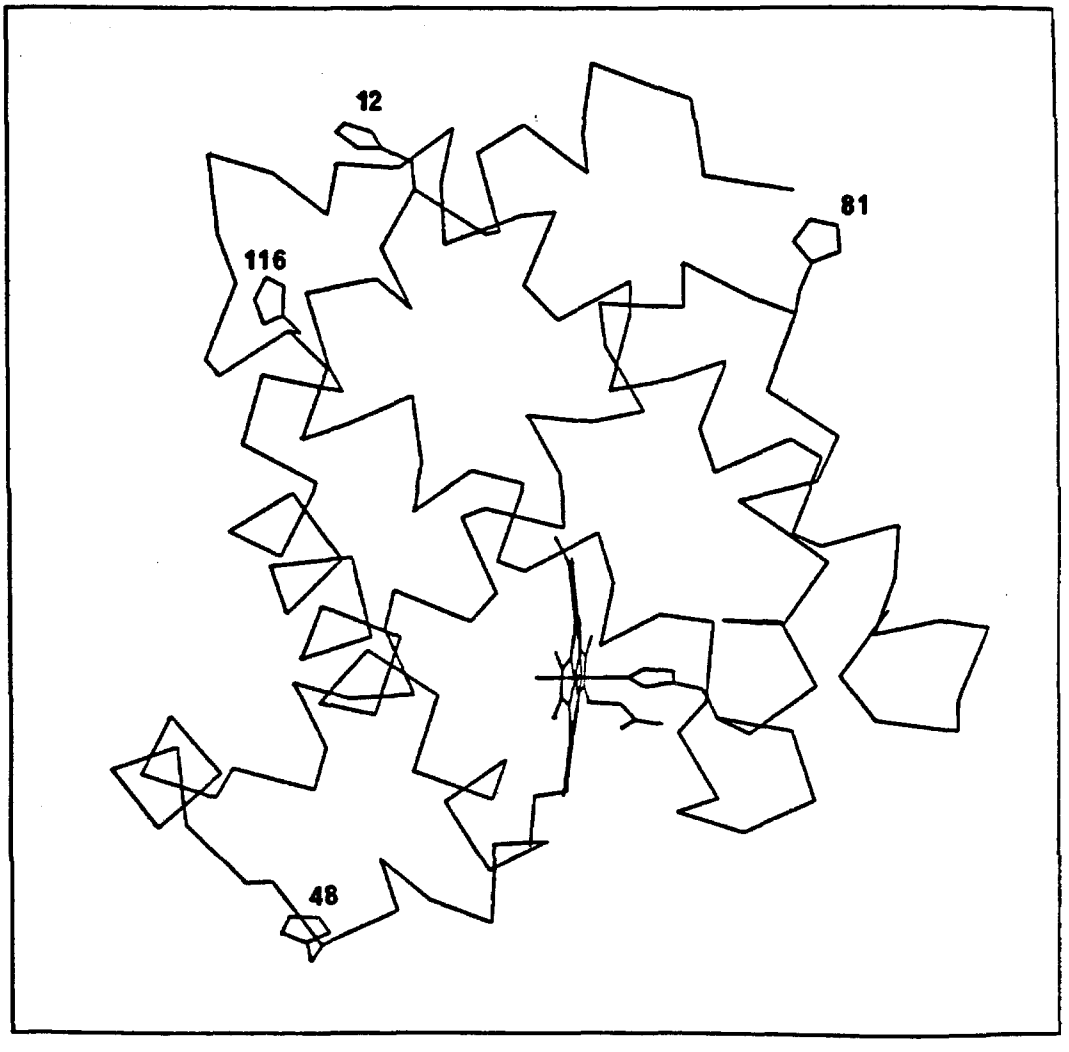
12
81
116
48

Figure 2.

Computer graphics projection showing the juxtaposition of the four a_5Ru(His-X) derivatives and the native redox center. In order to determine electron-transfer distances for these derivatives, each was optimized using a rigid-body conformational search routine.[11] The searches were performed by evaluating the van der Waals energy of the 10^4 unique conformations of each modified residue that are generated by successively incrementing each of the two histidine (modified with a_5Ru) sidechain dihedrals (C_α-C_β and C_β-C_γ) by 3.6°. The calculation included only the van der Waals contribution of those atoms within 8.5Å of the ruthenated histidine in each conformation. Pseudopotential-energy surfaces were then obtained by plotting conformational energy *vs.* electron-transfer distance. A comparison of the experimental structure[12] of a_5Ru(His-48)Mb reveals an uncertainty of at least 0.3eV in our calculations. That is, the experimental metal-metal (Ru-Fe) distance of 24Å falls on our potential-energy surface approximately 0.3eV above the calculated minimum. The distance ranges in our analysis of the rates reflect this 0.3eV uncertainty as summarized below.

ET Distances in Ruthenium-Modified Myoglobin[a]

Site (His-X)	M-M (Å)	E-E (Å)
48	16.6-23.9 (17.1)	11.8-16.6 (12.7)
81	24.1-26.6 (25.1)	18.8-19.3 (19.3)
116	26.8-27.8 (27.7)	19.8-20.4 (20.1)
12	27.8-30.5 (29.3)	21.5-22.3 (22.0)

a) Distance at potential minimum in parentheses.

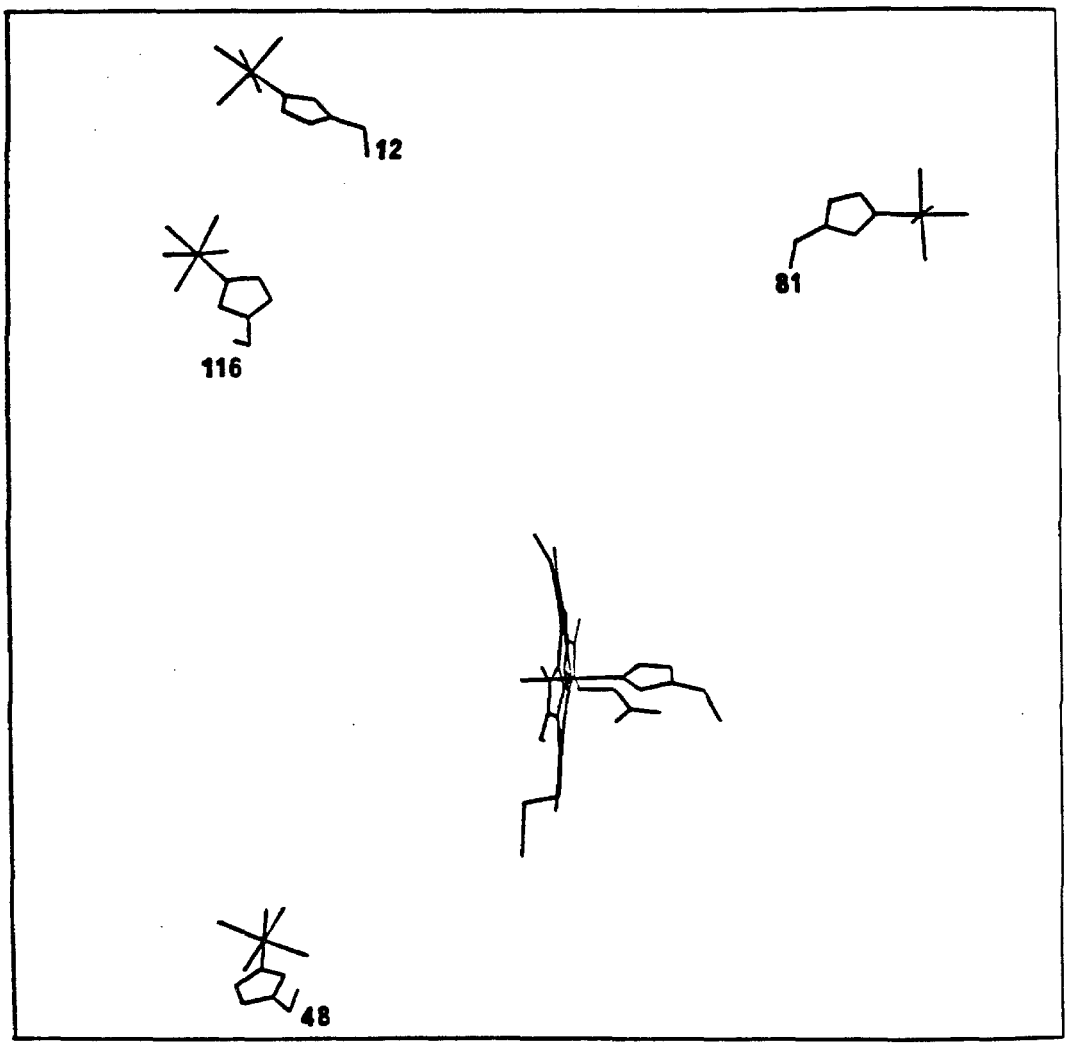
12
116
81
48

Figure 3.

Computer graphics projections comparing the native Mb structure and the a_5Ru(His-48)Mb structure.[12] The structures were matched by performing a least-squares fit of the C_α carbons. This comparison demonstrates that the native and ruthenium-modified structures are virtually the same with the exception of the expected rotation of the a_5Ru(His-48) side chain away from the protein (this rotation is expected because of the steric congestion in the region of His-48). (a) Comparision of C_α traces and native redox centers. (b) Zoom on region of His-48 showing both the native and modified conformations of the histidine.

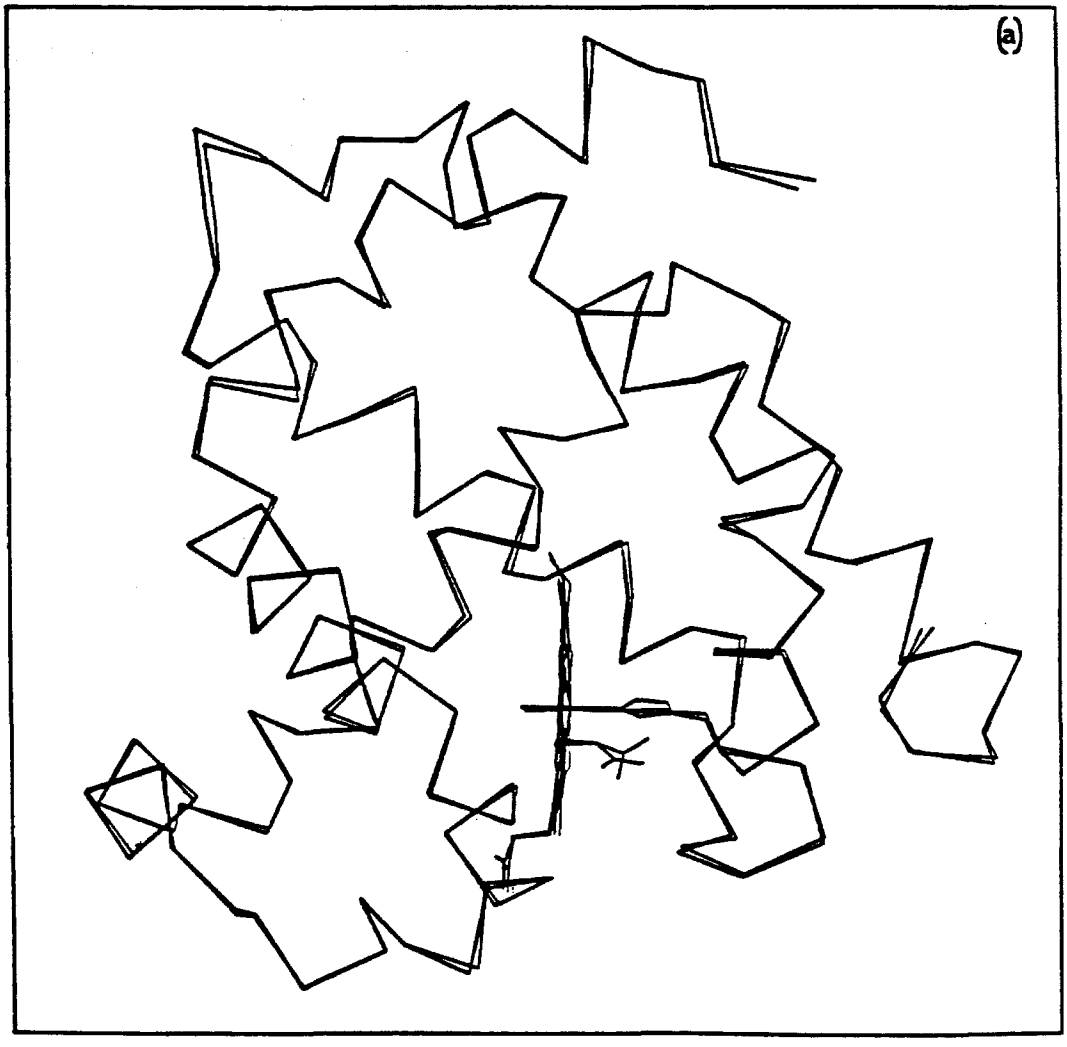
(a)

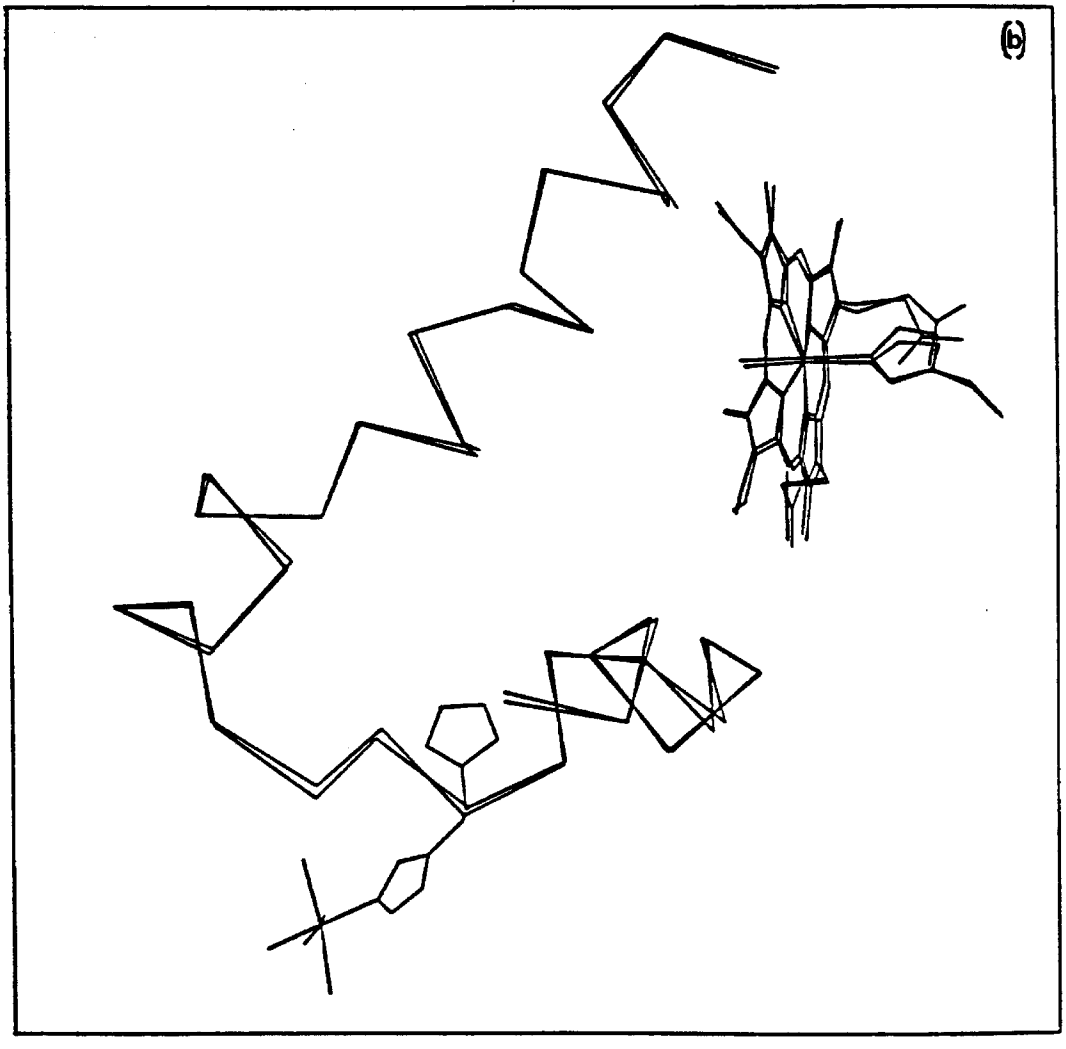
(b)

Figure 4.

Distance dependence of $\ln k_f$: 33, a_5Ru(His-33)cyt*c*(ZnP); other numbers are the a_5Ru(His-X)Mb(ZnP) derivatives. The lines are least-squares fits to 0.3eV lower-limit/upper-limit (- - -) and minimum energy (——) distance values. (a) Distance dependence of $\ln k_f$, using E-E distance values. The range of β obtained is 0.87-0.99Å^{-1}. (b) Distance dependence of $\ln k_f$ using M-M distance values. The range of β is 0.73-0.90Å^{-1}. (c) In order to illustrate the steepness of the calculated potential surfaces above 0.3eV, we plotted the distance dependence of $\ln k_f$ using E-E distance values obtained at 1eV above the energy minimum for each derivative. As can be seen from the plot, the range of β (0.86-0.99Å^{-1} is essentially unaffected by this variation.

(a) Edge-Edge at 0.3 eV

beta upper	:	0.99
pre-ex upper (d-3)	:	5.8E+09
beta middle	:	0.91
pre-ex middle (d-3)	:	7.8E+08
beta lower	:	0.87
pre-ex lower (d-3)	:	2.8E+08

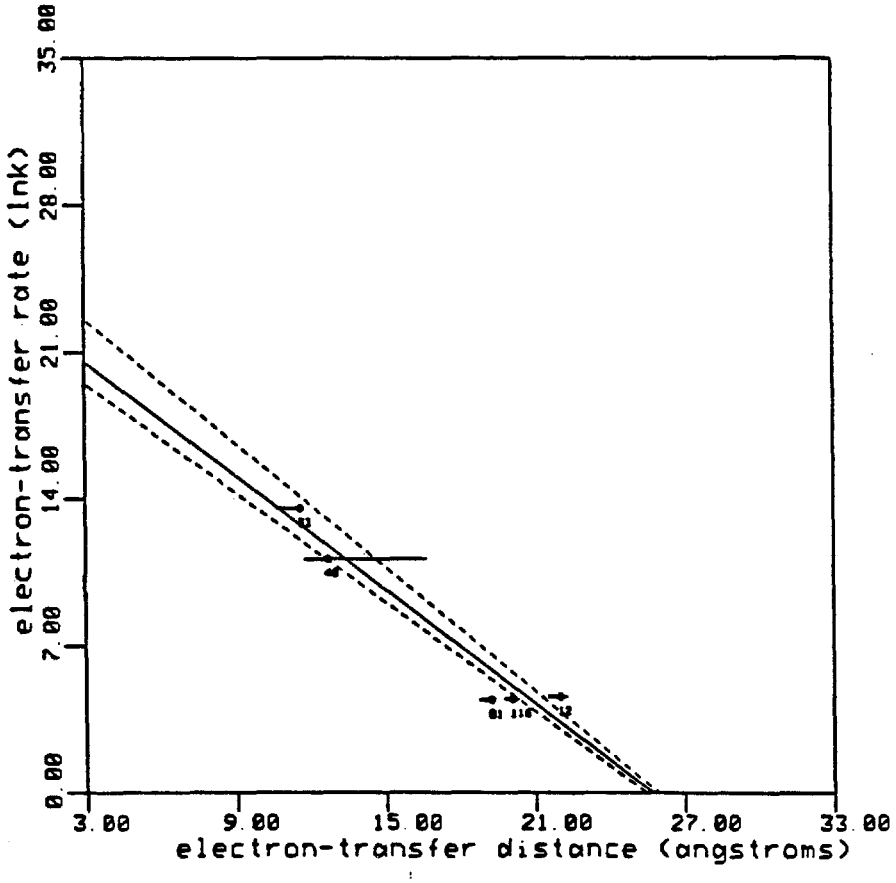

(b) Metal-Metal at 0.3 eV

beta upper : 0.90

beta middle : 0.73

beta lower : 0.75

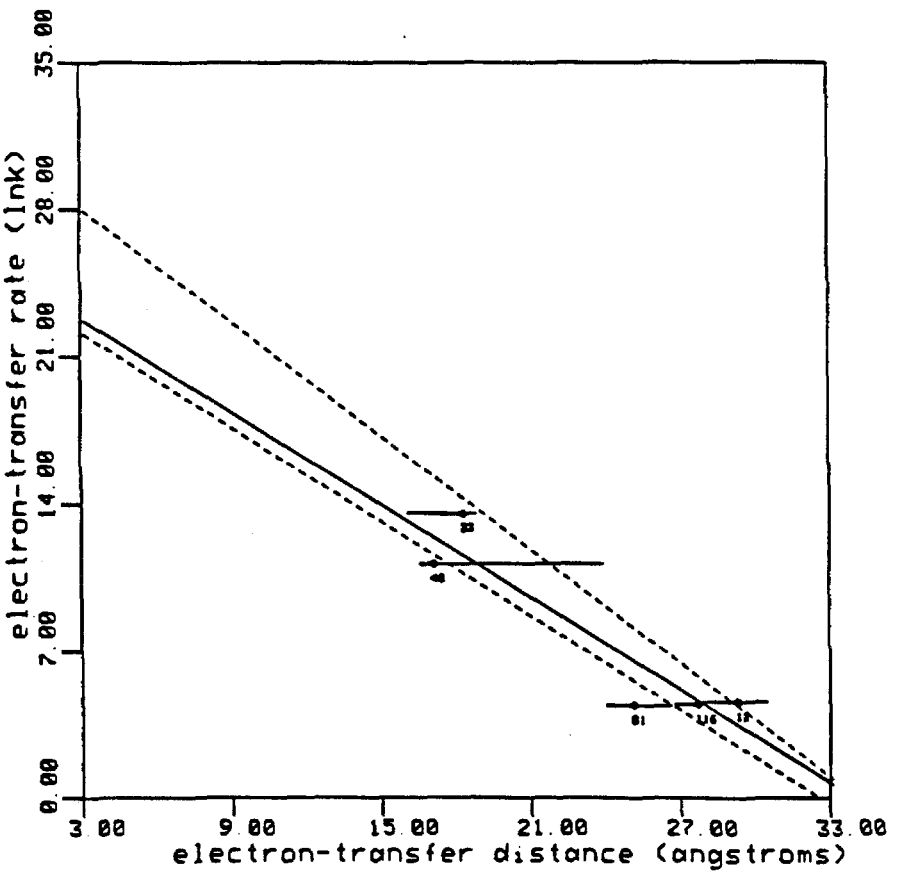

(c) Edge-Edge at 1 eV

beta upper	:	0.99
pre-ex upper (d-3)	:	5.8E+09
beta middle	:	0.91
pre-ex middle (d-3)	:	7.8E+08
beta lower	:	0.86
pre-ex lower (d-3)	:	1.6E+08

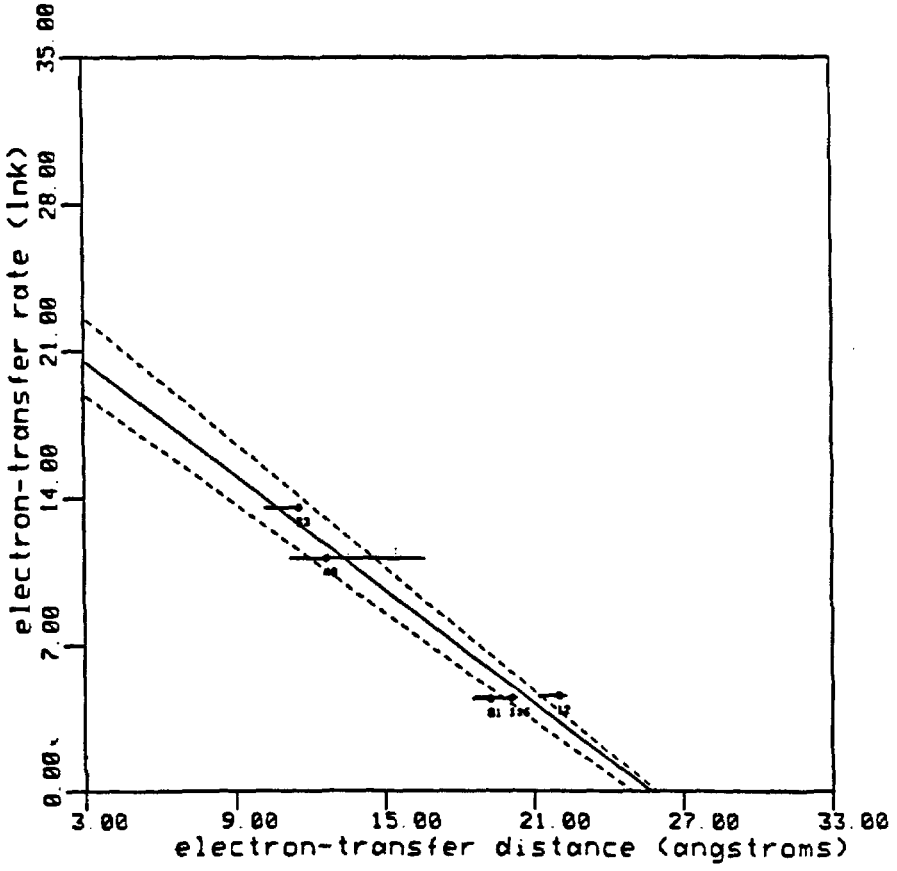

Figure 5.

Computer graphics projection of the Trp-14 aromatic group between the porphyrin and a_5Ru(His-12). The presence of this group raised the possibility that weak ^{3}ZnP*(Trp-14)a_5Ru(His-12)$^{3+}$ charge-transfer interactions might facilitate electron transfer.[14] However, an extensive theoretical analysis of the ZnP to a_5Ru(His-12) pathway by Kuki and Wolynes[15] does not support a special rote for the intervening tryptophan, and the relatively small departure of the His-12 derivative from the rate-distance correlation (Figure 4) may have an entirely different origin. Hoffman and coworkers have found only minor effects on cytochrome *c* peroxidase (^{3}ZnP*):cytochrome *c*(Fe^{3+}) long-range electron-transfer rates upon changing Phe-82 in cyt*c* to other residues, although dramatic differences in the reverse-direction transfers (Fe^{2+} to ZnP^+) were observed.[16]

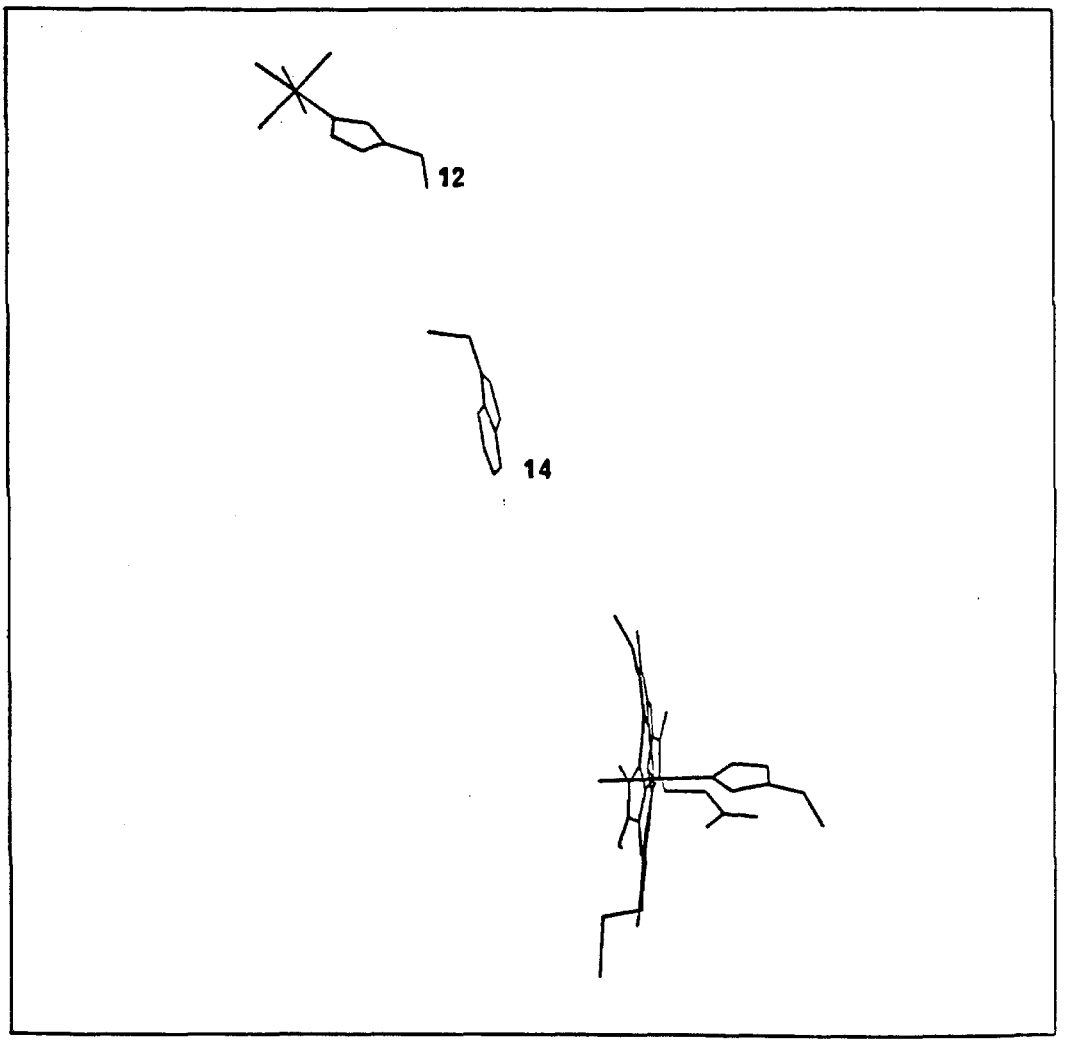
12
14

Figure 6.

Distance dependence of $\ln k_f$: 33, a_5Ru(His-33)cyt*c*(ZnP); other numbers are the a_5Ru(His-X)Mb(ZnP) derivatives. The lines are least-squares fits to 0.3eV lower-limit/upper-limit (- - -) and minimum energy (——) distance values. (a) Distance dependence of $\ln k_f$ using E-E distance values excluding the Mb His-12 data. The range of β obtained is 0.99-1.12Å^{-1}. (b) Distance dependence of $\ln k_f$ using M-M distance values excluding the Mb His-12 data. The range of β is 0.84-1.09Å^{-1}.

(a) Edge-Edge at 0.3 eV (w/o myo+hru12)

beta upper	:	1.12
pre-ex upper (d-3)	:	3.0E+10
beta middle	:	1.05
pre-ex middle (d-3)	:	3.6E+09
beta lower	:	0.99
pre-ex lower (d-3)	:	9.3E+08

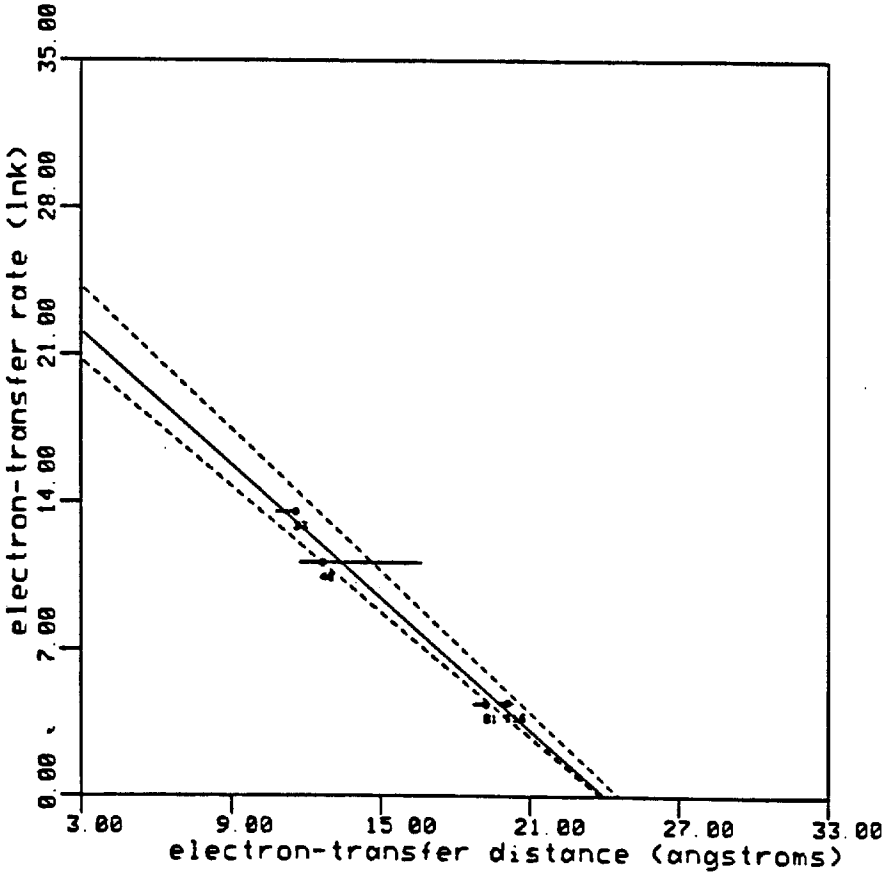

(b) Metal-Metal at 0.3 eV (w/o myo+hru12)

beta upper : 1.09

beta middle : 0.84

beta lower : 0.84

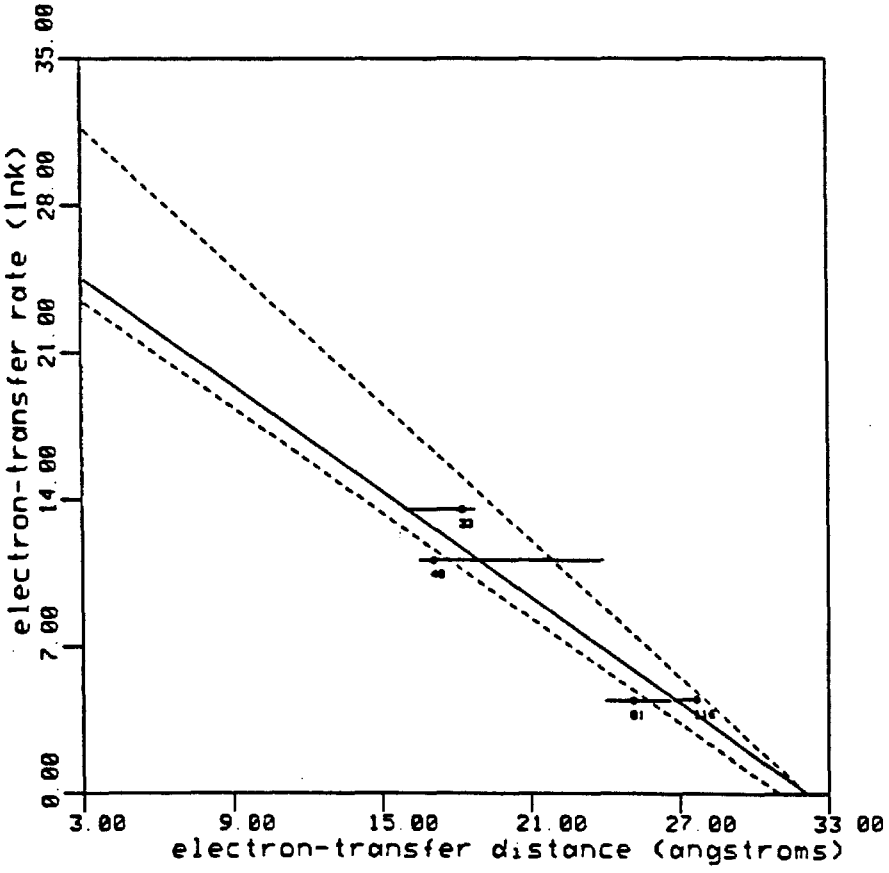

Figure 7.

The two curves were calculated for λ=1 and 2eV using a Marcus expression for the rate. The solid dots are the experimental points for a_5Ru(His-48)MbFe and $a_4$pyRu(His-48)MbFe. ΔE°=0.02V, k_{ET}=0.04s^{-1}; ΔE°=0.275V, k_{ET}=2.5s^{-1}.

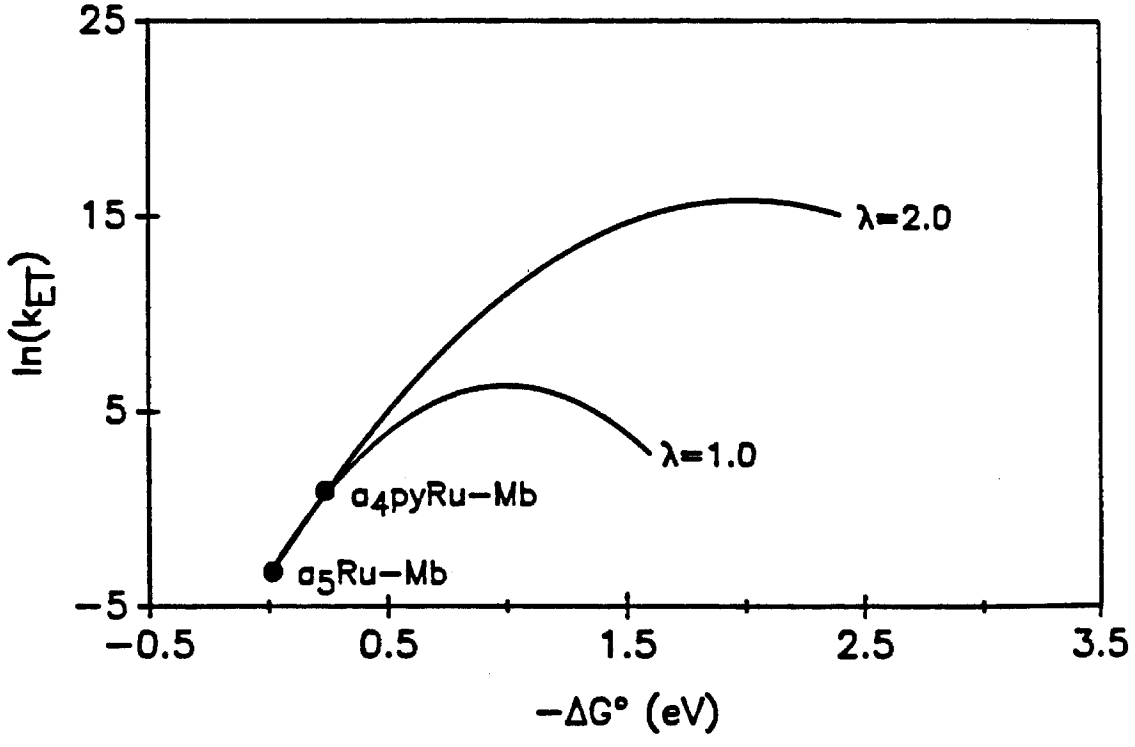
25
15
5
−5
ln(k_ET)
λ=2.0
λ=1.0
a4pyRu−Mb
a5Ru−Mb
−0.5
0.5
1.5
2.5
3.5
−ΔG° (eV)

Figure 8.

The solid dots are the experimental results at 25°C for $a_4LRu(His\text{-}48)MbM$ where M=Pd, Zn, or Fe and a=NH_3, L=NH_3 or pyridine. The data are given in the table below: The curves were calculated using a Marcus expression[2a] for the ET rate,

ET Distances in Ruthenium-Modified Myoglobin[a]

ET	$\Delta E°$ (V)	k_{ET} (s^{-1})
$a_5Ru^{III}MbFe^{II} \rightarrow a_5Ru^{II}MbFe^{III}$	0.020	0.040
$a_4pyRu^{III}MbFe^{II} \rightarrow a_4pyRu^{II}MbFe^{III}$	0.275	2.5
$a_5Ru^{III}MbPdP^* \rightarrow a_5Ru^{II}MbPdP^+$	0.72	9100
$a_5Ru^{III}MbZnP^* \rightarrow a_5Ru^{II}MbZn^+$	0.88	70,000
$a_4pyRu^{III}MbPdP^* \rightarrow a_4pyRu^{II}MbPdP^+$	0.98	90,000

$k=\nu_n exp[-\beta(d\text{-}3)]exp[-\Delta G°+\lambda)^2/4\lambda RT]$. The values of β (0.91Å^{-1}) and d (13.2Å) have been determined independently for RuMbZn.[9] The curves were fit to the experimental data by varying λ, with ν_n fixed at 10^{11}, 10^{12}, or $10^{13}s^{-1}$. The limits we place on the reorganization energy are 1.90 to 2.45eV.

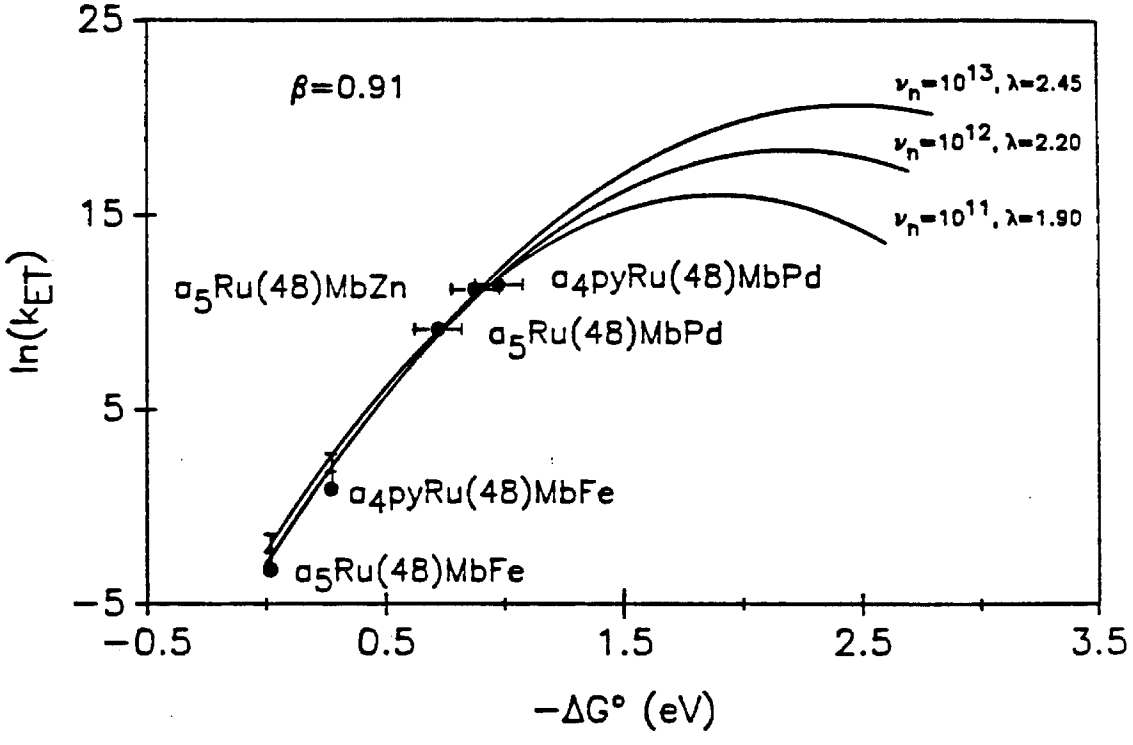
25
15
5
−5
−0.5
0.5
1.5
2.5
3.5
ln(k_ET)
−ΔG° (eV)
β=0.91
ν_n=10^13, λ=2.45
ν_n=10^12, λ=2.20
ν_n=10^11, λ=1.90
a5Ru(48)MbZn
a4pyRu(48)MbPd
a5Ru(48)MbPd
a4pyRu(48)MbFe
a5Ru(48)MbFe

Figure 9.

Biological ET reactions could be controlled by changes in reorganization energy. Such changes could be made by reducing the number of water molecules around the D and A sites by a conformational transition. Since rearrangements of solvent water molecules are usually associated with large reorganization energies, this type of conformational transition would be expected to lower λ. Below the figure depicting a water-eliminating conformational transition is a table of calculated ET rates for a range of ΔG° and λ values. These were calculated from Marcus theory using β=0.91Å^{-1} and ν_n=10^{13}s^{-1}.

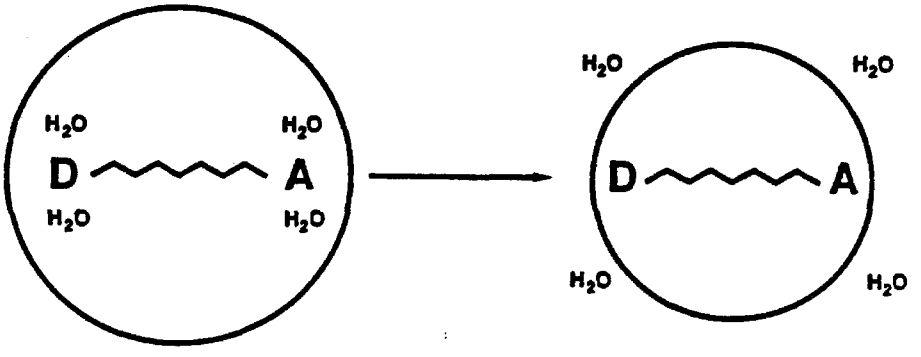

Electron-Transfer Rate: k_{ET} (s^{-1})

d(Å)	0.5			1.0			1.5			2.0			2.5			= λ(eV)
	0	0.2	0.5	0	0.2	0.5	0	0.2	0.5	0	0.2	0.5	0	0.2	0.5	= -ΔG°(eV)
8	1.3E10	2.8E11	1.6E12	1.0E8	2.3E9	1.4E11	8.1E5	8.0E7	2.6E9	6.4E3	2.5E5	8.1E7	1.1E1	2.1E3	3.1E5	
10	1.4E8	3.0E9	1.7E10	1.1E6	3.5E7	1.5E9	8.6E3	3.2E5	2.7E7	6.8E1	2.7E3	3.2E5	1.4E-1	2.2E1	3.3E3	
15	1.4E6	3.2E7	1.8E8	1.1E4	3.7E5	1.6E7	9.1E1	3.4E3	2.9E5	7.2E-1	2.8E1	3.4E3	1.7E-3	2.3E-1	3.4E1	
20	1.5E4	3.3E5	1.9E6	1.2E2	3.9E3	1.7E5	9.6E-1	3.5E1	3.0E3	7.6E-3	3.0E-1	3.6E1	6.0E-6	2.5E-3	3.6E-1	
25	1.6E2	3.5E3	2.0E4	1.3E0	4.1E1	1.8E3	1.0E-2	3.7E-1	3.2E1	8.0E-5	3.2E-3	3.8E-1	6.4E-7	2.6E-5	3.8E-3	
30	1.7E0	3.7E1	2.1E2	1.3E-2	4.3E1	1.9E1	1.1E-4	3.9E-3	3.4E-1	8.5E-7	3.3E-5	4.0E-3	6.7E-9	2.8E-7	4.1E-5	

$$k_{ET} = 10^{13}\exp(-0.91(d-3)\exp\left(-\frac{(\Delta G^{\circ}+\lambda)^2}{.1034\lambda}\right)$$

Appendix. Calculational Details

The goal of our geometery calculations was an estimation of the range of electron-transfer (ET) distances possible for the redox complexes described in the preceding papers. Assuming that the ruthenium reagent does little to perturb the structure of the protein (an assumption extensively supported by the experimental data), then the use of a low (or zero) perturbation computational technique is warranted. Given this consideration, we choose to employ rigid-body conformational-energy searching.

The simplest implementation of this technique requires that essentially all of the protein atoms remain in their native positions (zero perturbation), while the atoms of the residue of interest are driven through phase space by successively incrementing its sidechain dihedrals.[1] The energy of each conformation is then evaulated and stored for latter analysis.

For the case at hand, the side chain to be driven is a histidine with $Ru(NH_3)_5$ covalently attached[2] to its ϵ-nitrogen as shown in Figure 1. The energies of the 10^4 unique conformations generated by successively incrementing the C_α-C_β and C_β-C_γ side-chain dihedrals (see Figure 1) by 3.6° were calculated. Only the van der Waals energy was evaluated for the generated conformations.

The van der Waals energy was described in terms of a Lennard-Jones 12-6 potential function, which has the form

$$E_{vdW} = \sum_{R_{ij}<R_{cut}} (D_0)_{ij} \left\{ \left[\frac{(R_0)_{ij}}{R_{ij}} \right]^{12} - 2 \left[\frac{(R_0)_{ij}}{R_{ij}} \right]^{6} \right\},$$

where D_0 is the van der Waals bond strength in kcal/mol, R_0 is the van der Waals bond length in Å and R_{ij} is the interatomic distance in Å. The energy of each conformation is the sum over all pairs of atoms (i,j) that are separated by less than the cutoff distance, R_{cut}. For the cases studied, R_{cut} was set to 9.0Å. The van der

Waals parameters contained in the BIOGRAF-DREIDING parameter set were used unchanged.[3]

Typically, the results from such calculations are presented as phi-psi plots in which energy contours are plotted as a function of the dihedral angles phi and psi. But because of the obvious difficulties in extracting variations in the ET distances using this formalism, we decided to create pseudopotential-energy surfaces that plot ET distance[4] *vs.* conformational energy. Plots of this nature clearly show the variation of the ET distance for a given energy input (i.e., the curvature of the potential surface gives an indication of the possible variability in the ET distance: higher curvature indicates less distance variability). Figure 2 shows the plots resulting from this analysis.

By comparing our computational results for the conformation of a_5Ru(His-48)Mb with the conformation determined by X-ray diffraction,[5] we were able to derive an energy correction factor of 6.5 kcal (relative energy). That is, the experimental metal-metal (Ru-Fe) distance of 24Å falls on our potential surface (Figure 2f) approximately 6.5 kcal above the calculated minimum (this corresponds to a distance range of 16-24Å). Use of this correction factor led to the ET distance ranges described in this chapter.

References

[1] Gelin, B. R.; Karplus, M. *Biochemistry* **1979**, *18*, 1256-1268.

[2] (a) Protein coordinates were obtained from Brookhaven Protein Data Bank: Bernstein, F. C.; Koetzle, T. F.; Williams, G. J. B.; Meyer, Jr., E. F.; Brice, M. D.; Rodgers, J. R.; Kennard, O.; Shimanouchi, T.; Tasumi, M. *J. Mol. Biol.* **1977**, *112*, 535-542. (b) Tuna cytochrome *c* (Trp-33 replaced by a_5Ru(His)) served as the structural model for the horse heart protein. (c) a_5Ru modified histidines were generated by attaching this group to the ϵ-nitrogen of the appropriate histidine residues and minimizing the energy of the side-chain atoms (including a_5Ru) using the BIOGRAF DREIDING force field.[3]

[3] Calculations were performed using BIOGRAF/III version 1.23: BIOGRAF was designed and written by S. L. Mayo, B. D. Olafson, and W. A. Goddard III.

[4] The ET distances considered were the metal-metal distance and the edge-edge distance. The metal-metal distance for each conformation is defined as the distance between ruthenium and iron. The edge-edge distance for each conformation is defined as the *shortest* distance between the atoms comprising ruthenium's ligands (the five atoms of the histidine side-chain imidazole and the five ammine nitrogens) and the atoms comprising iron's ligands (the porphyrin-ring atoms and the five atoms of the ligand histidine imidazole and the sulfur of the methionine ligand in the case of cytochrome *c*)

[5] Mottonen, J; Ringe, D.; Petsko, G. A., unpublished results.

Figure 1.

Ruthenated histidine side chain. The bonds of interest for rigid-body conformational searching are C_α-C_β and C_β-C_γ. Rotation about the N_ϵ-Ru bond is not a consideration since strong 1-4 interactions between the ruthenium ammine groups and the histidine imidazole ring lock the ammines in the shown staggered conformation.

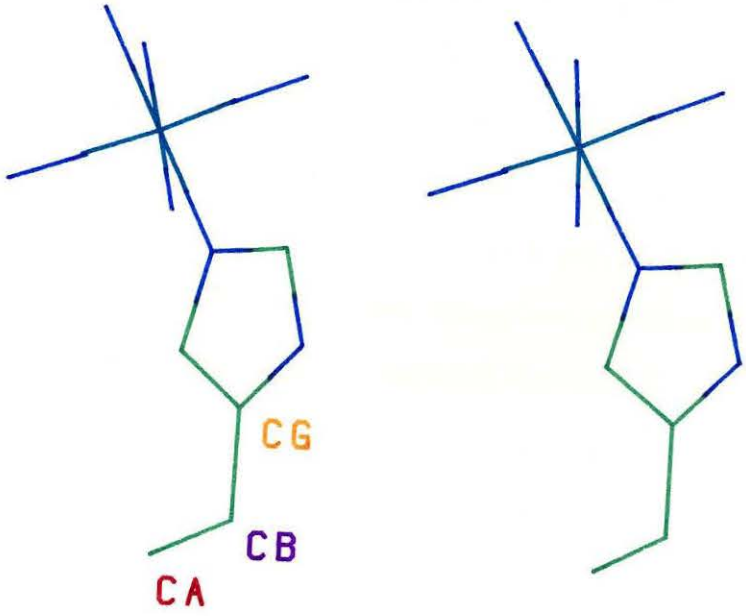
CG
CB
CA

Figure 2.

Potential energy surfaces for ET complexes. The plots on the following pages are the pseudopotential surfaces generated from the conformational searches described in the text. Two definitions of the ET distance were used in this analysis. The first is an edge-edge (E-E) distance and the second is a metal-metal (M-M) distance (Fe to Ru). In the E-E case the ET distance for a particular conformation is the shortest outersphere distance between the ligands on the ruthenium (i.e., the five ammine nitrogens and the five atoms of the histidine imidazole ring) and the ligands on iron (i.e., the atoms of the porphyrin ring – excluding pendant groups such as proprionic acid – and for myoglobin the five atoms of the proximal histidine imidazole and for cytochrome *c* the five atoms of the iron ligand histidine imidazole ring and the sulfur atom of the iron ligand methionine). For each plot all conformations having energies less than 25 kcals above the lowest energy are shown as points plotted at the conformational energy and the appropriate ET distance. Given all of the plotted data, the potential "surface" is envisioned as the smooth curve fitting below the mass of points. The vertical dotted lines shown on each plot are the minimum and maximum ET distances that are achievable by the indicated rotations. Although the possible range of distances is generally large (i.e., the separation between the minimum and maximum distances), the calculated range of distances (i.e., the spread in the potential surfaces) generally shows a much more restricted phase space. The plots are:

(a) E-E plot for ruthenated His-33 of cytochrome *c*

(b) M-M plot for ruthenated His-33 of cytochrome *c*

(c) E-E plot for ruthenated His-12 of myoglobin

(d) M-M plot for ruthenated His-12 of myoglobin

(e) E-E plot for ruthenated His-48 of myoglobin

(f) M-M plot for ruthenated His-48 of myoglobin

(g) E-E plot for ruthenated His-81 of myoglobin

(h) M-M plot for ruthenated His-81 of myoglobin

(i) E-E plot for ruthenated His-116 of myoglobin

(j) M-M plot for ruthenated His-116 of myoglobin.

(a) E-E His-33 cytochrome *c*: D_{min}=5.4Å, D_{max}=11.7Å, D_{mine}=11.6Å

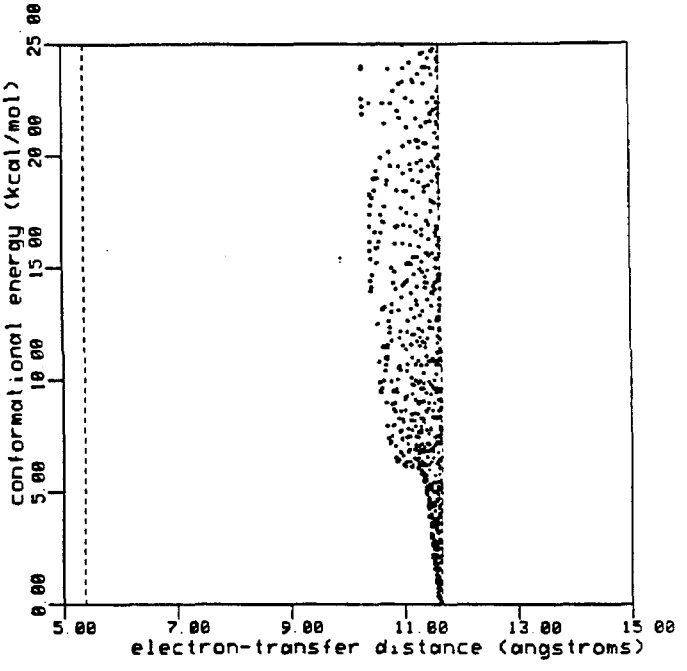

(b) M-M His-33 cytochrome *c*: D_{min}=10.8Å, D_{max}=19.1Å, D_{mine}=18.3Å

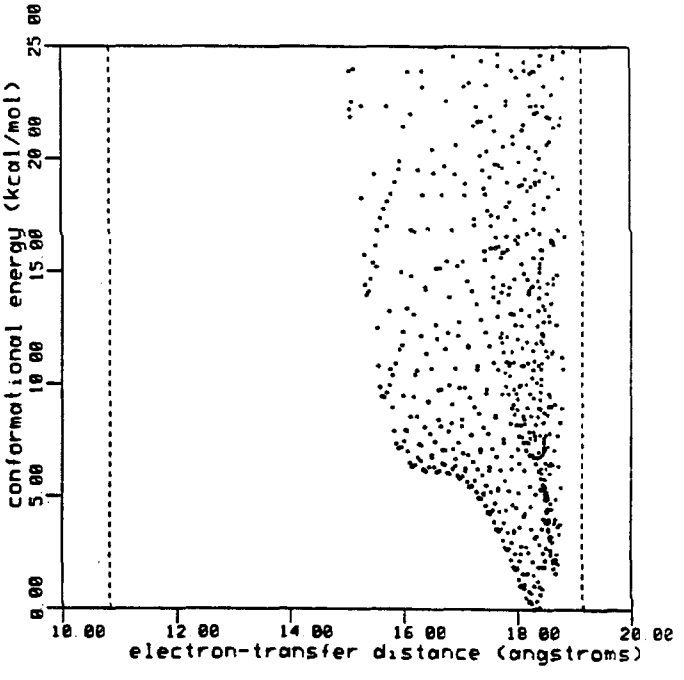

(c) E-E His-12 myoglobin: D_{min}=17.3Å, D_{max}=22.3Å, D_{mine}=22.0Å

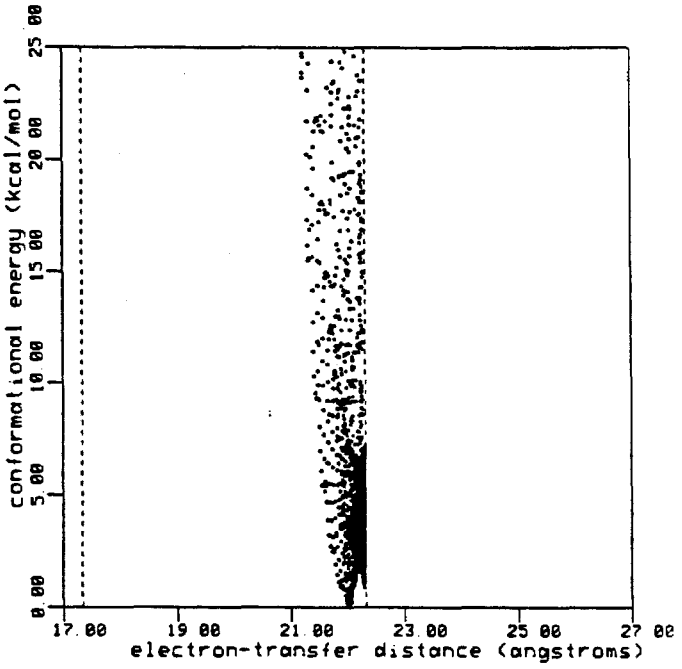

(d) M-M His-12 myoglobin: D_{min}=23.1Å, D_{max}=30.1Å, D_{mine}=29.3Å

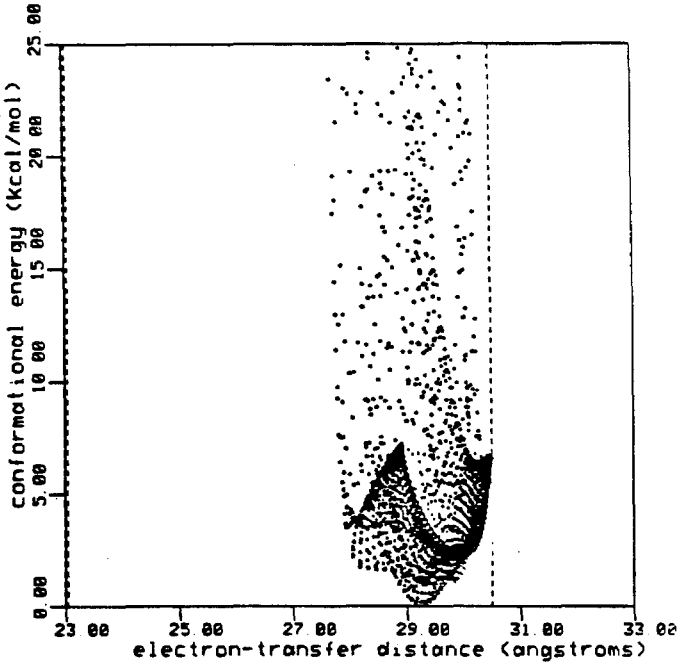

(e) E-E His-48 myoglobin: D_{min}=9.4Å, D_{max}=16.6Å, D_{mine}=12.7Å

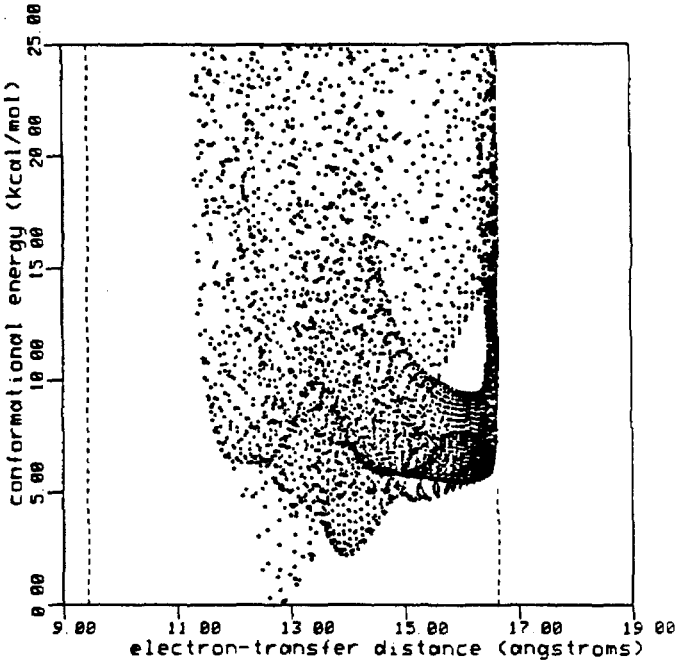

(f) M-M His-48 myoglobin: D_{min}=14.7Å, D_{max}=24.0Å, D_{mine}=17.1Å

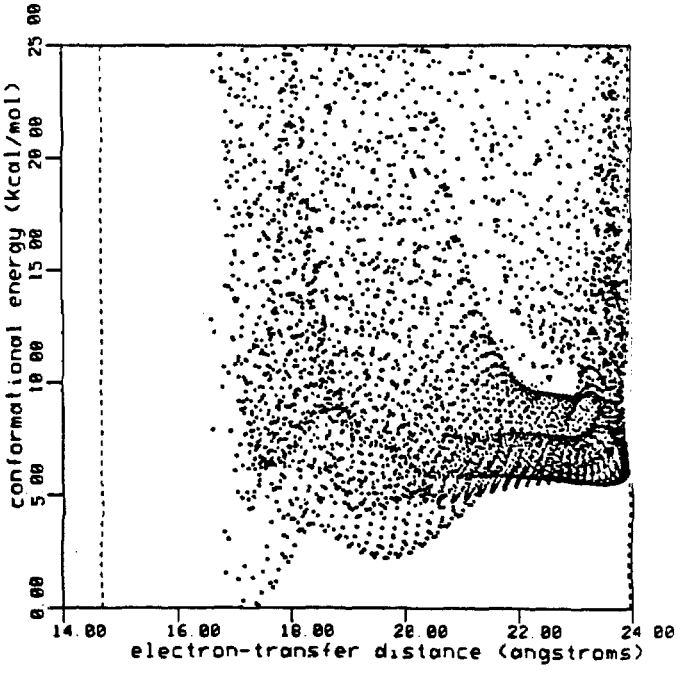

(g) E-E His-81 myoglobin: D_{min}=14.4Å, D_{max}=19.3Å, D_{mine}=19.3Å

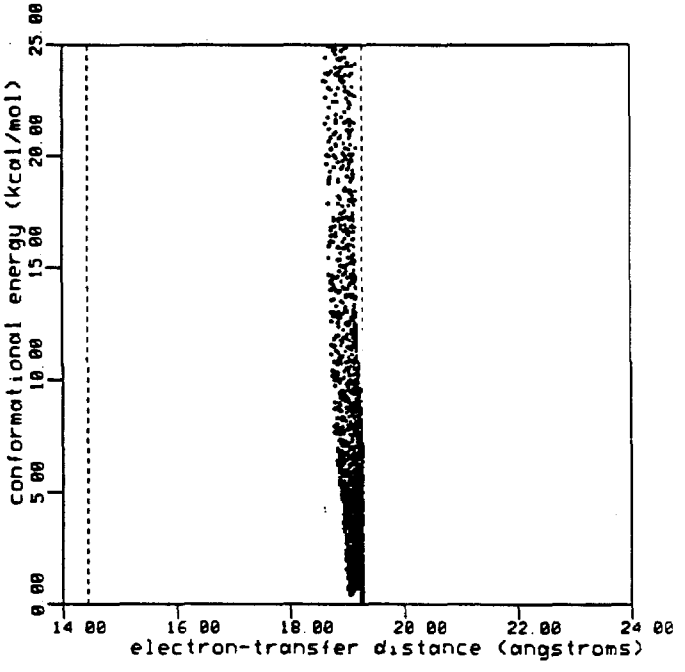

(h) M-M His-81 myoglobin: D_{min}=19.4Å, D_{max}=26.6Å, D_{mine}=25.1Å

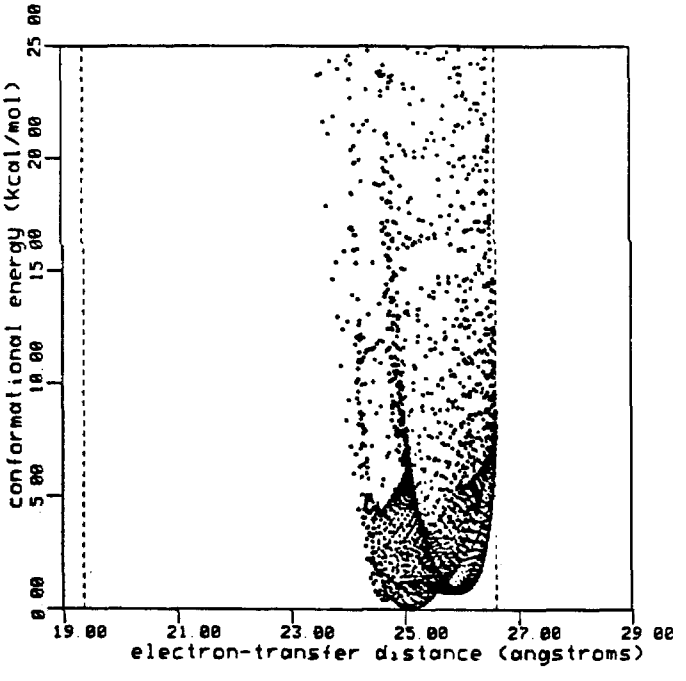

(i) E-E His-116 myoglobin: D_{min}=11.9Å, D_{max}=20.4Å, D_{mine}=20.1Å

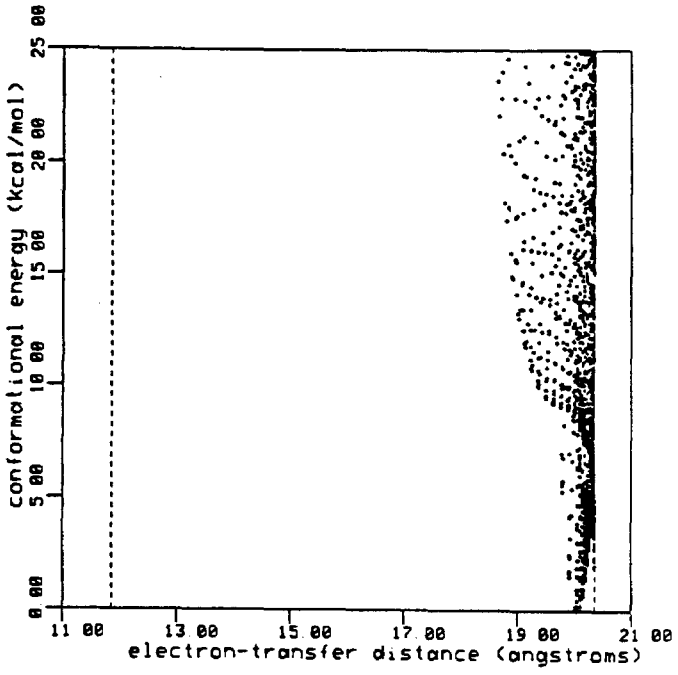

(j) M-M His-116 myoglobin: D_{min}=17.3Å, D_{max}=27.8Å, D_{mine}=27.7Å

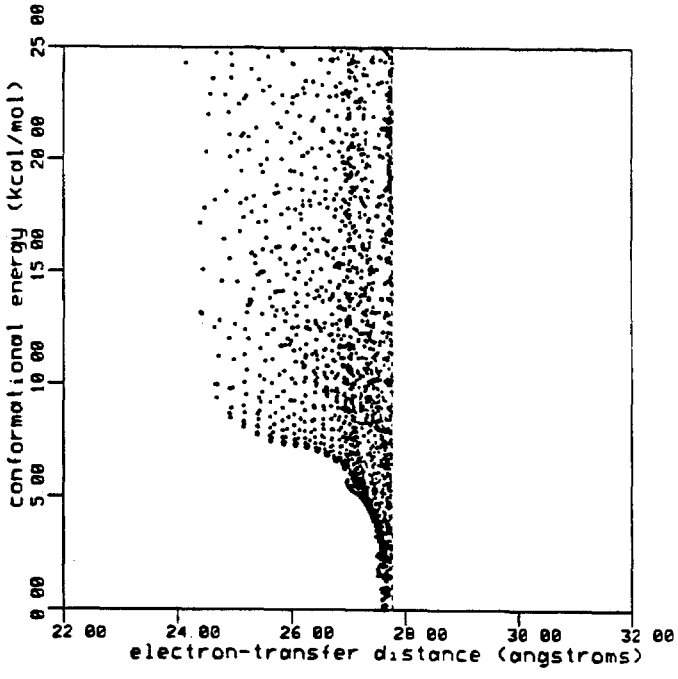

Chapter 3

The Design and Synthesis of Site-Specific Mutants of Yeast Iso-1 Cytochrome *c*

I. Introduction

After considering the currently available rate-distance data for electron transfer in metalloproteins (see Chapter 2), it is clear that much more data are needed before any definitive statement can be made concerning the viability of current electron-transfer theories. The single most obvious need is for rate data at distances in the range of 13-19Å. In addition, however, two other factors must be considered. The results presented in Chapter 2 indicate that the electron-transfer pathway may be important in attenuating the electron-transfer rate. If this proves to be correct, then rate-distance analyses should be carried out only for rates derived from sites with similar electron-transfer pathways. In addition, the orientation between the electron donor and acceptor may also play an important role in controlling the electron-transfer rate. Clearly then, the ideal metalloprotein system for studying the distance dependence of the electron-transfer rate is one in which multiple proteins are available with unique labeling sites that cover a range of distances, each with the same relative donor-acceptor orientation and intervening medium.

As a collaborative effort we are using site-directed mutagenesis to create such an ideal system. One route to such a system involves the use of site-directed mutagenesis to introduce *handles* at sites remote from the native catalytic center. The handles would then provide a means of probing that center without perturbing it in the process – i.e., nonperturbative site-directed mutagenesis. For long-range electron-transfer studies, the handle of choice is certainly histidine (modified with pentaamine ruthenium).

The goal of this collaboration has been the introduction of histidine residues onto the surface of yeast iso-1 cytochrome *c* at locations determined to be unimpor-

tant to the native catalytic process and the study of the electron-transfer kinetics from these remote sites to the heme-iron, using the ruthenium methods described in Chapter 2. Yeast iso-1 cytochrome *c* is particularly attractive for this purpose because of the extensive genetic[1] work done with this protein and the availability of its gene.[2,3,4,5,6,7,8] And, in general, the wealth of sequence and structural data available for c-type cytochromes[9] enhances the potential of designing isofunctional mutants. By judiciously choosing the new histidine positions, we are generating a series of proteins that will allow an unambiguous examination of the effects of distance on intramolecular electron-transfer rates in metalloproteins.

II. Methods

The Methods section is divided into three parts: mutant design, mutagenesis protocols and gene expression. The section on mutant design covers the generation and evaluation of a model of the structure of yeast iso-1 cytochrome *c* in terms of locating residues for use in the mutagenesis studies. Our primary concern relative to this section was the selection of a set of potentially mutatable sites, the selection of a subset of those sites that will yield a series of mutants optimized for an analysis of the distance dependence of the electron-transfer rate, and the design of the base protein onto which the individual surface histidines will be placed. The section on mutagenesis protocols includes a brief overview of the technique used to create the mutants described in latter sections. And the section on gene expression contains an overview of the expression system used to produce workable quantaties of the mutant proteins. Each of these will be considered in turn.

A. Experimental Design

1. Generation of a Model for Yeast Iso-1 Cytochrome *c*

Before we embarked on a detailed analysis of the yeast iso-1 cytochrome *c* structure, it was neccessary to generate a 3-D model of that protein since its x-ray crystal structure was not known at the time these experiments were initiated.[11] Our intent was to provide a working model of the yeast protein that could be used for future structural analyses.

Because of the extensive sequence homology found for c-type cytochromes[9] and the near superposability of the known cytochrome structures, the 3-D fold of eukaryotic c-type cytochromes is thought to be wholly conserved.[10,12] Based on these considerations, we felt that building a 3-D model for the yeast protein from the rice[13,14] and tuna[14,15,16] structures in the manner described below was scientifically justifiable.

The model was generated with the aid of an Evans and Sutherland PS300 (an interactive computer graphics system that allows for the real-time manipulation of complex 3-D objects), using the protein-engineering simulation capabilities of program BIOGRAF/III.[17] The protocol used for generating the model is listed below and the specific details of the side-chain replacements are listed in Table 1:

1. we started with rice cytochrome c because it contains the extra N-terminal amino acids needed for the yeast structure (yeast has five more N-terminal residues than tuna; rice has eight more than tuna);

2. we truncated the rice structure on its N-terminus so that it would conform to the length of the yeast protein;

3. we replaced a rice side chain with a yeast side chain whenever the sequences mismatched (see Table 1) and aligned the new side chain with the old rice side chain as closely as possible, *or* if the new side chain was more like its tuna counterpart, we aligned it with the tuna side chain (using superimposed rice and tuna structures); and lastly,

4. we minimized the energy of the new side chain positions using the BIOGRAF-DREIDING force field to remove unfavorable steric contacts and to regularize hydrogen bonds and salt bridges formed by the new side chains.

All future references to geometry (e.g., distances and angles) will refer to this model structure unless otherwise noted.

2. Selection of Potentially Mutatable Sites

Rather than look immediately for residue positions that could accommodate the incorporation of a histidine, we started by using the available sequence data[9] and our yeast cytochrome *c* model to eliminate positions that appeared *not* to be able to accommodate such a replacement. Residues were eliminated based on either sequence conservation or the direct observation of function as seen in our model protein (mainly hydrogen-bonding and salt-bridging). Although this approach seems to be somewhat backward, it has the advantage of forcing the consideration of *every* position in detail (both at the primary sequence level and the structural level). This approach, therefore, makes it much easier to spot important covariations in the primary sequence that might otherwise go unnoticed.

Table 2 summarizes the initial eliminations. Residues 12, 13, 16, 27, 72, 81, 86, and 87 were also eliminated because of their implication in model complexes between

cytochrome *c* and cytochrome b_5[18] and cytochrome *c* and cytochrome *c* peroxidase[19] (see Figure 1 for relative location of these residues). Chemical modification studies involving the Lys residues of horse heart cytochrome *c* indicate that position 8 (among others) is weakly involved in binding to cytochrome oxidase and cytochrome reductase.[20] However, the importance assigned to position 8 is low, relative to sites 13, 72, 86, and 87[20] and because yeast cytochrome *c* does not have a Lys in that position[9] (although Lys 11 is in the same general location), we decided not to eliminate it (or position 11) from our list of potentially mutatable sites (see Figure 2 for relative location of these residues). In addition, we also elected to eliminate positions containing Glu and Asp in order to avoid raising the already high pI of yeast cytochrome *c*. Extremely high pI's tend to lower the ruthenation efficiency (because of charge-charge interactions) and also to make the use of ion-exchange chromatography less effective in the purification of the ruthenated proteins. Positions -1 through -5 were also eliminated because of the lack of structural data for this region. The positions remaining after the elimination procedure are listed in Table 3 and are shown in Figure 3.

As expected, many of the positions listed in Table 3 have been previously classified as *hypervariable* (containing greater than seven residue types), suggesting that they have little or no involvement in the protein's catalytic function (substrate recognition and electron transfer).[9]

The approach we have taken in eliminating residue positions has, we hope, prevented us from making the generalization that variability *necessarily* indicates lack of function (structural or catalytic).[12] This is not our premise. Our premise is that variability, when analyzed at both the primary sequence and structural levels, can point to regions where this variability can be understood well enough to assess whether

incorporating a histidine into a particular position will adversely affect the structure or function of the protein. We feel that, while the 16 positions listed in Table 3 do not necessarily represent regions lacking function, they do represent regions that, based on past variations and structural information, could conceivably accommodate a histidine residue.

3. Picking a Set of Positions Optimized for the Analysis of the Effects of Distance on Intramolecular Electron Transfer

Since we are primarily concerned with a definitive analysis of the effect of site-to-site distance on intramolecular electron-transfer rates, we picked a subset of the positions listed in Table 3 that would allow us to address this issue rigorously. Positions 2, 3, 4, 5, 7, 8, and 11 make up the required subset. These positions have several nice features:

1. they are all located at the N-terminus of the protein (positions 7 through 16 using the yeast numbering scheme), which allows convenient characterization of both the ruthenated and unruthenated materials *via* automated N-terminal sequencing (see Figure 4);

2. they are all clustered in one region, which gives them the same relative donor-acceptor orientation and the same type of intervening medium – hydrophobic, nonaromatic;

3. they span a range of distances from approximately 12 to 18Å and are nicely distributed within that range (see Table 4); and, most importantly,

4. they appear in a region in which numerous stable mutants have already been made[1] (in the course of translation initiation studies).

4. Design of Base Protein

In order to make yeast iso-1 cytochrome *c* a more tractable experimental system, two initial mutagenesis experiments must be carried out:

1. replacement of Cys102 with Thr or Ser; and

2. replacement of the reactive, naturally occurring surface histidines.

Previous work in our laboratory,[22] and in others,[23,24] has indicated that Cys102 interferes with physical characterization by forming intermolecular disulfide dimers. Although modification of this residue with reagents such as iodoacetamide prevents this problem,[23,24] the x-ray crystal structures of rice[13,14] and tuna[14,15,16] cytochromes *c* suggest that such a modification would disrupt a structural feature found in the C-terminal helix (see Figure 5). Because of this consideration, we elected to use a genetic approach and to replace the Cys with a chemically inert residue (with respect to dimerization) that would preserve the feature shown in Figure 5. 54 of the 60 eukaryotic sequences examined have Thr in position 102, 2 have Cys, and 1 has Ser (the remaining are 2 Lys and 1 Ala).[9] The structural parallels among Thr, Ser, and Cys are obvious.

Since the purification of ruthenated proteins is much easier if there is only a single modifiable histidine (i.e., a single reactive histidine on the surface of the protein), we decided to replace the naturally occurring reactive surface histidine – His39 – with Gln (new residue selected based on sequence data[9] and computer-graphics analysis).

As anticipated from the computer-graphics analysis, His39 reacts rapidly the ruthenium label.[22] In addition, there is also evidence that His33 reacts with the ruthenium reagent, but its reactivity is minimal compared to that of His39. This observation is handily explained by the steric accessibilities of His39 and His33 as

shown in Figure 6. The implication is that relative reactivity of a set of histidines is largely determined by their relative steric accessibilities. This observation has also found utility in analyzing other protein systems.

To summarize, each protein that contains a new histidine position (from the list shown in Table 4) will also contain the His39→Gln and Cys102→Ser mutations. That is, each of the kinetically useful proteins will be a triple mutant.

B. Mutagenesis Protocols

Recent advances in genetic engineering methodologies and the advent of efficient DNA synthesis have made the task of oligonucleotide-directed, site-specific mutagenesis relatively simple.[25,26,27,28] Since protocols for the site-specific alteration of DNA sequences are well established, only a general overview of the method is presented.

As outlined in Figure 7, this method involves priming *in vitro* DNA replication with a chemically synthesized oligodeoxyribonucleotide that has been designated to have a sequence largely complementary to the wild-type DNA template in the region where the mutation is to be introduced. The synthetic oligonucleotide contains, however, one or more bases that are not complementary to the wild-type template; the mutation originates from these mismatched bases. Annealing of the synthetic oligonucleotide to the single-stranded wild-type M13 vector containing the gene of interest can be accomplished under conditions of sufficiently low stringency that a heteroduplex forms, in spite of some mismatching of bases. The site-specificity of this duplex formation is, nevertheless, exceedingly high. For example, in a 15 base oligodeoxynucleotide there will normally be 13-14 complementary base pairings and 1-2 mismatches at the site where the mutation is being introduced. Binding of the synthetic oligonucleotide to the template DNA at sites other than the desired site will

generally involve no more than 9-10 pairings by design. The heteroduplex region thus formed now serves as an initiation site for *in vitro* DNA synthesis that occurs in the presence of the four deoxynucleotide triphosphates and is catalyzed by the Klenow fragment of DNA polymerase I (which requires a 3'-OH primer terminus to begin DNA synthesis). After ligation, the heteroduplex is introduced into an appropriate bacterial host and multiplies as a result of normal semiconservative, *in vivo* replication into two types of homoduplexes; the mutant homoduplexes have a sequence that reflects the synthetic, mutagenic oligonucleotide; the other homoduplexes have the original, wild-type sequence.

An essential feature of any procedure for producing specific mutants is the necessity of identifying mutant colonies in a background of wild-type colonies. To be generally applicable, the procedure should allow identification of mutants at the level of DNA and should not rely on some phenotypic difference between mutant and wild type that may be difficult to predict and to assay. In this regard, oligonucleotide mutagenesis has the distinct advantage that mutants can be found by screening the single-stranded DNA contained in the M13 phage particles with the same synthetic oligonucleotide, now labeled with ^{32}P, that was originally used to introduce the mutation. In this case, the hybridization is carried out under conditions of high stringency such that even a single base mismatch between the oligonucleotide and the template can be readily distinguished from perfectly matching hybrids. This allows clear discrimination between wild-type and mutant phage particles dot-blotted onto nitrocellulose filter paper.

We have used two variations in forming the heteroduplex DNA described in Figure 7:

1. the "double-primer" method and

2. the "Eckstein" method.

For the double-primer method,[29] in addition to annealing the mutagenic oligo to the wild-type template (step A in Figure 7) a sequencing primer (i.e., an oligo that fully base pairs to the template) is also added to the reaction mixture. Its sequence is selected so that it hybridizes close (~100 bases away) to the 5′ side of the mutagenic oligo. The purpose of this additional primer is to protect the 5′ end of the mutagenic primer from *in vivo* degradation since much of the duplex material is not fully closed circular as shown in Figure 7. Efficiencies as high as 20% can be achieved under optimal conditions.

The Eckstein method[30] differs significantly from the double-primer method since it adds *in vitro* selection steps. The *in vitro* screening is added in order to remove unreacted single-stranded template and to render inactive the wild-type DNA strand. Removal of the unreacted (and heteroduplex material that is not completely closed circular) is achieved by filtering the primer extension reaction products through nitrocellulose. Nitrocellulose has a higher affinity for single-stranded DNA than for double-stranded DNA. The result of this differential affinity is that the double-stranded material passes through and the unwanted single-stranded material remains bound to the nitrocellulose. After removing ssDNA, the reaction mixture is treated with an endonuclease that is not capable of cleaving DNA containing alpha sulfur. It is then treated with exonuclease. The result of these treatments is the destruction of the wild-type template. The mutant containing template is protected from the action of these enzymes because of the use of alpha-S containing deoxynucleotide triphosphates in the primer extension reaction (step B in Figure 7). Efficiencies as high as 95% can be achieved under optimal conditions.

At the time these experiments were started, the double-primer method was rec-

ognized as the best protocal. Currently, however, the Eckstein method is considered to be among the best protocols.

C. Gene Expression

The gene expression system used in our experiments is shown Figure 8.[8,31] The goal of this system is twofold. First, it serves to shuttle the gene from its temporary prokaryotic state back to its native eukaryotic state; and secondly, it acts to facillitate the actual production of protein *in vivo*. Expression begins with moving the mutated gene from M13 (in which the mutagenesis was carried out) the multifunctional "shuttle" vector that allows the plasmid DNA to replicate in both bacteria and yeast. To this end, the vector contains both the bacterial origin of replication (derived from pBR322 sequences) and the yeast 2μ origin of replication. In addition, as an aid in identifying plasmids that carry inserted sequences, the vector also contains the Amp and Tet genes from pBR322. The intact plasmid illicits both ampicillin and tetracycline resistance, but those plasmids that carry an insert are tetracycline sensitive (Tet^s) as indicated in Figure 8.

Once recombinant material has been recovered, yeast transformation is carried out with a host that is a leucine auxotroph and is deficient in both iso-1 and iso-2 cytochromes *c*. Yeast transformants are first identified by their ability to complement the leucine auxotrophy (i.e., by showing growth on media lacking leucine). The Leu2 gene of the plasmid serves in this capacity. Cytochrome competency is then tested by requiring the transformants to undergo respiration (i.e., by requiring them to grow on nonfermentable carbon). Since the host strain lacks any endogenous cytochrome *c*, only an intact and functional protein derived from the recombinant plasmid will permit the cells to survive.

The genetic complementation described above plays an important role in our expression system, since its success (or failure) gives an immediate indication of the viability (or lack thereof) of the mutant proteins. In other words, the expression system guarantees that if complementation occurs, the mutant protein is very likely to be isofunctional (and isostructural). The importance of this cannot be overemphasized, since zero perturbation is the very basis of our designs.

III. Results

Since electron-transfer rate data are most needed in the distance range from 14-19Å, we decided to select sites from Table 4 that fall in this range. To this end, the Thr8→His and Lys5→His (14.4Å and 15.3Å, respectively) were selected to be the first kinetically useful mutations. Recall, however, that two initial mutations must be made in order to form the base protein: Cys102→Ser and His39→Gln. Each of these will be considered in turn.

A. Cys102→Ser

The goal of our initial experiment was to accomplish the first step in creating the base protein – removal of Cys102. To achieve this, we designed and synthesized[32] the 17 base, double mismatch, mutagenic primer shown in Figure 9. This primer encodes the required TGT to ACT alteration (Cys→Thr). We also synthesized a 15 base sequencing primer (located approximately 50 bases upstream) for use as the nonmutagenic primer in the double-primer mutagenesis protocal.

A double mutation (at both A and B in Figure 9) would yield the desired Cys102→Thr change as well as the introduction of a new DdeI restriction site. Also

note that any single mutation (at either A or B) would yield a Cys102→Ser mutation (a mutation at B would also give the new DdeI restriction site).

The mutagenesis procedure was carried out following the general protocal of Zoller and Smith.[26] 132 of the resulting transformants were selected for growth and phage dot-blotting. Screening by probe hybridization revealed a single positive as shown in Figure 10. Attempts to restrict this material with DdeI yielded gel patterns identical to those of the wild-type DNA, suggesting a single mutation at B giving the Cys102→Ser mutation. Subsequent DNA sequencing (using dideoxy chain termination[33,34] in M13) showed a single mutation at B verifying the result anticipated from the restriction analysis. Although the entire coding region was sequenced, only the data for the region around position 102 are shown in Figure 11. The resulting mutant was then subcloned into the previouly described shuttle vector and used to transform a yeast strain lacking both isozymes of cytochrome *c*.[8,31]

After confirming complementation of the cytochrome *c* deficiency in this strain, we isolated and purified approximately 20mg of protein from a 10-liter culture according to well-established procedures.[35] The mutant protein gave a UV/VIS spectrum that was indistinguishable from the wild type protein.[36] As anticipated from the removal of Cys102, the mutant protein showed completely reversible electrochemistry. An initial thin-layer spectroelectrochemical determination at 25°C, μ=0.1M (sodium phosphate buffer), pH=6.8 gave a redox potential of 272mV$\pm$2mV,[37] which is in good agreement with other values determined for c-type cytochromes.[38] In addition, recent NMR studies[39] on the purified protein showed that the chemical shifts of the observable histidines fall in their expected regions, further indicating that no structural alteration has taken place.

B. His39→Gln

The final step in creating the base protein was replacing His39 with Gln, using the template containing the Cys102→Ser mutation. Mutagenesis and screening were carried out using the 17 base, single-mismatch, mutagenic primer shown in Figure 12. The Eckstein protocal was used for the mutagenesis reaction.[40] Screening 60 plaques resulted in 3 positives as shown in Figure 13.

Subsequent sequencing confirmed the anticipated results. Although the entire coding region was sequenced, only the data for the region around position 39 are shown in Figure 14.

Attempts to express this mutant (Cys102→Ser, His39→Gln) are currently under way.

C. Thr8→His

Because this involved a triple mismatch as shown in Figure 15, we decided to use a 23 base, mutagenic primer for the actual mutagenesis reaction and a 15 base primer for screening. The Eckstein protocal was used for the mutagenesis reaction.[40] Screening 36 plaques resulted in 4 positives as shown in Figure 16.

We are currently in the process of sequencing a subset of the observed positives.

D. Lys5→His

Because this involved a double mismatch as shown in Figure 17, we decided to use a 23 base, mutagenic primer for the actual mutagenesis reaction and a 15 base primer for screening. Screening 36 plaques resulted in 2 positives as shown in Figure 18.

We are currently in the process of sequencing the observed positives.

IV. Summary

After an extensive evaluation of the structural data available for c-type cytochromes and the prospects of using *nonperturbative* site-directed mutagenesis in mechanistic studies, we have devised an experimental program that is allowing us to address, in a definitive fashion, the role played by donor-acceptor distance in biological electron transfer. The program involves the novel alliance of two relatively unrelated techniques – one biological, site-directed mutagenesis, and one chemical (inorganic), the ruthenium modification method. The product of this alliance is a series of semisynthetic, multisite redox metalloenzymes optimized for the study of the effect of distance on intramolecular electron-transfer rates. The distances covered in these experiments range from approximately 12 to 18Å. As a first step toward creating this series, we demonstrated the feasibility of making directed, isofunctional mutants of yeast iso-1 cytochrome *c* by replacing the reactive Cys102 sulfhydryl (which prevented convenient physical analyses) with the chemically inert Ser hydroxyl. Subsequent physical studies of this protein confirmed its expected structural and functional integrity. To date, three additional mutants have been made and partially characterized at the genetic level. Expression and electron-transfer analysis of these mutants are expected to proceed smoothly.

References

[1] Sherman, F.; Stewart, J. W. *The Molecular Biology of Yeast* Saccharomyces: *Metabolism and Expression*, Strathern, J. N.; Jones, E. W.; Broach, J. L., Eds.; Cold Spring Harbor Laboratories, Cold Spring Harbor, **1982**; pp. 301-333.

[2] Sherman, F.; Stewart, J. W.; Margoliash, E.; Parker, J.; Campbell, W. *Proc. Nat. Acad. Sci. USA* **1966**, *55*, 1498-1504.

[3] Stewart, J. W.; Sherman, F. *Molecular and Environmental Aspects of Mutagenesis*, Prakash, L.; Sherman, F.; Miller, M. W.; Lawrence, C. W.; Taber, H. W., Eds.; Thomas, Springfield, 1974; pp. 102-127.

[4] Gillam, S.; Rottman, F.; Jahnke, P.; Smith, M. *Proc. Nat. Acad. Sci. USA* **1977**, *74*, 96-100.

[5] Montgomery, D. L.; Hall, B. D.; Gilliam, S.; Smith, M. *Cell* **1978**, *14*, 673-680.

[6] Smith, M.; Leung, D. W.; Gilliam, S.; Astell, C. R.; Montgomery, D. L.; Hall, B. D. *Cell* **1979**, *16*, 753-761.

[7] Leung, D. W.; Smith, M. unpublished sequence of 2.5 Kb BamHI - HindIII fragment containing the yeast iso-1 cytochrome *c* gene.

[8] Yeast iso-1 cytochrome c gene, shuttle vectors, and yeast host kindly provided by M. Smith.

[9] Dickerson, R. E.; Timkovich, R. *The Enzymes*, Boyer, B. D., Ed.; Academic Press, New York, **1975**; pp. 397-547.

[10] Timkovich, R. *The Porphyrins*, Dolphin, D., Ed.; Academic Press, New York, **1979**; pp. 241-294.

[11] The structure of yeast iso-1 cytochrome *c* has been recently determined: Louie, G. V.; Hutcheon, W. L. B.; Brayer, G. D. submitted for publication.

[12] Ferguson-Miller, S.; Brautigan, D. L.; Margoliash, E. *The Porphyrins*, Dolphin, D., Ed.; Academic Press, New York, **1979**; pp. 149-240.

[13] Ochi, H.; Hata, Y.; Tanaka, N.; Kakudo, M.; Sakurai, T.; Aihara, S.; Morita, Y. *J. Mol. Biol.* **1983**, *166*, 407-418.

[14] Bernstein, F. C.; Koetzle, T. F.; Williams, G. J. B.; Meyer, E. F., Jr.; Brice, M. D.; Rodgers, J. R.; Kennard, O.; Shimanouchi, T.; Tasumi, M. *J. Mol. Biol.* **1977**, *112*, 535-542.

[15] Takano, T.; Dickerson, R. E. *J. Mol. Biol.* **153**, *153*, 79-94.

[16] Takano, T.; Dickerson, R. E. *J. Mol. Biol.* **1981**, *153*, 95-115.

[17] BIOGRAF/I was designed and written by S. L. Mayo, B. D. Olafson, and W. A. Goddard III for use in molecular modeling applications that have particular emphasis on display, design, and analysis of biologically relevant molecules.

[18] Salemme, F. R. *J. Mol. Biol.* **1976**, *102*, 563-568.

[19] Poulos, T. L.; Kraut, J. *J. Biol. Chem.* **1980**, *255*, 10322-10330.

[20] Mathews, F. S. *Prog. Biophys. Molec. Biol.* **1985**, *45*, 1-56.

[21] Knossow, M.; Daniels, R. S.; Douglas, A. R.; Skehel, J. J.; Wiley, D. C. *Nature* **1984**, *311*, 678-680.

[22] Selman, M.; Gray, H. B. unpublished results.

[23] Pielak, G. J.; Mauk, A. G.; Smith, M. personal communication.

[24] Zuniga, E. H.; Nall, B. T. *Biochemistry* **1983**, *22*, 1430-1437.

[25] McFarland-Dalbadie, G.; Richards, J. H. *Annual Reports in Medicinal Chemistry* **1983**, *18*, 237-245.

[26] Zoller, M. J.; Smith, M. *Methods in Enzymology* **1983**, *100*, 468-500.

[27] Messing, J. *Methods in Enzymology* **1983**, *101*, 20-78.

[28] Adams, S. P.; Kamila, S. K.; Wykes, E. J.; Holder, S. B.; Galluppi, G. R. *J. Am. Chem. Soc.* **1983**, *105*, 661-663.

[29] Zoller, M. J.; Smith, M. *DNA* **1984**, *3*, 479-488.

[30] Taylor, J. N.; Ott, J. Eckstein, F. *Nucl. Acids Res.* **1985**, *13*, 8764-8785.

[31] Faye, G.; Leung, D. W.; Tatchell, K.; Hall, B. D.; Smith, M. *Proc. Nat. Acad. Sci. USA* **1981**, *78*, 2258-2262.

[32] All oligonucleotides were chemically synthesized using solid phase synthesis. Purification was generally carried out by gel filtration on the Pharmacia FPLC system.

[33] Sanger, F.; Nicklen, S.; Coulson, A. R. *Proc. Nat. Acad. Sci. USA* **1977**, *74*, 5463-5467.

[34] Sanger, F.; Coulson, A. R.; Barrell, B. G.; Smith, A. J. H.; Roe, B. A. *J. Molec. Biol.* **1980**, *143*, 161-178.

[35] Sherman, F.; Stewart, J. W.; Parker, J. H.; Inhaber, E.; Shipman, N. A.; Putterman, G. J.; Gardisky, R. L.; Margoliash, E. *J. Biol. Chem.* **1968**, *243*, 5446-5456.

[36] Mayo, S. L.; Gray, H. B.; Campbell, J. L.; Richards, J. H. unpublished mutagenesis reults.

[37] Ellis, W. R., Jr.; Mayo, S. L.; Campbell, J. L.; Richards, J. H.; Gray, H. B. unpublished electrochemical results.

[38] Margalit, R.; Schejter, A. *Eur. J. Bioch.* **1973**, *32*, 492-499.

[39] Mead, T.; Mayo, S. L.; Campbell, J. L.; Richards, J. H.; Gray, H. B. unpublished NMR results.

[40] The Amersham oligonucleotide-directed *in vitro* mutagenesis system was used to carry out the indicated mutations. In an effort to simplify the procedure, we omitted the nitrocellulose filtration steps.

Table 1. Side-Chain Replacements for Yeast Model.

Number[a]	Tuna[b]	Rice	Yeast	Remarks
-5	-	Ser	Thr	matched with rice side chain[c]
-3	-	Ala	Phe	moved to unhindered position
-2	-	Pro	Lys	rotated into solvent
-1	-	Pro	Ala	-
2	Asp	Asn	ser	matched with rice side chain
3	Val	Pro	Ala	-
5	Lys	Ala	Lys	matched with tuna side chain[c]
7	Lys	Glu	Ala	-
8	Lys	Lys	Thr	rotated hydroxyl near water
9	Thr	Ile	Leu	matched with long branch of ILe
13	Lys	Lys	Arg	placed to preserve salt bridge (to 90)
15	Ala	Ala	Leu	placed in near Phe 110 (hydrophobic)
21	Glu	Asp	Glu	matched with tuna side chain
24	Gly	Ala	Gly	-
25	Lys	Gly	Pro	-
28	Val	Gln	Val	matched with tuna side chain
33	Trp	Asn	His	matched with 5 membered ring of tuna
35	Leu	Leu	Ile	matched with rice side chain
39	Lys	Gln	His	extended into solvent
42	Gln	Thr	Gln	matched with tuna side chain
43	Ala	Thr	Ala	-
44	Glu	Pro	Glu	matched with tuna side chain
49	Thr	Ser	Thr	matched with tuna side chain
50	Asp	Thr	Asp	matched with tuna side chain
52	Asn	Asp	Asn	matched with tuna side chain
53	Lys	Lys	Ile	matched with rice side chain
54	Ser	Asn	Lys	matched with rice side chain
55	Lys	Met	Lys	matched with tuna side chain
56	Gly	Ala	Asn	extended into solvent
58	Val	Ile	Leu	matched with rice side chain
60	Asn	Glu	Asp	matched with tuna side chain
63	Thr	Thr	Asn	matched H-bond components
64	Leu	Leu	Met	matched with rice side chain
65	Met	Tyr	Ser	matched with rice side chain
66	Glu	Asp	Glu	matched with tuna side chain
69	Glu	Leu	Thr	matched with rice side chain

Table 1. Side Chain Replacements for Yeast Model, continued.

Number[a]	Tuna[b]	Rice	Yeast	Remarks
81	Ile	Val	Ala	-
83	Ala	Pro	Gly	-
88	Lys	Pro	Glu	matched with tuna side chain
89	Gly	Gln	Lys	matched with rice side chain
90	Glu	Glu	Asp	placed to preserve salt bridge (to 13)
92	Gln	Ala	Asn	matched with tuna side chain
96	Ala	Ser	Thr	matched with rice side chain
100	Ser	Glu	Lys	matched with rice side chain
102	Thr	Thr	Cys	matched with rice side chain
103	Ser	Ser	Glu	extended into solvent

[a]residue numbers are based on tuna structure
[b]columns labeled "tuna rice yeast" show homologous positions
[c]means new and old side chains aligned as closely as possible

Table 2. Residue Eliminations.[a]

Number[b]	Residue	Reason for Elimination
1	Gly	conserved
6	Gly	conserved
9	Leu	usually large hydrophobic (48Ile,7Leu,3Val,2Thr)
10	Phe	conserved
12	Thr	implicated in model complex[c]
13	Arg	involved in salt bridge (48Lys,12Arg)[c]
14	Cys	heme attachment through thioether (58Cys,2Ala)
15	Leu	usually small (47Ala,9Ser,3Leu,1Asn)
16	Gln	conserved[c]
17	Cys	conserved
18	His	conserved
19	Thr	involved in H-bond (58Thr,2Ser)
20	Val	usually large hydrophobic (54Val,2Leu,1Ile,1Gly,1Cys)
21	Glu	usually negatively charged (44Glu,11Asp,2Gly,2Glx,1Ala)
23	Gly	always small (59Gly,1Ala)
24	Gly	usually small (35Gly,23Ala,1Glu,1Val)
26	His	involved in H-bond (55His,5Asn)
27	Lys	involved in H-bond (58Lys,1Ser,1Gly)[c]
29	Gly	conserved
30	Pro	conserved
31	Asn	involved in H-bond (58Asn,1Ser,1Gln)
32	Leu	conserved
33	His	already contains His
34	Gly	conserved
35	Ile	always large hydrophobic (51Leu,5Ile,2Val,2Phe)
36	Phe	always large hydrophobic (53Phe,3Ile,2Tyr,2Val)
37	Gly	usually small (58Gly,1Asn,1Ser)
38	Arg	conserved
39	His	already contains His
40	Ser	involved in H-bond (30Thr,29Ser,1Gln)
41	Gly	conserved
42	Gln	involved in H-bond (32Gln,25Thr,3Ser)
43	Ala	internal and usually small (34Ala,20Thr,6Val)
44	Glu	eliminated to save negative charge
45	Gly	always small (59Gly,1Ser)
46	Tyr	always aromatic, involved in H-bond (33Tyr,27Phe)
47	Ser	always small (52Ser,6Gly,2Thr)
48	Tyr	conserved
49	Thr	involved in H-bond (33Thr,27Ser)

Table 2. Residue Eliminations,[a] continued.

Number[b]	Residue	Reason for Elimination
50	Asp	involved in H-bond (26Asp,24Ala,5Asn,2Thr,1Lys,1Glu,1Asx)
51	Ala	always small (59Ala,1Gly)
52	Asn	conserved
55	Lys	involved in H-bond (42Lys,12Met,4Ala,1Ser,1Arg)
56	Asn	usually small (35Gly,24Ala,1Asn)
57	Val	usually large hydrophobic (32Ile,27Val,1Gln)
59	Trp	conserved
60	Asp	involved in H-bond (26Gly,19Glx,7Asx,3Lys,2Thr,2Ala,1Ser)
61	Glu	involved in salt bridge (47Glu,6Asp,2Asn,3Gln,1Tyr,1Pro)
63	Asn	involved in H-bond (56Thr,1Asn,1Asp,1Ser,1Val)
64	Met	always large hydrophobic (57Leu,2Met,1Phe)
65	Ser	crowded location (23Tyr,22Met,8Phe,3Ser,1Arg,1Asp,1His)
66	Glu	usually negative (33Glu,22Asp,2Val,1Lys,1Gln,1Ile)
67	Tyr	always aromatic (59Tyr,1Phe)
68	Leu	conserved
69	Thr	never positive (36Glu,23Leu,1Thr)
70	Asn	conserved
71	Pro	conserved
72	Lys	conserved[c]
73	Lys	conserved
74	Tyr	always aromatic (58Tyr,2Phe)
75	Ile	always large hydrophobic (58Ile,1Val,1Met)
76	Pro	conserved
77	Gly	conserved
78	Thr	conserved
79	Lys	conserved
80	Met	conserved
81	Ala	generally hydrophobic (27Val,25Ile,7Ala,1Ser)[c]
82	Phe	conserved
83	Gly	always small (28Ala,23Pro,6Gly,2Val,1Thr)
84	Gly	conserved
85	Leu	always large hydrophobic (36Leu,26Ile)
86	Lys	strongly conserved Lys (59Lys,1Ser)[c]
87	Lys	strongly conserved Lys (58Lys,1Ala,1Asx)[c]
88	Glu	eliminated to save negative charge
90	Asp	involved in salt bridge (38Glu,21Asp,1Gln)
91	Arg	conserved
92	Asn	crowded location (40Ala,6Asn,5Gln,3Glu,2Gly,2Val,1Lys,1Thr)

Table 2. Residue Eliminations,[a] continued.

Number[b]	Residue	Reason for Elimination
93	Asp	involved in H-bond (58Asp,1Asn,1His)
94	Leu	always large hydrophobic (58Leu,2Ile)
95	Ile	always large hydrophobic (55Ile,4Val,1Leu)
96	Thr	involved in H-bond (53Ala,6Thr,1Ser)
97	Tyr	always aromatic (59Tyr,1Phe)
98	Leu	always large hydrophobic (57Leu,3Met)
99	Lys	involved in salt bridge (55Lys,1Arg,1Glu,1Val,1Leu,1Glx)
101	Ala	usually small (39Ala,16Ser,2Leu,1Lys,1Glu,1Thr)
102	Cys	involved in H-bond (54Thr,2Cys,2Lys,1Ser,1Ala)
103	Glu	eliminated to save negative charge

[a]sequence data taken from [9]

[b]residue numbers are based on tuna structure

[c]also implicated in model complexes or chemical modification studies

Table 3. List of Potentially Mutatable Sites.

Number[a]	Residue	Other Residues Found in Position
2	Ser	Asp, Asn, Glx
3	Ala	Lys, Glu, Asn, Gln, Ser, Val, Ile, Pro
4	Lys	Asp, Glu, Ser, Thr, Ala, Glx
5	Lys	Arg, Asn, Ser, Thr, Ala, Val
7	Ala	Lys, Asp, Gln, Gly, Ala
8	Thr	Lys, Arg, Asn
11	Lys	Glu, Thr, Val, Ile
22	Lys	Glu, Asp, Gln, Gly, Ala
25	Pro	Lys, Gly, Ala
28	Val	Gln, Thr, Ile
53	Ile	Lys, Ala
54	Lys	Arg, Asp, Asn, Gln, Ser, Gly, Ala
58	Leu	Glu, Asn, Gln, Thr, Gly, Ala, Val, Ile
62	Asn	Lys, Asp, Glu, Gln, Ser, Ala, Pro
89	Lys	Asp, Glu, Asn, Gln, Ser, Thr, Gly, Ala
100	Lys	Asp, Glu, Asn, Gln, Ser, Thr, His, Ala, Ile

[a]residue numbers are based on tuna structure

Table 4. Positions Targeted for Incorporating Histidine.

number[b]	residue	distance,[a] Å
11	Lys	11.6
7	Ala	12.1
8	Thr	14.4
5	Lys	15.3
3	Ala	16.5
4	Lys	17.4
2	Ser	18.2

[a]distances determined using a 225 point conformational energy search (see Chapter 2).
[b]tuna numbering scheme

Figure 1.

Residues implicated in model complex studies. The following stereo projection shows those residues on cytochrome *c* that have an implied structural and/or functional role as indicated from model complex studies of cytochrome *c* and cytochrome *c* peroxidase and cytochrome *c* and cytochrome b_5 (residues 12, 13, 16, 27, 72, 81, 86 and 87). See text for additional details. The C_α trace is shown in yellow, the heme is shown in red, and the implicated residues are shown in blue.

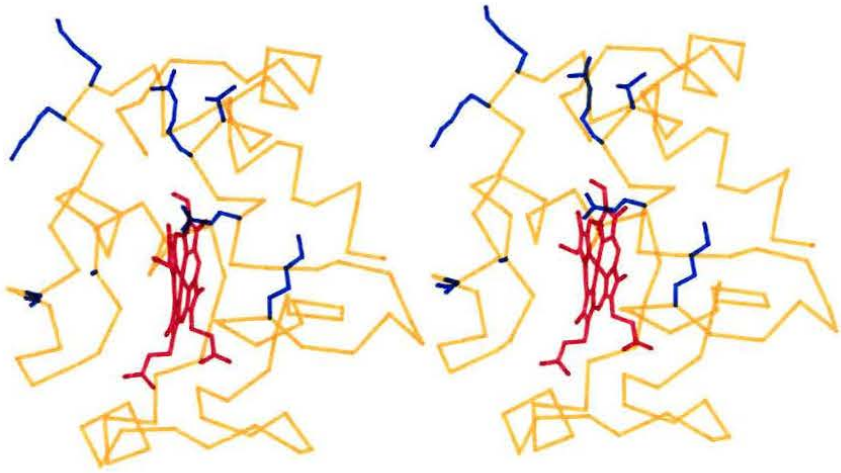

Figure 2.

Residues implicated in chemical modification studies. The following stereo projection shows those residues on cytochrome c that have an implied structural and/or functional role as indicated from chemical modification studies (residues 13, 72, 86 and 87). See text for additional details. The C_α trace is shown in yellow, the heme is shown in red, and the implicated residues are shown in blue.

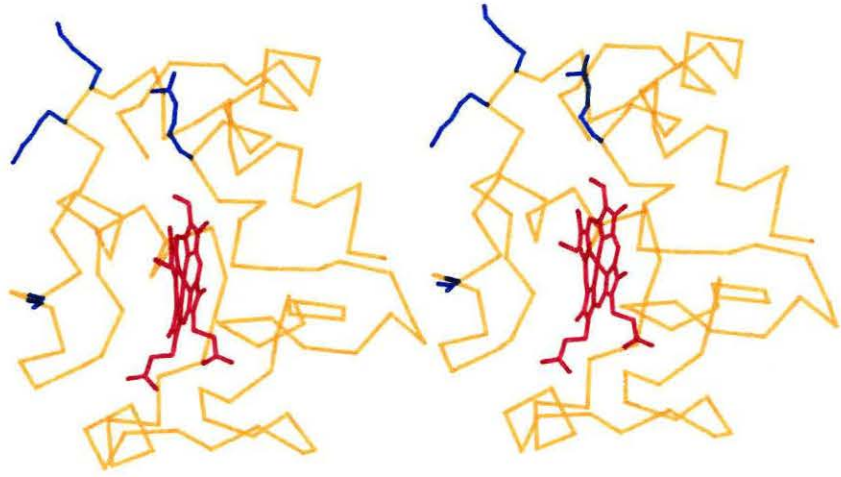

Figure 3.

Residues remaining after elimination procedure. The following stereo projection shows those residues that remain after the elimination procedure described in the text. Note that these residues are located on the periphery of what have been determined to be the "active" regions of the molecule. See Table 3 for residue numbers. The C_α trace is shown in yellow, the heme is shown in red, and the residues remaining after the elimination procedure are shown in blue.

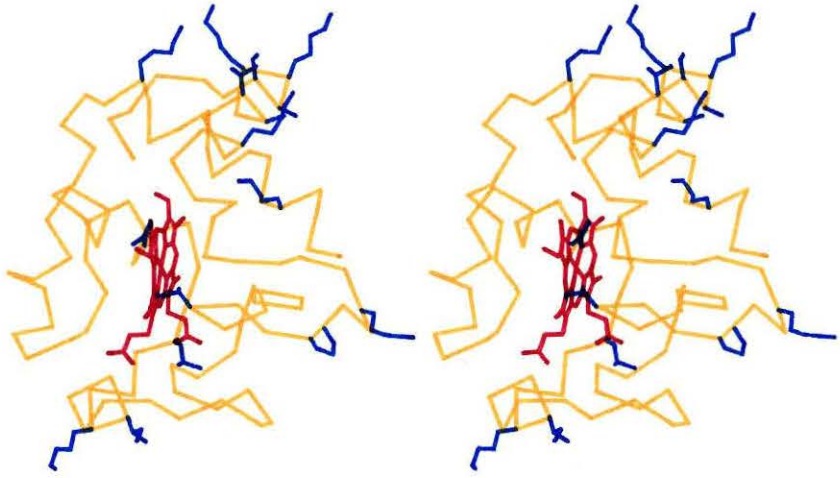

Figure 4.

Residues targeted for mutation to histidine. The following stereo projection shows the residues that have been targeted for mutation to histidine as described in the text and Table 4. Note how these residues cluster on the top and side of the N-terminal helix. Also note the relatively constant orientation with respect to the heme. The intervening media for these residues is hydrophobic and nonaromatic (not shown). The C_α trace is shown in yellow, the heme is shown in red, and the residue targeted for mutation to histidine are shown in blue.

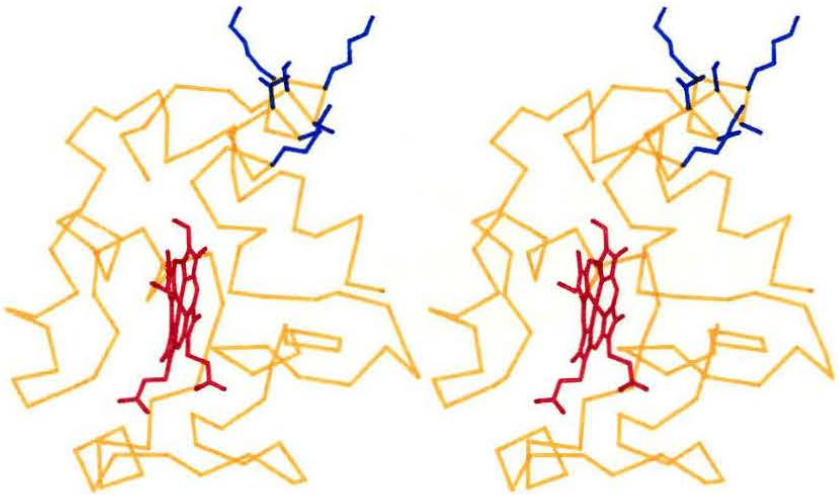

Figure 5.

Hydrogen-bond network in C-terminal helix. The following stereo projection shows the hydrogen-bond network that was responsible for our decision to mutate Cys102→Ser rather than to solve the "dimerization" problem by chemical modification. See text for additional details. The structure shown is from the yeast model. The purple lines indicate the hydrogen bonds formed between the carbonyl oxygen and side-chain sulfur of Cys102 and the amide nitrogen of residue 98.

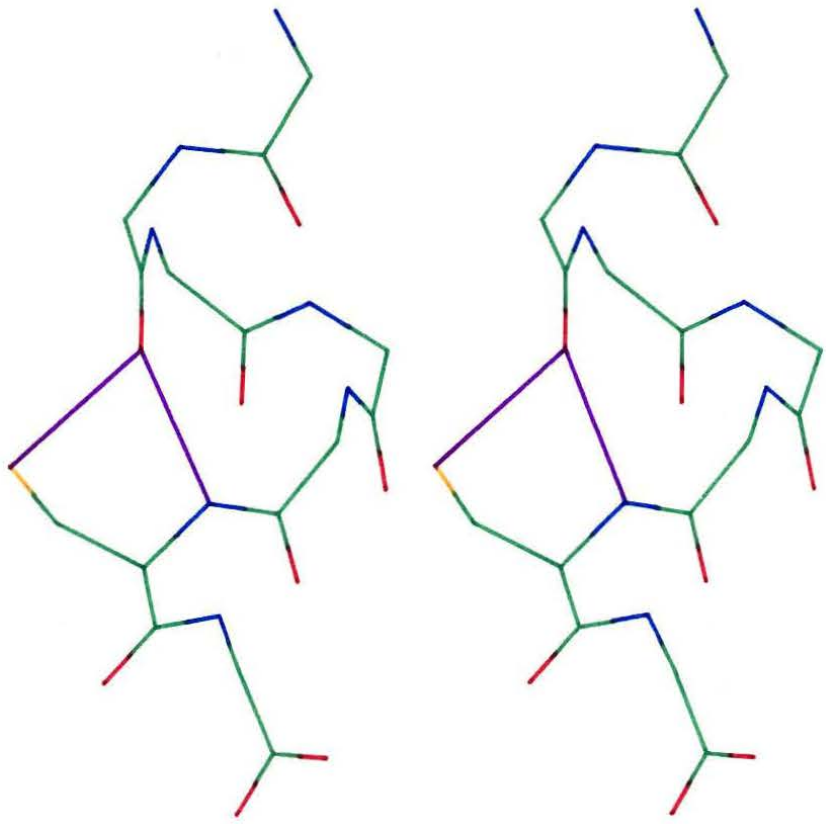

Figure 6.

Solvent accessible surfaces of His33 and His39. The following stereo projections show the solvent accessible surfaces of His33 (a) and His39 (b). It is our belief that solvent accessibility is a key factor in determining the rate of ruthenation. In *candida* cytochrome *c*, the product ratio between ruthenated His33 and His39 indicates that His39 reacts much faster than His33.[22] This is consistent with the observed solvent accessibility. Because of this observation, we decided that removal of His33 was not necessary for the construction of the base protein. See text for additional details.

(a)

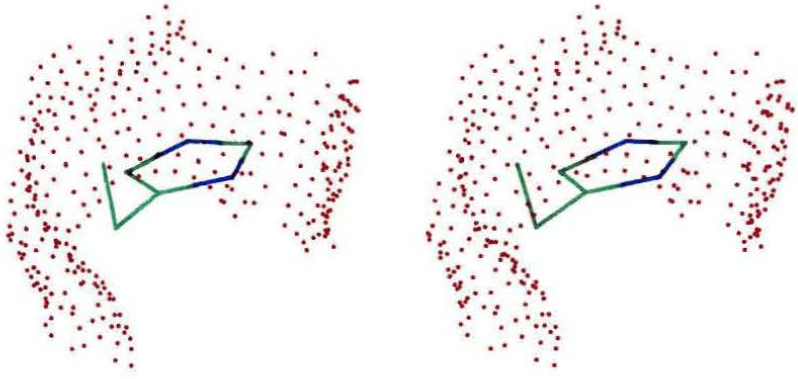

(b)

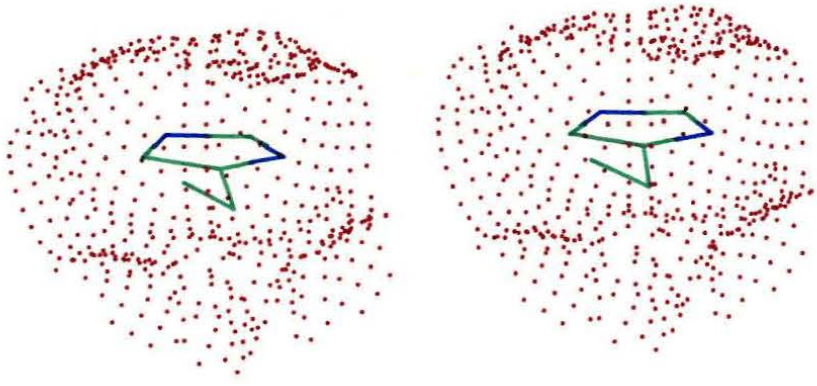

Figure 7.

General scheme for oligonucleotide-directed, site-specific mutagenesis. The following figure illustrates a general scheme for site-directed mutagenesis. The first step (A) is the annealing of the synthetic oligonucleotide to the single-stranded DNA template that contains the gene of interest. The mutagenic primer is then extended in the presence of the four deoxynucleoside triphospates with DNA polymerase (B). DNA ligase is also present to ensure that closed duplexes are formed. The product of this enzymology is then used to transfect E. *coli* (C). After culturing, the phage from individual plaques are spotted onto nitrocellulose filter paper. The filter, which contains single-stranded phage DNA, is developed at room temperature in a solution containing the mutagenic probe that has been radioactiviley labeled (D). Autoradiography reveals "spots" at all locations. Washing the filter at a discriminating temperature and autoradiographing reveals the required "positives" (E).

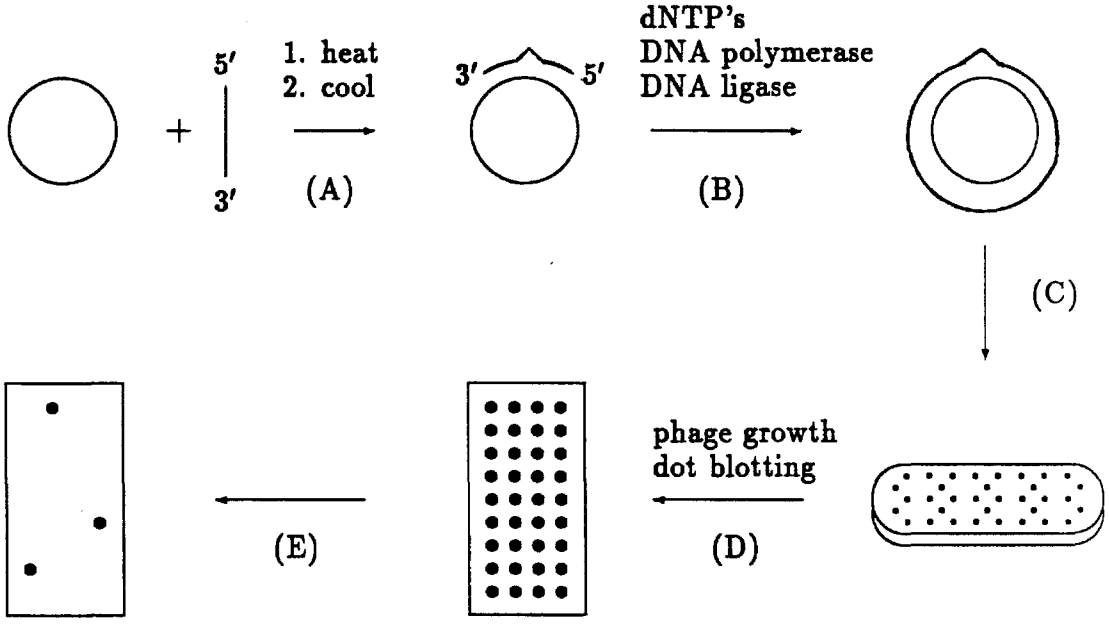
5′
3′
1. heat
2. cool
(A)
3′
5′
dNTP's
DNA polymerase
DNA ligase
(B)
(C)
phage growth
dot blotting
(D)
(E)

Figure 8.

Yeast expression and shuttle vector. The following figure indicates the functional regions of the vector used to shuttle the cytochrome *c* gene between yeast and bacteria and to express the gene in yeast. In addition to containing a bacterial origin of replication (ORI), this vector contains the ampicillin (AMP) and tetracycline (TET) genes, which allow convenient identification of recombinant plasmids in bacteria. The areas labeled 2μ and LEU2 are yeast sequences that confir high copy number and complement a host-strain leucine auxotroph, respectively. All of the control elements for expression of the CYC1 gene are contained on the 2500 base pair BamHI/HindIII fragment that contains the genes coding sequences. See text for additional details.

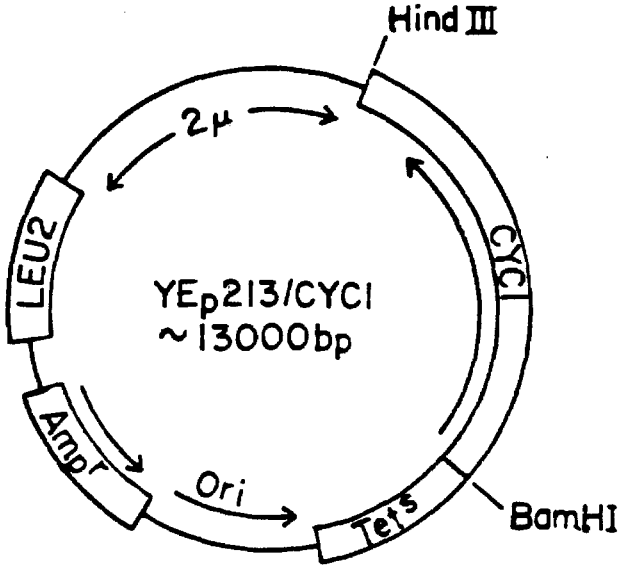
Hind III
2μ
LEU2
CYC1
YEp213/CYC1
~13000bp
Amp^r
Ori
Tet^s
BamHI

Figure 9.

The Cys102→Ser mutation. The following figure shows the details of the Cys102→Ser transformation. A 17 base mutagenic oligonucleotide was synthesized with the shown sequence. The possibility of incorporating one or both mismatches leads to three possible results. Incorporation at (A) gives only Cys102→Ser and no new restriction site. Incorporation at (B) gives only Cys102→Ser and a new DdeI restriction site. Incorporation at both (A) and (B) gives Cys102→Thr and a new DdeI restriction site. See text for additional details.

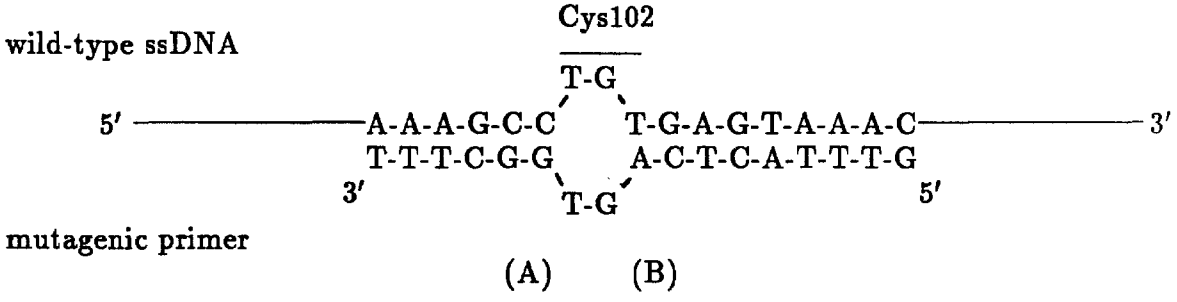

Ser102	Thr102	Ser102
GCC-AGT-GAG	GCC-ACT-GAG	GCC-TCT-GAG
CGC-TCA-CTC	CGC-TGA-CTC	CGC-AGA-CTC
	DdeI site	DdeI site
(A) only	(A) and (B)	(B) only

Figure 10.

Dot blots for Cys102→Ser. Dot-blot data for Cys102→Ser at room temperature (a) and at 41°C (b). Of the 132 plaques cultured and spotted, a single positive was found (only the filter containing positive is shown). See text for additional details.

(a) room-temperature wash

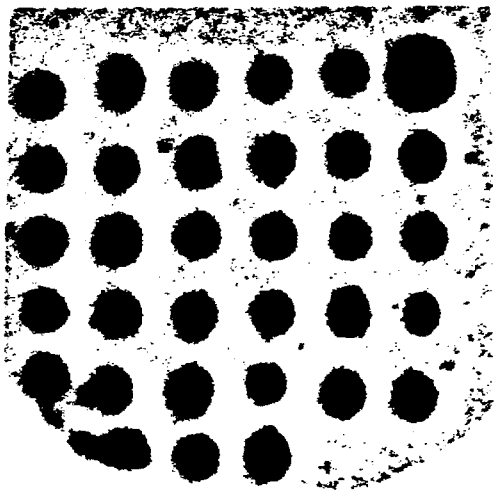

(b) 41°C wash

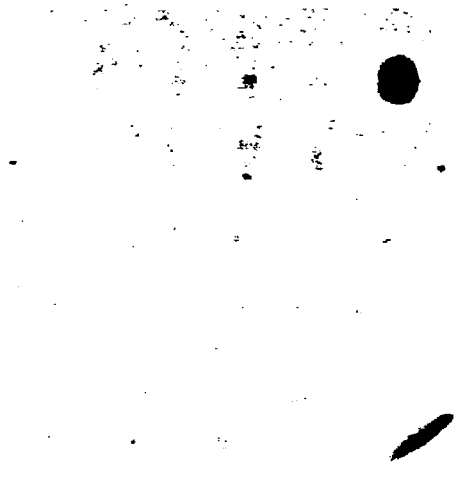

Figure 11.

Sequence data for Cys102→Ser. Although the entire coding region was sequenced, only data for the region surrounding the mutation are shown. (a) is the wild-type sequence and (b) is the mutant sequence. The sequences are for the "nonsense" strand and read 3′ to 5′ from top to bottom. The lanes are A, T, G, C from left to right. The arrows indicate the location of the single base change (A→T). See text for additional details.

(a) wild-type (b) Cys102→Ser

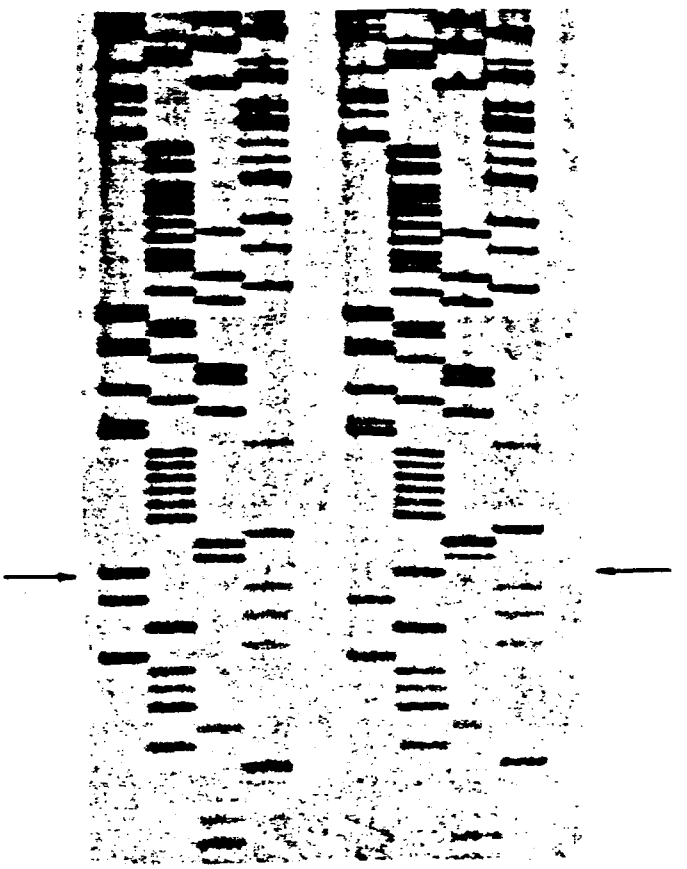

Figure 12.

The His39→Gln mutation. The following figure shows the details of the His39→Gln transformation. A 17 base single mismatch, mutagenic oligonucleotide was synthesized with the shown sequence. See text for additional details.

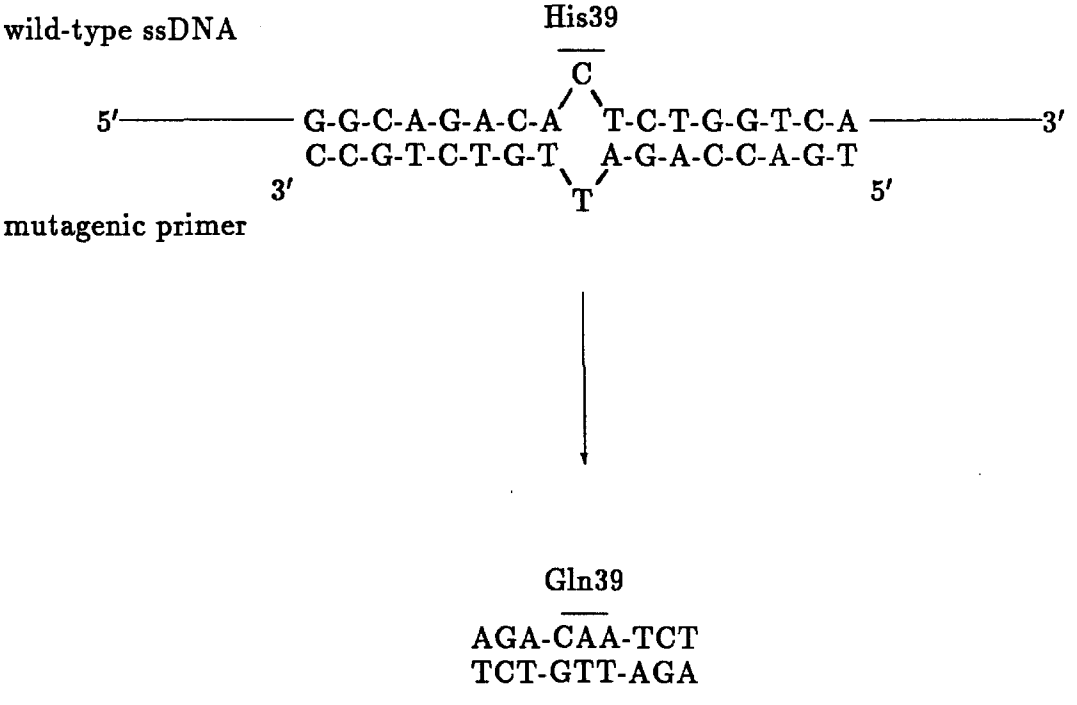
wild-type ssDNA
His39
C
5′
G-G-C-A-G-A-C-A
T-C-T-G-G-T-C-A
3′
C-C-G-T-C-T-G-T
A-G-A-C-C-A-G-T
3′
T
5′
mutagenic primer
Gln39
AGA-CAA-TCT
TCT-GTT-AGA

Figure 13.

Dot blots for His39→Gln. Dot-blot data for His39→Gln at room temperature (a) and at 50°C (b). Of the 60 plaques cultured and spotted, 3 positives were found. See text for additional details.

(a) room-temperature wash

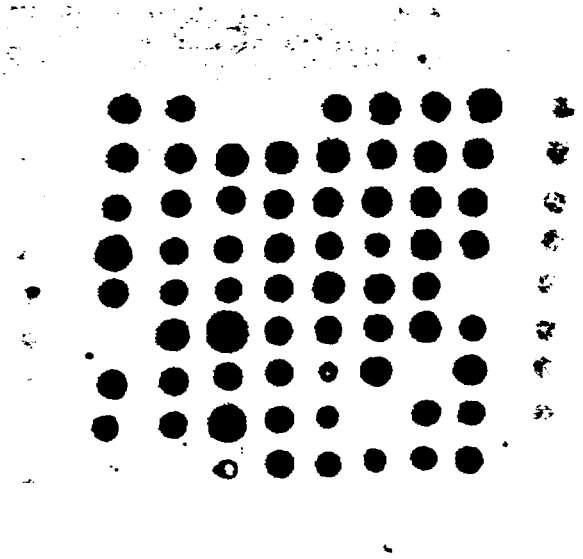

(b) 50°C wash

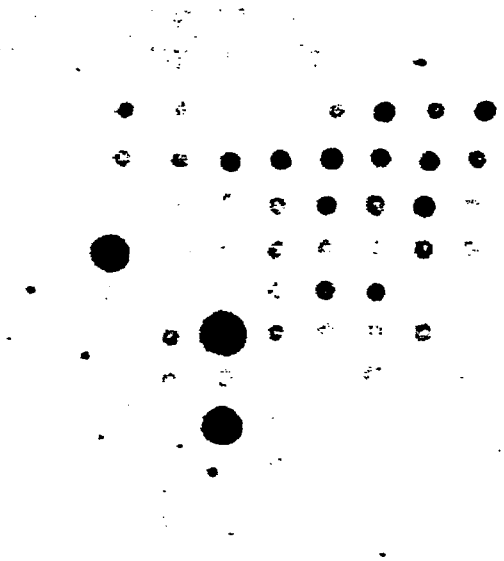

Figure 14.

Sequence data for His39→Gln. Although the entire coding region was sequenced, only data for the region surrounding the mutation are shown. (a) is the wild-type sequence and (b) is the mutant sequence. The sequences are for the "nonsense" strand and read 5′ to 3′ from top to bottom. The lanes are A, T, G, C from left to right. The arrows indicate the location of the single base change (G→T) See text for additional details.

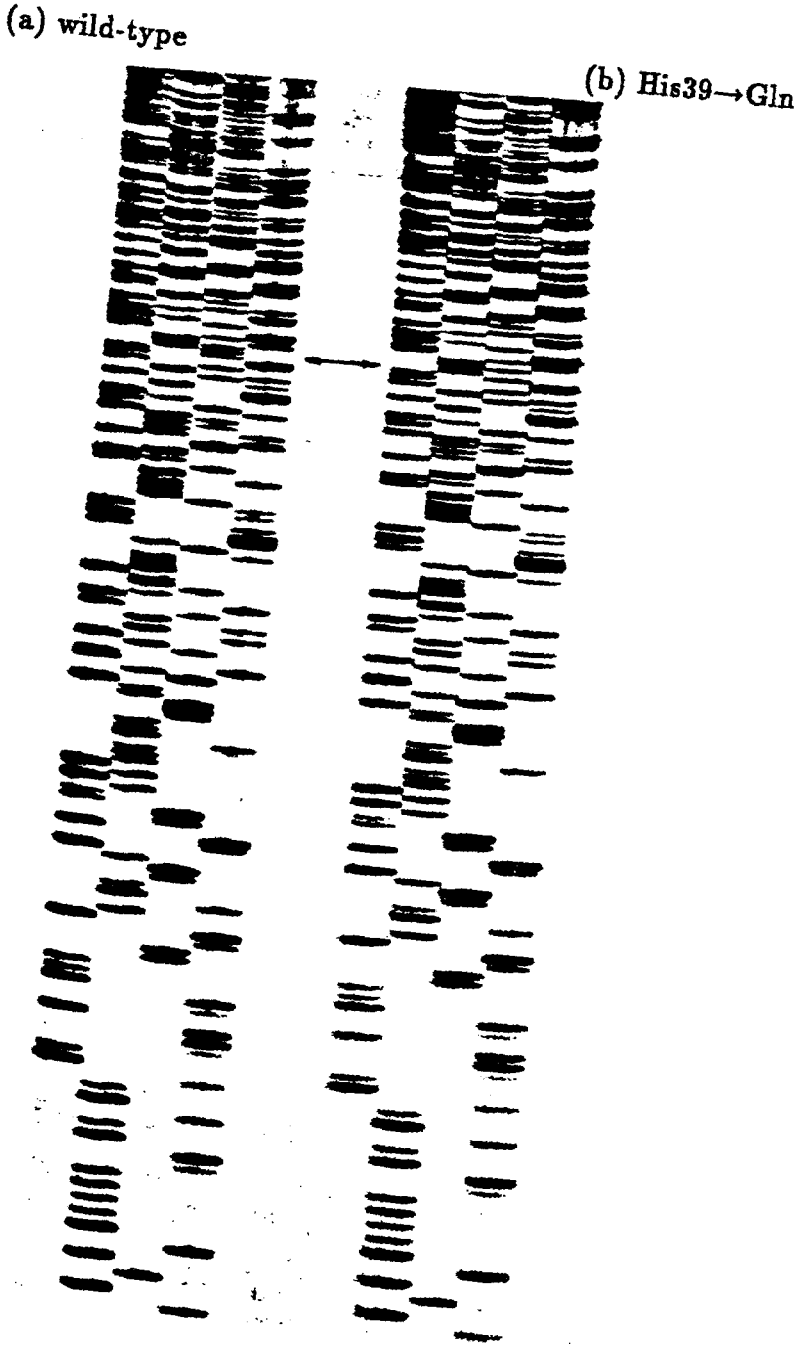
(a) wild-type
(b) His39→Gln

Figure 15.

The Thr8→His mutation. The following figure shows the details of the Thr8→His transformation. A 23 base triple mismatch, mutagenic oligonucleotide was synthesized with the shown sequence. See text for additional details.

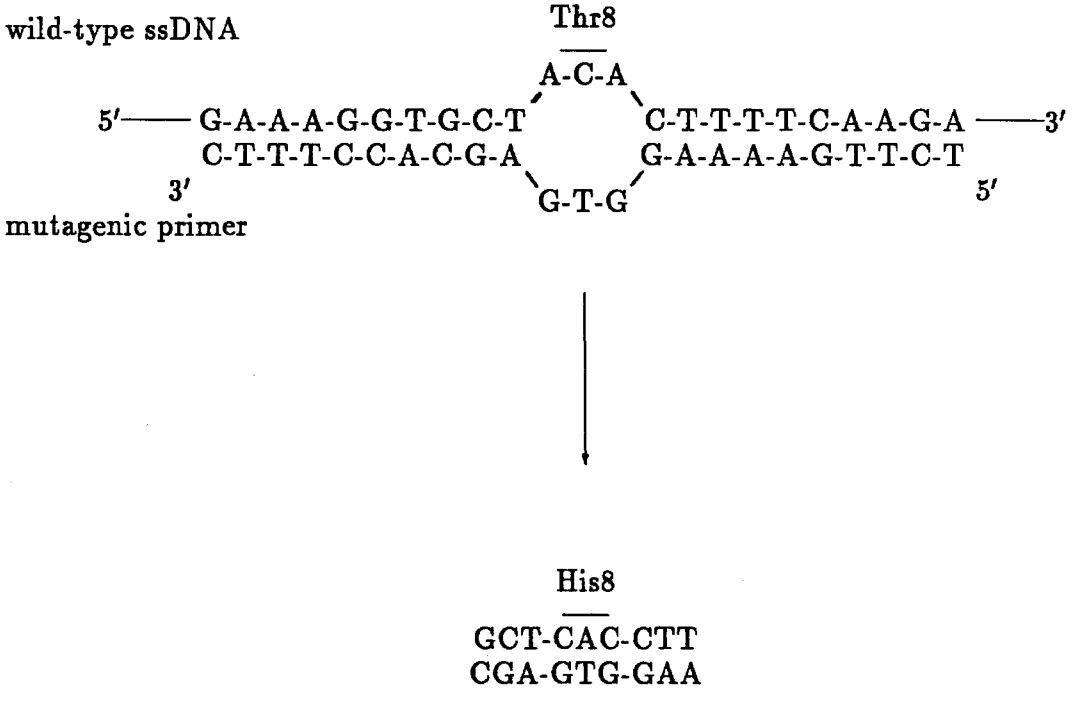
wild-type ssDNA
Thr8
A-C-A
5′—— G-A-A-A-G-G-T-G-C-T
C-T-T-T-C-C-A-C-G-A
C-T-T-T-T-C-A-A-G-A ——3′
G-A-A-A-A-G-T-T-C-T
3′
5′
G-T-G
mutagenic primer
His8
GCT-CAC-CTT
CGA-GTG-GAA

Figure 16.

Dot blots for Thr8→His. Dot-blot data for Thr8→His at room temperature (a) and at 44°C (b). Of the 36 plaques cultured and spotted, 4 positives were found. See text for additional details.

(a) room-temperature wash

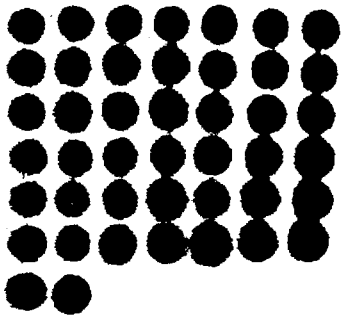

(b) 44°C wash

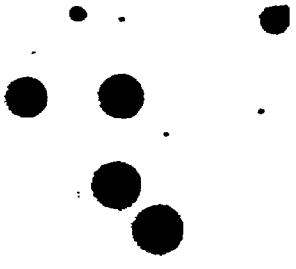

Figure 17.

The Lys5→His mutation. The following figure shows the details of the Lys5→His transformation. A 23 base double mismatch, mutagenic oligonucleotide was synthesized with the shown sequence. See text for additional details.

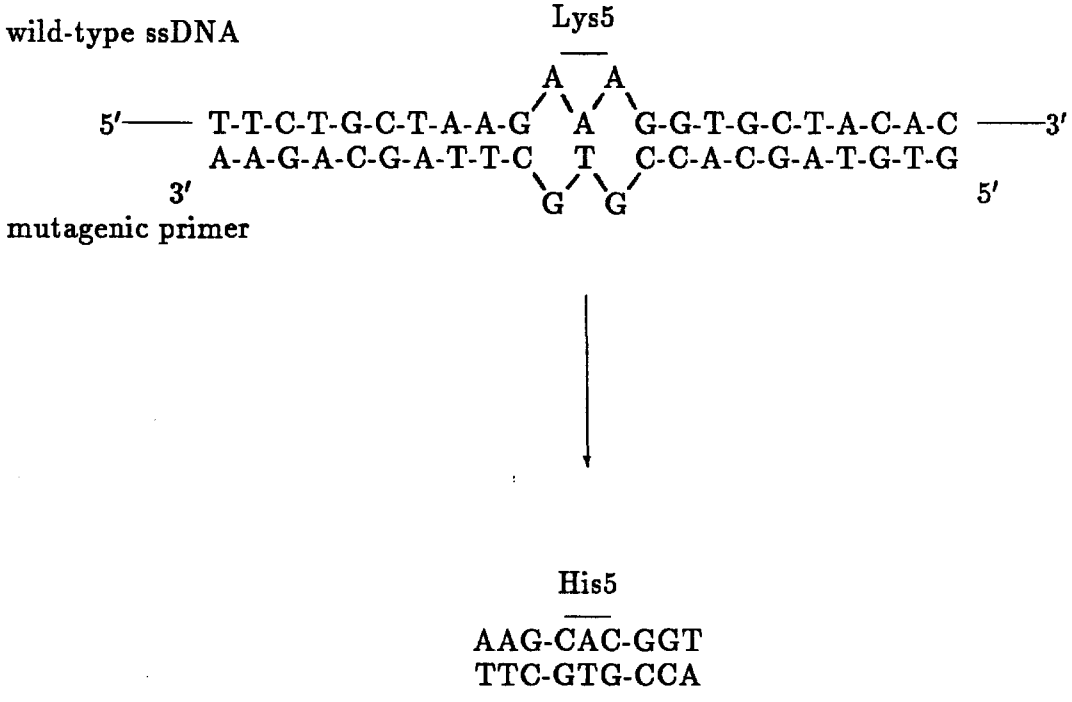
wild-type ssDNA
Lys5
A A
5′—— T-T-C-T-G-C-T-A-A-G A G-G-T-G-C-T-A-C-A-C ——3′
A-A-G-A-C-G-A-T-T-C T C-C-A-C-G-A-T-G-T-G
3′
G G
5′
mutagenic primer
His5
AAG-CAC-GGT
TTC-GTG-CCA

Figure 18.

Dot blots for Lys5→His. Dot-blot data for Lys5→His at room temperature (a) and at 44°C (b). Of the 36 plaques cultured and spotted, 2 positives were found. See text for additional details.

(a) room-temperature wash

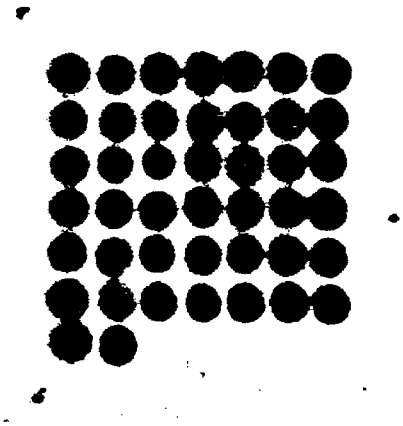

(b) 44°C wash

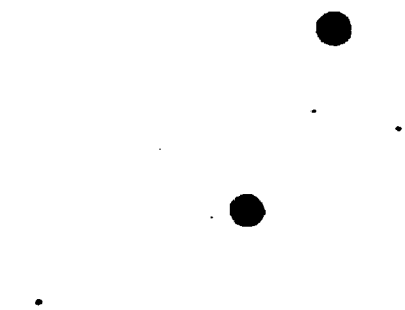

Thesis Summary

The material presented in the preceding chapters illustrates an evolution of experimental approaches in studying electron-transfer mechanisms in metalloproteins. The move from bimolecular to unimolecular model systems led to the first meaningful rate-distance analysis for metalloprotein systems. It is our hope that the experimental evolution suggested by the last chapter leads to an even more profound advance in the way we think about experiments aimed at elucidating the mechanism of biological electron transfer.